MEMORANDUM
RM-6093-PR
NOVEMBER 1969

NUMERICAL PREDICTION OF THE THERMODYNAMIC RESPONSE OF ARCTIC SEA ICE TO ENVIRONMENTAL CHANGES

G. A. Maykut and N. Untersteiner

PREPARED FOR:
UNITED STATES AIR FORCE PROJECT RAND

The RAND Corporation
SANTA MONICA • CALIFORNIA

This study is presented as a competent treatment of the subject, worthy of publication. The Rand Corporation vouches for the quality of the research, without necessarily endorsing the opinions and conclusions of the authors.

Published by The RAND Corporation

MEMORANDUM
RM-6093-PR
NOVEMBER 1969

NUMERICAL PREDICTION OF THE THERMODYNAMIC RESPONSE OF ARCTIC SEA ICE TO ENVIRONMENTAL CHANGES

G. A. Maykut and N. Untersteiner

This research is supported by the United States Air Force under Project RAND—Contract No. F11620-67-C-0015—monitored by the Directorate of Operational Requirements and Development Plans, Deputy Chief of Staff, Research and Development, Hq USAF. Views or conclusions contained in this study should not be interpreted as representing the official opinion or policy of the United States Air Force.

The RAND Corporation
1700 MAIN ST • SANTA MONICA • CALIFORNIA • 90406

PREFACE

This Memorandum describes a mathematical simulation model of sea ice growing and dissipating with the seasons and interacting with the atmosphere and the ocean. The model was developed by G. A. Maykut, performing research at the University of Washington under supervision of Rand consultant N. Untersteiner. It was a product of an arctic research program sponsored by the Office of Naval Research, which because of its immediate application to Rand weather studies has concurred with the publication of the work by Rand.

The subject is interrelated with a continuing line of Rand investigations into climatic change, its nature, its causes, and the possibilities for influencing climate (whether deliberately or inadvertently) on a large scale. The general aim of the program is to understand the dynamics of the thermally forced motion of the global atmosphere and ocean and to simulate this behavior using mathematical models and high-speed computers. Related work by other Rand staff members and consultants includes the development of simulation models of the atmosphere (Y. Mintz and A. Arakawa) and of the wind-driven ocean (W. L. Gates), studies of large-scale variations in thermal forcing of the global system (J. Bjerknes, J. O. Fletcher, R. E. Huschke, S. Olenicoff, and R. R. Rapp), and the development of simulation models of convective processes which heat the atmosphere and produce rain (L. R. Koenig and F. W. Murray).

Variations in ice extent on the sea are associated with variations in thermal forcing of the global system. Previous Rand reports exploring this interaction include: The Heat Budget of the Arctic Basin and its Relation to Climate, R-444, 1965, Proceedings of the Symposium on the Arctic Heat Budget and Atmospheric Circulation, RM-5233, 1966, and Ice Extent on the Southern Ocean and its Relation to World Climate, RM-5793, 1969. This Memorandum represents one more step toward understanding and simulating the dynamics of the global system.

SUMMARY

A one-dimensional thermodynamic model of sea ice is presented which includes the effects of snow cover, ice salinity, and internal heating due to penetration of solar radiation. Surface-energy balances determine rates of ablation and accretion; diffusion equations govern heat transport within the ice and snow. The incoming radiative and turbulent fluxes, oceanic heat flux, ice salinity, snow accumulation, and surface albedo are specified as functions of time. Starting from an arbitrary initial condition, the model is integrated numerically until annual equilibrium patterns of temperature and thickness are achieved. The model neglects the effects of mechanical stresses on the ice and the influence of surface conditions on the turbulent fluxes. Leads and melt ponds are considered only insofar as they indirectly affect the energy fluxes over the bare ice. The model is applied to the Central Arctic.

The input data for the initial test of the model were drawn largely from J. O. Fletcher, The Heat Budget of the Arctic Basin and Its Relation to Climate, The Rand Corp., Santa Monica, (1965). Values predicted by the model for the average ice thickness (288 cm), amount of surface ablation (40 cm), and the temperature field all agree closely with field observations. To define the response of sea ice to changes of its environment, various sets of values for the input parameters were specified, and additional solutions obtained. The roles of oceanic heat flux, snow cover, internal heating, albedo, incoming energy fluxes, and ice salinity were examined. Under present conditions, the ocean must supply 1 to 2 kcal/cm^2 year to the ice; an additional 4 kcal/cm^2 year would cause the ice to vanish. Analysis of these results has also shown that the response time of sea ice for a given set of parameters is determined primarily by the final equilibrium thickness, rather than the initial thickness. Annual snow depths less than 70 cm have little effect on equilibrium thickness because of mutually compensating changes in ice temperature, ice ablation, and internal heating; snow depths greater than 70 cm result in much thicker ice. Comparison of observed

and calculated temperature profiles indicate that 2.0 to 2.5 kcal/cm^2 year of the short-wave radiation penetrates the ice and contributes to internal heating, but as a larger fraction is allowed to penetrate the ice, less energy is available for melting at the surface and the average thickness increases. An increase in the amount of either incoming long-wave or short-wave radiation by 10 percent results in a 50 percent decrease in ice thickness. Although the turbulent fluxes are small in comparison to the radiative fluxes, they are significant in terms of the net energy balance. If their sum is reduced from -0.5 kcal/cm^2 year to zero, a 70 percent decrease in thickness occurs. Average ice albedos under 0.50 cause the ice to vanish in a few years.

The present model indicates that, of the various techniques proposed for large-scale ice removal, those involving modification of the surface would be the most feasible and effective. It is suggested that, in future field projects, priority be given to studies investigating the interaction of leads and melt ponds with the ice.

ACKNOWLEDGMENTS

This research was made possible by the continuing support from the Office of Naval Research (Arctic Program, Dr. Max Britton, Head, Contract NR 307-252, No. 477-24) with the Department of Atmospheric Sciences, University of Washington.

Our special thanks are due to Col. J. O. Fletcher (The Rand Corporation) for providing the instrumental input data and many fruitful discussions. Professors J. Holton, F. Badgley, J. Businger and Dr. J. Deardorff helped with valuable suggestions during all stages of the work. We wish to acknowledge the cooperation given by the Computer Center of the University of Washington.

Finally, we would like to express our gratitude to Mr. Ben Keller and Dr. W. L. Gates (The Rand Corporation) and Mr. Alan Thorndike (University of Washington) for their painstaking editorial work in preparing the final version of the manuscript, and Mrs. Alice Jefts for the exercise of her talents in preparing the tables.

CONTENTS

LIST OF FIGURES

Figure

SYMBOLS

c	Specific heat (cal/gm °K)
F_c	Flux of sensible heat by conduction (cal/cm^2 sec)
F_L	Flux of incoming long-wave radiation (cal/cm^2 sec)
F_ℓ	Flux of latent heat (cal/cm^2 sec)
F_r	Flux of incoming short-wave radiation (cal/cm^2 sec)
F_s	Flux of sensible heat (cal/cm^2 sec)
F_w	Oceanic heat flux (cal/cm^2 sec)
H	Thickness of the ice layer (cm)
h	Thickness of the snow layer (cm)
I_o	Flux of short-wave radiation passing through the upper surface (cal/cm^2 sec)
K	Eddy diffusivity (cm^2/sec)
k	Thermal conductivity (cal/cm sec °K)
q	Latent heat of fusion (cal/cm^3)
$S(z)$	Ice salinity at a depth z(gm/cm^3 or °/$_{oo}$)
T	Temperature (°K)
$\tilde{T}$	Temperature calculated by step A of the Sauliev method (°K)
$\hat{T}$	Temperature calculated by step B of the Sauliev method (°K)
t	Time (sec)
w	Upward velocity of ice due to hydrostatic adjustment (cm/sec)
z	Depth (cm)
α	Surface albedo (dimensionless)
β	Constant = 0.28 (cal cm^2/gm sec)
γ	Constant = 4100 (cal °K/gm)
Δt	Time increment (sec)

Δz	Depth increment (cm)
$\Delta \varepsilon$	Incremental change of the thickness at the boundaries (cm)
ε_L	Long-wave emissivity (dimensionless)
κ	Bulk extinction coefficient (cm^{-1})
ξ	$k\Delta t/pc\Delta z^2$ (dimensionless)
ρ	Density (gm/cm^3)
σ	Stefan-Boltzmann Constant (cal/cm^2 sec $°K^4$)

Subscript

f refers to fresh (pure) ice
H refers to the bottom of ice layer
h refers to the bottom of snow layer
i refers to the sea ice
o refers to the upper surface (snow or ice)
s refers to the snow
w refers to the water

I. INTRODUCTION

1.1 SEA ICE AND THE POLAR REGIONS

The polar regions, as the major heat sinks of the Earth, influence the general circulation patterns in both hemispheres. The heating at high and low latitudes is unequal, and the consequent general horizontal temperature gradient from the polar regions to the lower latitudes forces heat into the polar regions. In the Northern Hemisphere the annual heat transport into the region bounded by the Arctic Circle is approximately 75 kcal/cm^2, averaged over the entire area. (This is roughly equivalent to the yearly total of incoming short-wave radiation reaching the surface of the Arctic.) Most of this advected heat is lost in space in the form of long-wave radiation, thereby helping to maintain the radiative equilibrium of the earth.

Heat also is carried into the Arctic Basin by ocean currents, but only about one-tenth as much as is carried by the atmosphere because of the relative slowness of oceanic transport and the relative inefficiency of the transfer of heat between ocean and atmosphere. Still, the oceanic heat flux is sufficient to affect the sea ice significantly, both in thickness and extent.

Sea ice is a dominant feature of both polar oceans. The Arctic Ocean (as defined by Zubov, 1943), covering some 10^{17} cm^2, is about 80 percent ice-covered during the winter and 60 percent in the late summer. The pack ice surrounding the Antarctic Continent has a maximum area over one and a half times as great as in the Arctic. The annual variation in areal extent is about 85 percent (Treshnikov, 1967), contrasting with 25 percent in the Arctic. These broad changes make sea ice one of the most variable physical features on the surface of the earth.

Because of differences in the configuration of oceans and land masses, sea ice plays different roles in the Arctic and the Antarctic. In the Arctic, with its ice-covered ocean, the extent of sea ice is critical to the energy balance over the entire region. Even small anomalies in the energy fluxes at the surface can greatly vary the

percentage of ocean that is ice-covered. In fact, a mere 22 kcal/cm^2 surplus (only a third of the yearly energy flux into the Arctic) would obliterate the entire ice pack. The case of the Antarctic is strikingly different. There, the sea ice surrounding the continent, while greatly influencing the regional heat budget and the seasonal variations in atmospheric heat advection, still probably affects the general features of atmospheric circulation only about as much as do the stable continental ice masses. The continental region, under its 2000 to 4000 meters of ice is comparable in extent to the area covered by pack ice in the Arctic. Although antarctic sea ice could vanish with much the same energy input as that required for the Arctic, the masses of continental ice could be significantly affected by nothing less than a drastic climate change. Rapid removal of the southern pack ice would produce changes of unknown magnitude, but changes certainly ameliorated by the stabilizing effect of the relatively permanent ice sheets, and no radical change in the general circulation would necessarily follow.

For studying processes in the Northern Hemisphere, the Arctic appears to be of considerable concern, and the situation also is less complex, in the absence of large-scale continental ice. Considering further that the great annual variation in the extent of antarctic sea ice has made research difficult, the Arctic lends itself more readily to studies of sea ice and its large-scale effects. The following paragraphs will examine in more detail the role of sea ice in the Arctic.

1.2 CLIMATIC CONSEQUENCES OF ICE COVERING THE ARCTIC SEA

Sea ice modifies its environment in a number of ways. During the dark winter months, intense atmospheric cooling occurs; surface temperatures in the Arctic usually reach -30 to -40°C. The resulting increase in latitudinal temperature gradients produces an increase in the general circulation which then causes large quantities of warm air to be drawn into the Arctic from lower latitudes. Moreover, an ice cover transfers little heat from the ocean to the atmosphere, since

molecular conduction is the controlling mechanism. During the summer the pack ice is even more influential. Because of a relatively high albedo, only 30 to 40 percent of the incoming short-wave radiation is absorbed by an ice surface, as compared to 90 percent by open water. The large amount of radiation reflected contributes somewhat to atmospheric warming and a reduction in the intensity of atmospheric circulation. Heat storage in the Arctic Ocean is severly limited, while wind stress and wind mixing in the ocean is suppressed. Because little of the ocean surface is open for evaporation, arctic winters are characterized by light snowfall. Even during cloudy summers, precipitation remains low, being on the order of 10 to 15 g/cm^2 year.

The climatic consequences of ice covering the Arctic Ocean can best be understood through an examination of some possible results of an Arctic Ocean freed of ice. Fletcher (1965), in an extensive evaluation of existing literature dealing with the heat budget of the Arctic, visualizes an ice-free Arctic in roughly the following manner: in the summer the ocean would absorb and store up to 90 percent of all incoming solar radiation. This would imply a slightly cooler atmosphere and hence a small increase in the intensity of atmospheric circulation. Greater amounts of evaporation would produce general cloudiness over the area. During the winter the ocean would slowly release heat stored from the summer. Surface temperatures would be slightly above freezing in contrast to -35°C under present conditions. Advection of heat from lower latitudes would be only slightly less than at present. An ice-free Arctic would thus be characterized by a constant, vigorous, year-round zonal flow with cool moist summers and warm moist winters. This situation should, according to Fletcher, induce heavy snowfall along coastlines with onshore flow and might possibly lead to accumulation of continental ice sheets. Quantitative results from a model of zonal temperature distribution (Rakipova, 1966) generally tend to corroborate Fletcher, although the model predicts a slight decrease in the intensity of both zonal and meridional circulation in the summer, as well as winter. In either case, the climatic changes in the more populous regions of the Northern Hemisphere could be drastic indeed. The primary difficulty in evaluating the magnitude of

any of these effects is that the complex interrelationship between the atmosphere and the oceans cannot yet be adequately described.

1.3 RESPONSE OF ARCTIC SEA ICE TO ITS ENVIRONMENT

The extent and the thickness distribution of the pack ice depend on conditions in the atmosphere and ocean. Laikhtman (1959) investigated the ways in which the atmosphere may affect the speed of surface ablation and concluded that air temperature and cloudiness are the two major factors controlling ice melt. Anomalies of cloudiness can cause great departures from the normal radiation balance, whereas higher air temperatures raise the sensible heat flux. He also suggests that wind speed would have little influence on summer melting because a larger downward sensible heat flux would be offset by a correspondingly larger evaporative heat loss. Budyko (1966) contends that the ice is so sensitive to temperature that a positive summer anomaly of only 4°C would cause the entire ice pack to melt in four years; a 2-degree anomaly would produce the same result in a few decades. However, the validity of these conclusions is open to some doubt.

Although the winds exert little direct influence on surface ablation, they provide the principal mechanism through which ice movements occur. Figure 1 shows the average pressure patterns at high latitudes, superimposed over the mean ice drift. It may be seen that the ice motions tend to parallel the isobars. Two important features arise from the motions of wind-driven ice: pressure ridges and open leads. Overthrusting by ice flows can create zones where the ice thickness is up to an order of magnitude greater than that of the surrounding ice. Wittmann and Schule (1966) have found that 13 to 18 percent of the ice-covered portion of the Canadian Basin consists of pressure ridges. If pressure ridging proves to be this extensive throughout the Arctic Basin, existing estimates of the total amount of ice in the Arctic must be reviewed. Leads, especially during the winter, are zones of intense heat loss. Badgley (1961) found experimentally that the heat loss is at least two orders of magnitude larger from open leads than from perennial ice. Areas of open water thus stimulate rapid ice production.

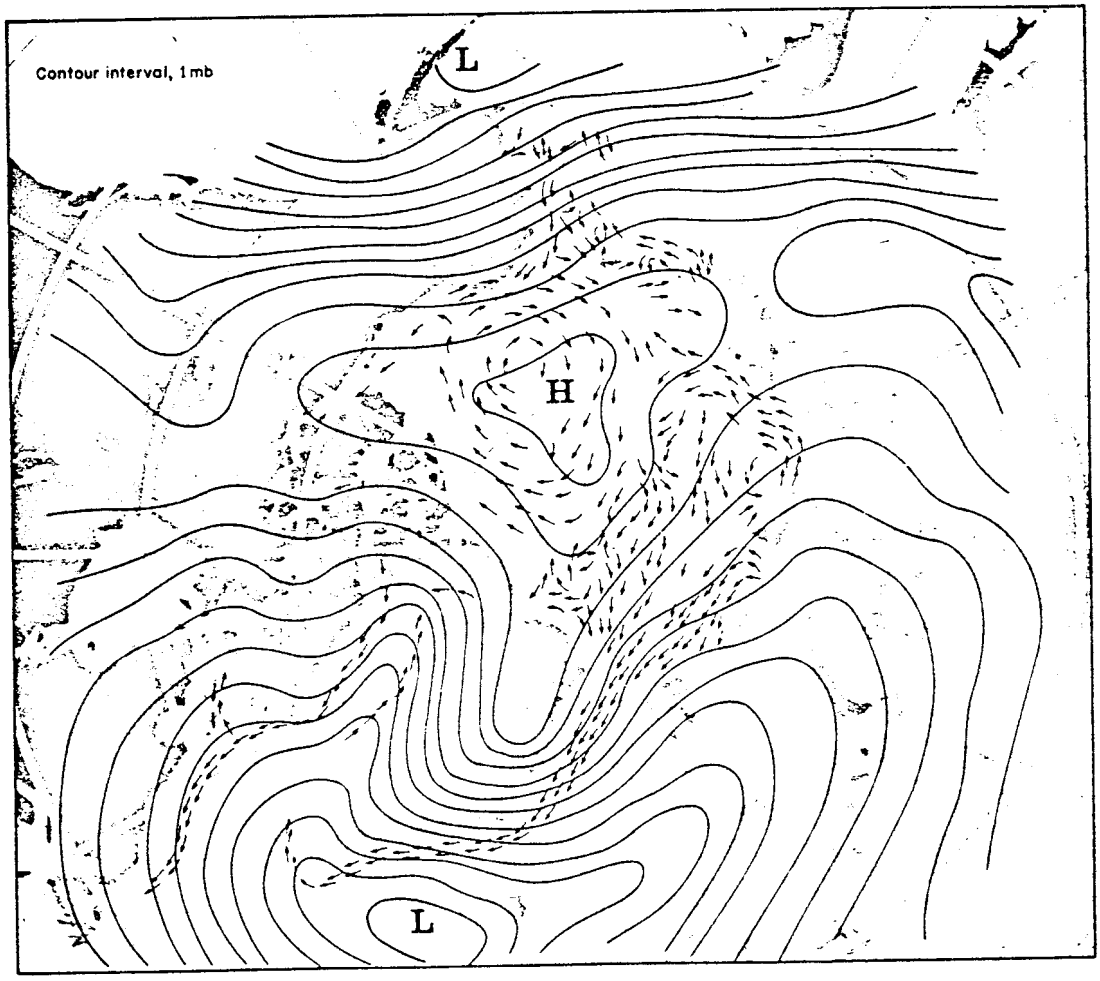

Fig. 1 -- Annual mean patterns of surface pressure and ice movement in the Arctic (Fletcher, 1965; data from Dunbar and Wittman, 1963).

The oceans influence arctic sea ice in only two principal ways: through turbulent heat transfer from the water to the ice and ice export by winds and surface currents. The oceanic heat flux ultimately results from the advection of warmer water into the Arctic Ocean; the rate of heat transfer depends upon the magnitude of water exchange, the ocean temperatures, and the density stratification in the ocean. The primary exchange mechanism is the influx of warm Atlantic water through the Faroe/Shetland Channel and the outflux of cold arctic water via the East Greenland Current. A small amount of water enters by the Bering Strait and by continental runoff from rivers, but the heat transported by these sources is an order of magnitude less than that from the Atlantic. Nearly all the ice leaving the Arctic drifts through the Greenland/Spitsbergen Strait. The exact total of this ice export is in some doubt; many authors prefer the estimate of Zubov (1950) of 3000 km^3 per year. This figure represents roughly 10 percent of the total ice contained in the Arctic Basin. If the ice exported each year were evenly distributed over the entire Polar Ocean, it would form a layer some 30 cm in thickness. Assuming that the pack ice is in near-equilibrium, average yearly ice production must lie near this value. The heat added to the region by the export of unmelted ice thus is about 2 $kcal/cm^2$ year.

Because the water transfer is restricted and the ice cover is widespread, the structure of the Arctic Ocean is quite different from that of other oceans. As the ice insulates the ocean from the atmosphere and reduces mechanical mixing, it is the primary determinant of vertical structure. The structure of the Arctic Ocean is horizontally quite uniform and characterized by an extremely stable density gradient. However, during periods of rapid ice accretion and consequent brine expulsion by the ice, a shallow convective layer is formed. Vertical overturning of this unstable layer brings up warmer water from the lower layers, generating an increased heat flux toward the bottom of the ice. Therefore, analogously to the atmosphere, the ocean not only influences the extent and thickness of the ice, but also is itself modified by the ice.

1.4 SURVEY OF PREVIOUS RESEARCH

The scientific literature dealing with the Arctic has multiplied many-fold since the pioneering voyages of the Fram (1893-1896) and the Maud (1918-1925). In 1937 the Soviets began a systematic study of the arctic interior by setting up the drifting station "North Pole 1 (NP-1)" on the pack ice. With the establishment of "Fletcher's Ice Island (T-3)" in 1952, the United States initiated its own long-range scientific program in the Arctic. Both the American and Soviet research efforts continue. Recently data from the ice stations have been supplemented by observations from air-borne and satellite-borne instruments and submarine transits. The resulting mass of observational and experimental data has been summarized in several comprehensive surveys which are discussed in this section.

By 1940 a coherent, although somewhat crude, picture of the Arctic and its physical environment had begun to emerge. N. N. Zubov in 1943 published "Arctic Ice," a classic reference devoted entirely to arctic ice and oceanography. Zubov's presentation of the geophysical aspects of the Arctic was, at the time, comprehensive. Besides such topics as the distribution, growth, forms, and physical, chemical, and mechanical properties of sea ice, he dealt in detail with the ocean/atmosphere system and its relationship to the pack ice. In addition to qualitative description of the physical events, he often gave them a quantitative formulation through the use of empirical or carefully derived mathematical expressions. Although subsequent research has shown some of Zubov's work to contain oversimplifications, many of his contributions remain of value and his text is still regarded as a standard reference.

Emphasis during early arctic reasearch was upon observing and describing events occurring on the ice and in the ocean. Not until the early 1950's did the concept of relating the energy balance to the mass budget begin to gain favor. Earlier there had been only sporadic attempts to measure the radiative components, but, with the establishment of NP-II in 1950 and T-3 in 1952, began a serious effort to acquire representative data on both short-wave and long-wave radiation. These measurements, combined with calculations of the turbulent

heat fluxes, produced for the first time good quantitative estimates of the heat-transfer processes in the Central Arctic. The results of a decade of observations have been summarized by Gavrilova (1963). Not only has she presented the geographical distribution of the radiation components in the Arctic and peripheral areas, but she has also described Soviet techniques of observation and methods of analysis. Because the Soviet data are supported by the most field observations and thus seem to be the most representative, Gavrilova's summary must be considered as a prime source of data concerning the arctic radiation regime.

In 1962 the Arctic Meteorology Research Group at McGill University, led by S. Orvig, undertook a project to correlate and evaluate all available data relating to the arctic heat budget. Included in these studies were such topics as atmospheric advection of heat and moisture, heat flux through the ice, sensible and latent heat fluxes, radiative components, and surface albedos. Despite certain limitations (see Section 4.1.4), the resulting technical papers, published during the next four years, represent a significant contribution to knowledge of the arctic regions.

Pursuing a similar theme, Fletcher (1965) related the arctic heat budget to hemispheric climate. In this study he discusses the interaction of the arctic ice mass with the ocean and atmosphere, mentions possible methods by which man may influence the heat balance, comments on the present direction of arctic research, and specifies the research topics deserving priority. One aim of this study was to obtain an average heat budget for the central Arctic Basin today for comparison with a possible ice-free regime. After a detailed analysis, he proposed a heat budget that relied heavily on Soviet sources, but which did not correspond exactly with any other single author. This budget is internally consistent and, according to Fletcher, has a probable error less than the year-to-year variations. Much of the work described in the present report makes use of these values. By interpolating cloud and energy exchange data from the normally ice-free portions of arctic seas, Fletcher devises a probable energy budget for an ice-free central Arctic Basin. The net energy balance for this

situation is very slightly positive, suggesting that the ice would not immediately re-establish itself once it is removed. However, resulting changes in atmospheric circulation could tip this delicate balance in either direction. Thus the stability of an ice-free Arctic remains an open question.

1.5 UNSOLVED PROBLEMS

It has long been observed that unusual weather in Europe seems to be correlated with abnormal extent of the pack ice. This feature is to be expected since storms generally tend to follow the margins of the ice, drawing energy from the temperature difference between ice and water. In an attempt to define the factors influencing climatic change, for example, Lamb (1959, 1961) made a detailed study of world-wide weather records and found that during the period 1800 to 1940 there was a definite tendency toward a stronger general circulation. The edge of the pack ice at the same time showed such a large northward migration that by 1938 it had receded further north than ever before in modern times. Whether the abnormally small amount of sea ice caused the circulation to be more vigorous, or whether the greater heat transport by the atmosphere was responsible for less ice, is a question that has not been adequately answered. Lamb attributes the recession of the ice to increased atmospheric heat advection associated with a more vigorous global circulation. More recently, Fletcher (1969) has suggested that the fluctuations in global atmospheric circulation and in the state of the ice and general circulation in the Northern Hemisphere may be related to the great changes in ice cover which occur in the Antarctic, but data remain so sparse that evaluation is very difficult. Until theoretical models describing the entire ocean/ice/atmosphere system can be solved, all that may be definitely stated is that some causal relationship must exist between the ice extent and hemispheric weather patterns.

Since relatively small changes in the energy balance over the pack ice can produce large changes in the areal extent of the ice cover, numerous investigators have looked to the Arctic for a source

of the sweeping climatic changes associated with the ice ages of the Quaternary. The present pattern of atmospheric and oceanic circulation and the distribution of ice may be only one of several quasi-stable situations. This possibility has evoked speculation on the various consequences of an ice-free Arctic Ocean. Many investigators conclude that an open Arctic, if it indeed represents an equilibrium situation, could lead to the accumulation of continental ice sheets. The central question to be answered is then: "What natural processes could produce an ice-free Arctic, and, once an open Arctic is achieved, could it remain so?" Brooks (1949) postulated a critical size of the ice pack above which its own cooling effect would ensure its continued growth, but, below which, a warming climate would ensure its continued wastage. Budyko (1966) presents a similar positive feedback mechanism to explain the formation of an open Arctic Ocean. In their theory of the ice ages, Ewing and Donn (1956, 1958, 1966) advanced data from a multitude of sources arguing for the existence of an ice-free Arctic, concurrent with the continental ice sheets. They suggest that variations in the oceanic heat flux, caused by a rising and falling sea level, could explain the appearance and disappearance of the pack ice. Because it is not known how large the oceanic heat flux must become before the ice would vanish, it is not clear whether the rise in sea level, associated with the melting of continental glaciers, could increase the supply of energy enough to melt the ice. In fact, recent evidence (Hunkins, 1965; Ku, 1965) strongly indicates that sedimentation rates on the floor of the Arctic Basin have remained relatively constant over at least the last 70,000 years. If so, it would appear that the Wisconsin Glaciation occurred without a coincident open Arctic.

As man's technological capabilities increase, it becomes more and more urgent that the factors influencing climate on a large scale be understood. For example, it now may be possible for man to remove the arctic ice pack; the result can only be surmised. Another possibility is that in man's increasingly effective tampering with nature, he may accidentally intervene at some critical stage in the climatic

process, producing unexpected effects on a world-wide scale. Such considerations cannot be neglected in the formulation of climatic experiments.

Because the physical principles governing the operation of each part of the system are relatively well understood, theoretical models of each part can be designed and methods of solution devised. The complexity of the resulting equations usually necessitates a numerical solution, employing the use of high-speed computers. Although storage limitations in present-day computers make it possible to solve only simplified versions of each component of the system, forthcoming computers offer hope that more realistic models may be solved. The ultimate goal then must be the incorporation of all the individual models into a single program that will provide a simultaneous description of each component.

II. FORMULATION OF A THEORETICAL MODEL

2.1 APPROACH TO THE PROBLEM

Among the many unsolved problems concerning the Arctic, that of quantitatively predicting the response of sea ice to changes in its environment stands out. Not only is it of major importance, but it also is a relatively straightforward problem amenable to current computer techniques. However, since theoretical treatment of the atmosphere and the ocean is beyond the scope of this report, their effects must be specified as external parameters. The outcome will be that the environment may influence the ice, but not vice versa. The objectives of this study will then be to forecast ice temperatures and thickness and to define the role of each component of the energy budget in relation to its effects upon the ice.

2.1.1 Previous work

A large number of studies have been made to develop empirical relationships predicting ice growth from observed temperatures at the surface. Two of the best known empirical formulas are those of Barnes (1928) and Zubov (1938). Somewhat more complex equations have been developed by Bilello (1961, 1964) from long-term observations of ice growth in the Arctic. While empirical and statistical approaches have practical value, they offer little physical insight into the problem.

Since the classical work of Stefan (1891), theoretical studies of the rate of ice growth have generally been limited to those in which simple analytical, approximate solutions could be attained. One of the most successful of these is due to Kolesnikov (1946). His equation predicts the thickness of sea ice by setting up heat-balance equations and solving them in conjunction with the heat conduction equation. Solution requires specification of such parameters as wind speed, humidity, air temperature, cloudiness, snow thickness, surface roughness, and ice salinity. This equation predicts growth rates in almost exact agreement with observed ones (Calloway, 1954). In practice, it would be difficult to acquire values for all these parameters over a large

region. Doronin (1959, 1966) calculated growth rates for an ice slab by using the heat-conduction equation, allowing for the variation of specific heat with ice salinity. He reports good agreement with observations on thin ice, but gives no specific examples.

In a more sophisticated model, Kolesnikov (1958) proposed a set of steady-state Fourier equations to describe the air/snow/ice/water system; approximate analytical solutions were then given. However, several serious errors have been pointed out in the model (U. S. Naval Civil Engineering Lab., 1965), and hence its applicability is doubtful.

With the development of high-speed computers, it is no longer mandatory that models have analytical solutions. A system of integro-differential equations can now be rapidly solved by finite-difference techniques. An advanced model is reported by Budyko (1966). Using a method of successive approximations, he reports that he has calculated ice thicknesses and the horizontal extent of the ice pack in good agreement with observational evidence. This model requires specifying the heat flux from the ocean at the bottom of the ice; ablation at the upper surface is determined by assuming values for humidity, wind speed, ice temperatures, air temperatures, and the radiative fluxes. The principal criticism of Budyko's model is that its upper boundary condition is more or less physically independent of heat conduction within the ice. By specifying surface temperatures, Budyko ignores any effects of heat conduction on surface ablation and surface temperature. No provisions are made to account for snow cover or the effects of ice salinity on heat transport between the boundaries of the slab. A model described by Untersteiner (1966) eliminates all these difficulties.

2.1.2 Idealized picture of the ice

In an idealized fashion, arctic sea ice may be viewed as an infinite, horizontally homogeneous slab, floating on its own liquid phase, having various energy fluxes impinging at both surfaces. The ice transfers heat between ocean and atmosphere by conduction; however, the transfer is affected by the brine pockets in the ice and by shortwave radiation penetrating the upper surface during certain seasons.

The annual snow cover influences the radiative and conductive transfer in important ways. It is taken into account by addition of an appropriate second layer to the model. An internal boundary condition ties together the diffusion equations describing conduction of heat in the snow and in the ice.

The boundaries of the slab are pictured as mathematically idealized planes. Energy is assumed to be absorbed at these planes, although in reality the energy absorption occurs in a finite layer. Mass changes may occur at either the upper or the lower surface. At the upper boundary, ice or snow may melt, but mass may be increased only through addition of snow. Either ablation or accretion can take place at the bottom of the slab. Whether ablation or accretion occurs is determined by the energy balance at the boundary under consideration. If, for example, there is more energy being absorbed at the boundary than is being lost from it, then either ablation or warming must occur.

The external energy fluxes, which are basic in determining mass changes of the slab, are taken to repeat themselves in a constant annual cycle. Thus an equilibrium situation must eventually be reached, that is, the net yearly bottom accretion will exactly balance the amount of ice lost through melting at the upper surface. This means that the net mass balance for the year is zero and that the mass changes and temperature patterns will begin to exactly repeat themselves in an annual cycle. Either condition may be used to define equilibrium.

Conditions are often uniform over vast areas in the Arctic. Available radiation data (Gavrilova, 1953) show only a slight latitudinal variation over the ice-covered portions of the ocean. Thus the assumption of horizontal homogeneity appears to be justified.

2.2 HEAT CONDUCTION

2.2.1 Heat conduction in the ice

The basic equation governing heat flow in solids is the thermal diffusion equation:

$$\rho c \frac{\partial T}{\partial t} = \nabla \cdot (k \nabla T), \tag{1}$$

where ρ is the density, c the specific heat, T the temperature, and k the thermal conductivity, and t refers to time. This well known equation has received intensive study, and numerous analytical solutions have been developed for certain situations (Carslaw and Jaeger, 1959). However, because of the deep penetration and absorption of short-wave radiation, Eq. (1) does not completely describe the situation as it exists for sea ice. Untersteiner (1964) used the following modifications of Eq. (1):

$$(\rho c)_i \frac{\partial T}{\partial t} = \frac{\partial}{\partial z} \left(k_i \frac{\partial T}{\partial z}\right) + \kappa_i I_o \exp(-\kappa_i z) - (\rho c)_i w \frac{\partial T}{\partial z}, \tag{2}$$

where κ_i is the extinction coefficient, I_o is the amount of short-wave radiation passing through the surface, and w is the upward flux of ice due to thickness changes. The subscript "i" refers to variables in the ice. The third term in Eq. (2) represents the heat generated by absorption of solar radiation per unit of time per unit volume at a depth z, and the last term describes the heat flux associated with the hydrostatic readjustment of the ice in response to mass changes at the boundaries. In keeping with the assumption of horizontal uniformity, the problem was reduced to one spatial dimension.

Both $(\rho c)_i$ and k_i are variables in sea ice, because small pockets of brine, trapped during freezing, remain in the ice. The brine is assumed to be at its freezing point and in phase equilibrium with the surrounding ice. The equilibrium is maintained by volume changes in the brine pocket. A rise in temperature causes the ice surrounding

the pocket to melt, diluting the brine and raising its freezing point to the new temperature. The brine pocket, thus, is a thermal reservoir, retarding the heating or the cooling of the ice. It is obvious, hence, that density, specific heat, and thermal conductivity are all functions not only of salinity, but also of temperature.

The variations of $(\rho c)_i$ and k_i were first investigated by Malmgren (1927), and a thorough theoretical analysis of the problem has been presented by Schwerdtfeger (1963). Untersteiner (1961) introduced the following formulas to describe these variations:

$$(\rho c)_i = (\rho c)_{i,f} + \frac{\gamma S(z)}{(T - 273)^2} \tag{3}$$

and

$$k_i = k_{i,f} + \frac{\beta S(z)}{T - 273}, \tag{4}$$

where $S(z)$ is the ice salinity at a depth z; $\gamma = 4100$ cal °K/gm and $\beta = 0.28$ cal cm^2/gm sec are constants. The subscript "f" refers to pure ice and $(\rho c)_{i,f} = 0.45$ cal cm^3 °K and $k_{i,f} = 0.00486$ cal/cm sec °K. Ono (1966) derived expressions for $(\rho c)_i$ and k_i on theoretical grounds. The resulting equations, while slightly more complex than Untersteiner's, proved to be similar in form and to give values which are in remarkably good agreement. For simplicity, Eqs. (3) and (4) were chosen for use in this model.

Substituting Eqs. (3) and (4) into (2), Untersteiner (1964) derived a complete description of energy transfer within the ice:

$$\left[(\rho c)_{i,f} + \frac{\gamma S(z)}{(T - 273)^2}\right]\frac{\partial T}{\partial t} = \left[k_{i,f} + \frac{\beta S(z)}{T - 273}\right]\frac{\partial^2 T}{\partial z^2} + \frac{\beta}{T - 273}\frac{dS}{dz}\frac{\partial T}{\partial z} -$$

$$\frac{\beta S(z)}{(T - 273)^2}\left(\frac{\partial T}{\partial z}\right)^2 + I_o \kappa_i \exp(-\kappa_i z) - \left[(\rho c)_{i,f} + \frac{\gamma S(z)}{(T - 273)^2}\right] w \frac{\partial T}{\partial z}. \tag{5}$$

Solution of this equation, with specified boundary temperatures, provided a temperature field consistent with observations.

For the present experiment, Eq. (5) is cumbersome and its solution time consuming, but an examination of the equations reveals that several terms may be dropped without substantial loss of accuracy. The last term in Eq. (5), the vertical advection term, is small and was eliminated. Its removal has the effect of allowing the upper and lower boundaries to move independently of one another; i.e., there is no hydrostatic readjustment. The terms $\frac{\beta}{T - 273} \frac{dS}{dz} \frac{\partial T}{\partial z}$ and $\frac{\beta\, S(z)}{(t - 273)^2} \left(\frac{\partial T}{\partial z}\right)^2$ express the variation of conductivity within the layer under consideration. Because these terms are awkward to handle, we decided to assume that the conductivity was constant within an incremental layer of thickness Δz. This assumption still allows the equation to take into account the variation of conductivity from layer to layer. An order-of-magnitude analysis performed on the equation indicated that both terms are three orders of magnitude smaller than the major terms; hence their removal seemed justified. An experiment described in the next chapter further serves to demonstrate that their effect is truly negligible.

With the above simplifications, Eq. (5) becomes:

$$\left[(\rho c)_{i,f} + \frac{\gamma\, S(z)}{(T - 273)^2}\right] \frac{\partial T}{\partial t} = \left[k_{i,f} + \frac{\beta\, S(z)}{T - 273}\right] \frac{\partial^2 T}{\partial z^2} + \kappa_i I_o \exp(-\kappa_i z). \tag{6}$$

Eq. (6) is now taken to be the basic equation describing heat flow in the ice.

2.2.2 Heat conduction in the snow

An analogous equation may be employed to describe passage of heat through a snow cover. Assuming horizontal homogeneity and a constant thermal conductivity, Eq. (1) becomes for the snow:

$$(\rho c)_s \frac{\partial T}{\partial t} = k_s \frac{\partial^2 T}{\partial z^2} + \kappa_s I_o \exp(-\kappa_s z) , \qquad (7)$$

where the subscript "s" refers to values in the snow.

Snow, unlike ice, undergoes great changes in density and crystal fabric during its metamorphism. Also the extinction coefficient for short-wave radiation varies widely. Observations by Liljequist (1956) and Ambach (1962) indicate that κ_s may range from 0.07 cm^{-1} to 0.5 cm^{-1}, depending on temperature, density, and crystal structure. A laboratory experiment by Mellor (1965) produced values between 1.3 cm^{-1} and 1.7 cm^{-1} for cold snow. The consequence of such large values is that essentially all incoming radiation is absorbed in the first few centimeters of the snow. Thus, in the model, the heating effect from this source is indistinguishable from absorption at the surface. In the absence of any detailed information on the behavior of κ_s, heat conduction in the snow may be described simply by:

$$(\rho c)_s \frac{\partial T}{\partial t} = k_s \frac{\partial^2 T}{\partial z^2} . \qquad (8)$$

2.3 BOUNDARY CONDITIONS

The crux of the present problem is the description of mass changes at the boundaries of the slab. They are stated as heat-balance equations, relating the various energy fluxes toward and away from the surface to the rate of freezing or melting. Solution of the boundary equations, along with the two heat-conduction equations, will allow computation of surface temperatures, temperature profiles within the ice and snow layers, and mass changes at both boundaries of the slab. The present model thus will represent a generalization of Untersteiner's (1964) model.

2.3.1 Upper surface

The major energy fluxes at the upper boundary include incoming long-wave radiation from the atmosphere and clouds (F_L), incoming

short-wave radiation (F_r), reflected short-wave radiation from the surface (αF_r), and outgoing long-wave radiation ($\varepsilon_L \sigma T_o^4$). In addition to these, there are several smaller but important fluxes: the fluxes of sensible heat (F_s) and latent heat (F_ℓ), heat conduction flux in the ice or snow (F_c), and a flux of radiative energy through the surface into the ice (I_o). These fluxes are schematically illustrated in Fig. 2. In describing the energy fluxes, the convention will be adopted that a flux toward the surface is positive and one away from the surface is negative.

To determine a balance equation for the upper boundary, it is necessary to consider two possible situations. If the surface temperature (T_o) is below the freezing point, then T_o must be adjusted in order that all the fluxes balance. If, on the other hand, T_o is at the freezing point, a certain amount of ice will have to melt to accommodate any surplus of energy flux toward the surface:

$$(1-\alpha)F_r - I_o + F_L - \varepsilon_L \sigma T_o^4 + F_s + F_\ell + k\left(\frac{\partial T}{\partial z}\right)_o = \begin{cases} 0 & , T_o < 273°K \\ -\left[q\frac{d}{dt}(h+H)\right]_o & , T_o = 273°K, \end{cases} \tag{9}$$

where h is the thickness of the snow layer, H is the thickness of the ice layer, ε_L is the long-wave emissivity, σ is the Stefan-Boltzmann constant, q is the latent heat of fusion, and α is the surface albedo. I_o is contained in $(1-\alpha)F_r$; however, since I_o passes into the interior of the ice, it represents an energy loss by the surface and must be treated accordingly (see Section 2.4.2). The subscript "o" refers to the upper surface. The turbulent fluxes have been given as positive terms, but they may in fact be in either direction. The quantities in Eq. (9) which must be specified as time-dependent external parameters are α, F_r, F_L, I_o, F_s, and F_ℓ; all temperatures and ice-thickness changes result from integration of the model. Snow deposition must also be treated as an external parameter (see Section 2.4.4).

Although Eq. (9) is quite general, it is only one of several possible formulations. For example, instead of specifying the downward long-wave and short-wave radiation at the surface, one might develop the equation in terms of solar radiation incident at the top of the atmosphere and assumed conditions of cloudiness, atmospheric absorption, humidity, and temperature. Added complexities of this sort, however, were not felt to be justified at the present stage of development.

2.3.2 Ice/water interface

At the bottom of the ice there are only two fluxes to be considered: the turbulent heat flux from the ocean and the conductive heat flux in the ice close to the boundary. The magnitude of the two fluxes is similar, with one or the other dominating during different seasons. The boundary equation has the form:

$$k_i \left.\frac{\partial T_i}{\partial z}\right|_{h+H} - (\rho c)_w \left.K_w \frac{\partial T_w}{\partial z}\right|_{h+H} = q \left.\frac{d}{dt}(h+H)\right|_{h+H}, \qquad (10)$$

where K_w is the coefficient of eddy diffusivity in the water, and the subscript "w" refers to values in the water; h and H are the thicknesses of snow and ice. Without a theoretical model of the ocean, it is not possible to calculate the heat flux from the water. Thus $(\rho c)_w \left(K_w \frac{\partial T_w}{\partial z}\right)_{h+H}$ is specified as an external parameter, while bottom growth is determined by the model. As a convenience, the following notation will be adopted throughout the remainder of the text:

$$F_w \equiv (\rho c)_w \left(K_w \frac{\partial T_w}{\partial z}\right)_{h+H}. \qquad (11)$$

2.3.3 Ice/snow interface

When snow covers the ice, it becomes necessary to specify another restriction at the ice/snow interface (z = h):

$$k_i \left.\frac{\partial T_i}{\partial z}\right|_h = k_s \left.\frac{\partial T_s}{\partial z}\right|_h . \qquad (12)$$

Equation (12) simply states that conduction through the ice/snow interface is continuous and assumes that any effects from penetration of short-wave radiation are negligible down to the depth h. Also, it is required that at $z = h$, $T_i = T_s$.

In summary, the problem is to solve the four equations (6), (8), (9), and (10) for the four unknowns: snow temperature, ice temperature, thickness change at the top, and thickness change at the bottom. This model, which is equivalent to the one outlined by Untersteiner (1966), is presented graphically in Fig. 2.

2.4 EXTERNAL PARAMETERS

The model formulated in the preceeding sections views temperature and thickness changes as a result of arbitrarily imposed energy fluxes at the upper and lower boundaries of the slab. Solution of the equations depends upon specification of these fluxes, along with a number of other parameters. In the initial integration of the model, values which closely resemble actual conditions were chosen; results could then be compared with observations as a test of the validity of the model.

2.4.1 Energy fluxes

At the upper boundary, four energy fluxes must be specified: F_r, F_L, F_s, and F_ℓ. After a detailed analysis, Fletcher (1965) chose the values given by Marshunova (1961) for F_r and F_L as the most representative of the region. Her values were based on the results from Soviet drifting stations NP-3 and NP-6. Fletcher also considers the turbulent fluxes calculated by Doronin (1963) physically plausible and

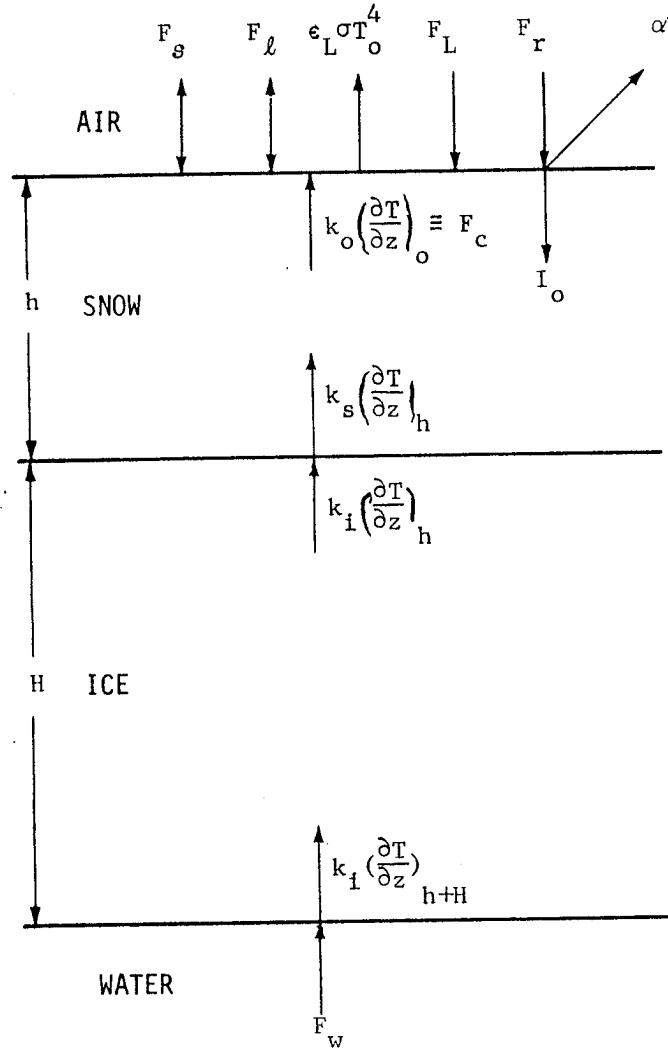

Balance of fluxes

$$(1-\alpha)F_r - I_o + F_L - \epsilon_L \sigma T_o^4 + F_s + F_\ell + k_o\left(\frac{\partial T}{\partial z}\right)_o = \begin{cases} 0 & , T_o < 273\ ^oK \\ -\left[q\frac{d}{dt}(h+H)\right]_o & , T_o = 273\ ^oK \end{cases}$$

$$(\rho c)_s \frac{\partial T}{\partial t} = k_s \frac{\partial^2 T}{\partial z^2}$$

Heat required for ablation

Heat conduction

$$k_s\left(\frac{\partial T}{\partial z}\right)_h = k_i\left(\frac{\partial T}{\partial z}\right)_h$$

Balance of fluxes

$$\left[(\rho c)_{i,f} + \frac{\gamma S(z)}{(T-273)^2}\right]\frac{\partial T}{\partial t} = \left[k_{i,f} + \frac{\beta S(z)}{T-273}\right]\frac{\partial^2 T}{\partial z^2} + \kappa_i I_o \exp(-\kappa_i z)$$

Heat conduction with internal heat source

$$k_i\left(\frac{\partial T}{\partial z}\right)_{h+H} - F_w = \left[q\frac{d}{dt}(h+H)\right]_{h+H}$$

Balance of fluxes

Fig. 2 -- Schematic illustration of the sea-ice model.

consistent with what is known about the other components. Following Fletcher's suggestion, these values were adopted for use in the initial test of the model and are reproduced in Table 1. The only major researchers to deviate substantially from the above findings are Vowinckel and Orvig (1966, 1967). Their studies indicate values for the absorbed short-wave radiation which seem extremely high. The consequences of the heat budget of Vowinckel and Orvig are examined in detail in Section 4.1.4.

Compared with the fluxes at the upper surface, the magnitude of the oceanic heat flux (F_w) is relatively little known. Direct measurements have proved difficult, at best, and estimates have been based primarily on indirect evidence. Malmgren (1927) used temperature profiles in the ice to produce his estimate of 6.8 kcal/cm^2 year. However, equating the annual heat flux in the ice with that in the water is incorrect (Untersteiner, 1964), since this method ignores the heat released from accretion at the underside of the ice and heat contributed by the penetration of visible radiation (similarly Mosby, 1963).

One method of approximating F_w is to estimate the heat content and the residence time of the waters entering the Arctic Basin. Rough values of the heat loss can then be calculated for various areas. Crary (1960) used the data from Timofeev (1958) to construct lines of equal heat content for the North Polar Basin. His chart indicates a heat loss of approximately 2 kcal/cm^2 year from the ocean in the Central Arctic. A more recent calculation (Panov, 1964) demonstrates that the heat flux undergoes large year-to-year variations. In the Chukchi Sea, for example, the annual upward heat loss from Atlantic waters fluctuated between 1038 and $1800 \cdot 10^{12}$ kcal during the 1930 to 1964 period; the average being $1426 \cdot 10^{12}$ kcal/year. Assuming an area of 86,400 km^2, the annual heat flux then varied from 1.1 to 2.0 kcal/cm^2, with an average of 1.65 kcal/cm^2. It would be reasonable to expect a slightly greater value in the Central Arctic.

Badgley (1961) used a more direct method to determine F_w. By choosing a period when the lower part of the ice was isothermal and then measuring bottom ablation, he calculated a yearly value of 1.5 kcal/cm^2. Independent results from Untersteiner's 1964 model suggest

almost exactly the same value. Although all these methods involve numerous assumptions, the true values of F_w must lie close to 1.5 kcal/cm^2 year. This value was adopted for the test run of the model.

A final problem connected with heat flux from the ocean is that there is probably a slight time dependence. During the summer, fresh water drains into the ocean and forms a stable layer near the underside of the ice (Untersteiner and Badgley, 1958; Hanson, 1965). But without more precise knowledge than is currently available, it seems pointless to speculate on time variations of F_w. Therefore it was assumed to be constant during the entire year.

2.4.2 Penetration by short-wave radiation

During the snow-free summer months, solar radiation penetrating the ice surface (I_o) is the prime source of internal heating. In this section we will be concerned with the amount of penetrating radiation and its effect.

Temperature profiles taken at the height of the melt season indicate an internal heating of the slab of approximately 700 cal/cm^2 in only 14 days (Untersteiner, 1961). A further examination of these profiles shows that the temperature gradients (and therefore the conductive heat fluxes) remained nearly constant during this period, implying that the observed heating was not the result of conduction. Thus the source of the energy used to heat the deeper layers must be ascribed to penetration of incoming short-wave radiation. Untersteiner's data indicate that about 32 percent of the net short-wave radiation makes no contribution to the surface melting. On the basis of these observations and his radiation measurements, Untersteiner (1964) arrived at an annual value for I_o of 1.2 kcal/cm^2.

Because absorption of solar energy by the ice is a function of wavelength, angle of incidence, and physical character of the surface, a theoretical description of I_o would be complex. Ice is nearly opaque to some wavelengths, and the incoming energy at these wavelengths is absorbed in the top few centimeters. At other wavelengths, the radiation penetrates farther. Thus, for modeling purposes, we

may consider the ice slab as having two layers: a thin surface layer that absorbs most of the short-wave energy, overlying another layer in which the remaining energy is absorbed. Numerical limitations decrease the resolution of the model to the point that absorption of radiation in this surface layer is indistinguishable from direct surface melting. As a first approximation, we may assume that Beer's Law is valid within the lower layer and determine a bulk (integrated over all wavelengths and solid angles) extinction coefficient (κ_i). Direct photometric measurements (Chernigovskii, 1963) indicate values for κ_i of 0.014 cm^{-1} to a depth of 150 cm, and 0.012 cm^{-1} below this. Untersteiner (1961) utilized temperature profiles to make indirect calculations of energy transmission in the ice. His results give an average value of 0.015 cm^{-1} between 50 and 150 cm. Since both of these methods have shown that extinction in the lower layer closely follows Beer's Law, Eqs. (6) and (9) offer a reasonable description of the effects of penetration and absorption of short-wave radiation.

Although κ_i could easily be specified as a function of depth in the model, little is known of such variations and a constant value of 0.015 cm^{-1} was therefore chosen. To specify I_o in the model, values for incoming short-wave radiation were combined with the albedo to calculate net short-wave radiation; a predetermined percentage of this quantity was then assigned to I_o (subtracted from the net short-wave radiation) and the remaining portion was used to determine the surface energy balance. Lacking more detailed evidence, this percentage was taken to be constant during the snow-free period. Imposing the restriction that I_o be 1.2 $kcal/cm^2$ year on Fletcher's suggested heat budget means that only 17 percent of the net short-wave radiation may penetrate the ice. This is in apparent conflict with Untersteiner's 32 percent and it is possible that his 1964 value underestimates I_o. The model's predictions of surface ablation and ice thickness should help to resolve these discrepancies.

Table 1. AVERAGE MONTHLY VALUES FOR THE INPUT DATA AT THE UPPER BOUNDARY ACCORDING TO FLETCHER (1965).

Symbol	Variable	Jan	Feb	Mar	Apr	May	Jun	Jul	Aug	Sep	Oct	Nov	Dec	Year
F_r	Incoming short-wave radiation ($kcal/cm^2$)	0	0	1.9	9.9	17.7	19.2	13.6	9.0	3.7	0.4	0	0	75.4
F_L	Incoming long-wave radiation ($kcal/cm^2$)	10.4	10.3	10.3	11.6	15.1	18.0	19.1	18.7	16.5	13.9	11.2	10.9	166.0
F_s	Flux of sensible heat ($kcal/cm^2$)	1.18	0.76	0.72	0.29	-0.45	-0.39	-0.30	-0.40	-0.17	0.10	0.56	0.79	2.71
F_ℓ	Flux of latent heat ($kcal/cm^2$)	0	-0.02	-0.03	-0.09	-0.46	-0.70	-0.64	-0.66	-0.39	-0.19	-0.01	-0.01	-3.20
α	Surface albedo	...	...	0.83	0.81	0.82	0.78	0.64	0.69	0.84	0.85	...	...	...

2.4.3 Ice salinity

Brine inclusions in sea ice are thermodynamically important because they affect density, conductivity, and latent heat. Equations (3) and (4) describe the influence of salinity on $(\rho c)_i$ and k_i and hence upon heat conduction. At temperatures near the freezing point, $(\rho c)_i$ may change by almost two orders of magnitude, while k_i shows a 10-percent change. Also the latent heat of fusion (q) is influenced by the initial brine volume. At the bottom of the ice, for example, the brine volume is roughly 10 percent (Schwarzacher, 1959), and the heat of fusion 64 cal/cm^3 (rather than 72 cal/cm^3). This difference is important in the calculation of bottom growth.

Although it is relatively easy to treat the effects of salinity, when it is known, acquisition of representative salinity profiles has proved difficult because of the large scatter in the field data. To further compound the problem, the shapes of the profiles probably depend upon the season, the growth rate, and the thermal history of the slab. Many of these difficulties could be resolved by a theoretical description of the desalination process, however at the present time, there is still doubt as to what mechanism controls brine removal. A recent study (Untersteiner, 1968) has shown that solute diffusion and gravity drainage are too small to account for the observed features. Both "flushing" and "brine expulsion" could produce

brine withdrawal at a reasonable rate, but it is now known which is dominant.

Ideally, salinity should be described as a function of growth rate and thermal history of the slab; however, a proven theory of desalination is lacking, and it is difficult to guess how the profile would change under varying conditions of temperature and speed of growth. Fortunately an examination of Eqs. (3) and (4) indicates that, unless the temperature is higher than -2 or -3°C, salinity has only a small effect upon $(\rho c)_i$ and k_i. Thus it is important only that salinity be known accurately during the summer and in the vicinity of the ice/water interface. Salinity in the lower portion of the ice is relatively constant at around 3.2 parts per thousand. The best documented equilibrium profile is that of Schwarzacher (1959) shown as Fig. 3. In the absence of more extensive data, this profile was adopted to represent mean annual conditions.

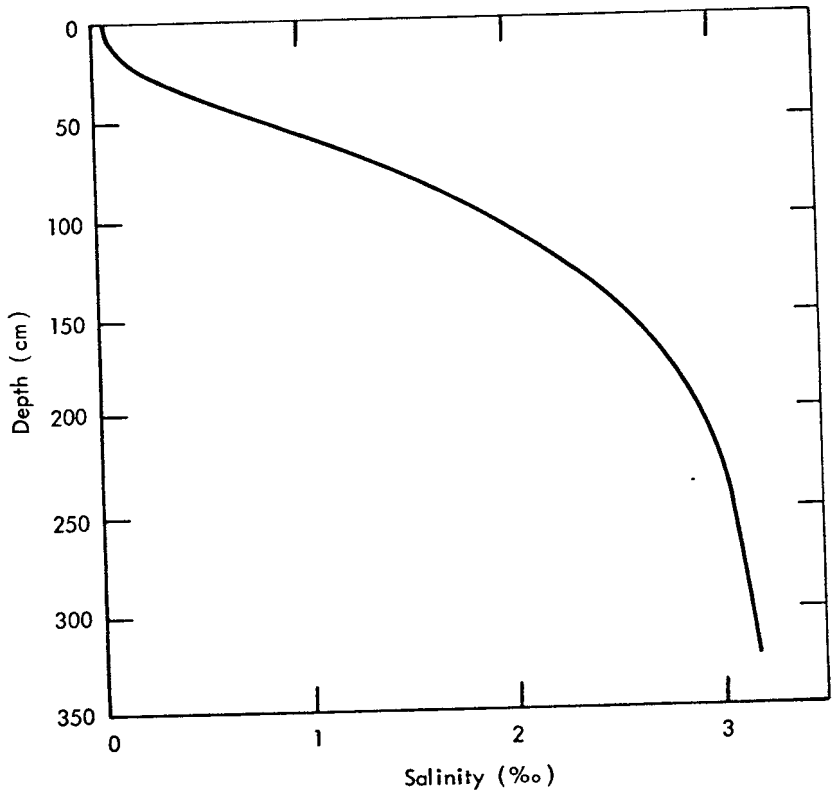

Fig. 3 -- Salinity profile for equilibrium sea ice.

The salinity of Fig. 3 is approximated by the expression:

$$S(z,t) = A + B \sin\left[C\left(\frac{z}{H}\right)^{n/\left(\frac{z}{H}+m\right)} + D\right], \qquad (13)$$

where A, B, C, D, m, and n are constants and H is the thickness of the ice. Equation (13) thus gives the salinity as a function of depth and is related to time through H. Details of the evaluation of the constants are given in the following chapter. The equation, while complex, provided an extremely good fit to the data. Implicit in the equation is the assumption that shape and end-points of the profile are retained during all fluctuations of ice thickness.

2.4.4 Snow cover

Nearly two decades of observations from various drifting stations have produced a fairly good knowledge of the snow distribution in time and space. After the freeze-up in late August, snow accumulates rapidly for the first month or two, followed by a more gradual increase during the winter months. In May, snow accumulation again slightly increases, reaching a maximum depth of about 40 cm in June (Untersteiner, 1961; Hanson, 1965). During the melt season, sporadic storms deposit small amounts of snow that directly influence the mass budget only slightly, but which, by changing the albedo, may affect the heat and mass budget considerably (see Section 2.4.5). Although surface features, such as pressure ridges, cause some small-scale variations, snow depth is generally uniform throughout the Central Arctic.

To represent this pattern of snowfall, it was assumed that there is a linear accumulation of 30 cm between 20 August and 30 October, a linear increase of 5 cm from 1 November to 30 April, and an additional 5 cm during the month of May. In cases where the summer melt season extends past 20 August, snow accumulation is delayed until freeze-up occurs. If the surface temperature reaches the melting

point before 1 June, then snow accumulation is cut off before it reaches 40 cm. No attempt was made to model the occasional summer snowfalls.

The fine-grained structure of arctic snow, combined with compaction by the wind, causes it to have a fairly high density. A value of 0.33 g/cm^3 (Untersteiner, 1961) was chosen for the model. It is assumed that the snow density (ρ_s) is independent of depth and remains constant as long as the snow temperature remains below freezing. At the onset of melting, the density increases rapidly to a limiting value of 0.45 g/cm^3 (E. LaChappelle, personal communication) as melt water penetrates the snow and is refrozen. Thermal conductivity (k_s) is quite variable, even in snows of equal density, and depends upon grain size, snow structure, and the temperature gradient. Mellor (1964) has collected and graphed experimental results from 75 years of observations. Abels' Formula (Abels, 1892) represents a reasonable compromise of all the diverse measurements and was used in the experiment:

$$k_s = 0.0068\ \rho_s^2 (\text{cal/cm sec } ^\circ\text{K}) \ . \qquad (14)$$

A major problem encountered in treating the snow cover is how to take into account water percolation and densification of the melting snow. It would be possible, for example, to add a forcing function term to Eq. (8) that would describe the heat released by refreezing. Equation (14) could then be combined with an assumed ρ_s to solve the modified heat-conduction equation. Before this method was tried, a calculation was made to determine the heat content of the snow layer at the onset of melting. The results indicated that the melting and subsequent refreezing of only 2 cm of snow would add enough heat to make the entire layer isothermal. No field data are available on the length of time necessary to melt the first 2 cm of snow; however an initial test of the model predicted that only about 5 days are required. In order to avoid unnecessary complications, the model was then set up to ignore heat added by melt water. The integration proceeds, considering only conduction in the snow, until 2 cm

of snow are melted. At this time, the snow layer is made isothermal and the density is increased from 0.33 to 0.45, with a consequent discontinuity in snow depth. This procedure preserves the essential features of the densification process. The only significant deviation from reality is that the temperature at the ice/snow boundary will be too cold for a few days and then will suddenly jump to the freezing point of the ice (-0.1°C). Consequences of this treatment are discussed more thoroughly in Section 2.5.

2.4.5 Surface albedo

The surface albedo (α) and its variations are probably the most important regional factor affecting the heat and mass budgets of the Arctic Basin. Albedo values determine the net short-wave radiation, and small changes in α can account for dramatic changes in the amount of surface ablation. As an example, if the albedo were decreased by only 10 percent during the month of June, yearly ice ablation would increase by about 25 cm or 60 percent.

During the spring and fall, when surface conditions are uniform, α is high and relatively constant. Incident short-wave radiation is relatively small during this time. The critical period occurs during June and July, when there is a sharp increase in available energy and melting is rapid. As melting progresses, wide albedo fluctuations occur in response to the changing micro-relief of the surface. Yakovlev (1958) reports that α varied between 0.44 and 0.89 on NP 2 during the summer ablation season.

Snow patches, bare ice, and melt ponds, all with different radiative characteristics, may coexist over a relatively small area. In addition, snowfall can cause a 30-percent increase in α in a matter of hours. It is obviously impossible to duplicate such random fluctuations and horizontal variations in a one-dimensional model.

Most authors agree on spring and fall values for α, but there is disagreement regarding albedo averages during the summer. The majority view is that the effective albedo of ice that is melting lies between 0.60 and 0.70. Untersteiner (1961) assumed an average of 0.66,

while Soviet measurements indicate a value of 0.64 (Marshunova, 1961; Chernigovskii, 1963). Aircraft measurements (K. Hanson, 1963) also support these values. Unpublished data from Arlis-II show hourly albedo values fluctuating from 0.55 to 0.70 on melting ice.

Vowinckel and Orvig (1966, 1967) hold a value of 0.45 to be representative. This view is supported by the fact that albedo measurements on melting, dirty ice have often been as low as 0.40 and integrated albedo values from a 15 meter tower are even lower (Langleben, 1968). These facts, combined with the prevalence of melt ponds, cause Vowinckel's estimate to appear reasonable; however acceptance of a value this low is incompatible with other considerations. From energy-balance calculations, the increase in net short-wave radiation resulting from an albedo of 0.45 would cause about 120 cm of ablation during the summer, an amount roughly three times the observed quantity. On this basis, Fletcher (1965) accepted Marshunova's value of 0.64.

Neglecting the influence of melt ponds, the average ice albedo is certainly closer to 0.64 than to 0.45, although an areal average is probably substantially lower. The question which must be considered is how the depth of the melt ponds affects the average ice thickness over an annual cycle. A melt pond which exists at the end of the ablation season will freeze during the fall and, except for acting as a heat source to retard cooling, has little effect on annual thickness. During the summer, however, at least half of the melt ponds drain, forming channels and hollows in the surface topography. Snow accumulated in these depressions remains longer, retards ablation in these areas, and tends to level the ice relief. Increased ablation beneath melt ponds therefore has only a limited effect on the general ice thickness. In consequence, averages over large areas were set aside, and the albedo of melting ice was taken as 0.64. Fall and spring snow albedos were also taken from Marshunova (1961) and are reproduced in Table 1.

A further problem is how to model the albedo during the transition from a snow cover to bare ice. Lacking any detailed information, a simple linear decay of albedo with snow depth was assumed:

$$\alpha = \alpha_i + (\alpha_o - \alpha_i) \frac{h}{h_o} \qquad (15)$$

where h_o is the snow depth when the snow begins to melt, α_o is the snow albedo at the onset of melting, and α_i is the albedo of the bare ice (0.64). Thus, if the snow albedo was 0.84 at the onset of melting, it would have a value of 0.74 when half the snow had melted, 0.69 after three-quarters had melted, etc. Although it is not known how well Eq. (15) approximates reality, the errors introduced should be no larger than those from other sources.

2.4.6 Other assumptions

For convenience, the year was divided into twelve months of 30 days each. Since both ice and snow radiate in the long-wave region much like a black body (Kellogg, 1964), the long-wave emissivity (ε_L) in Eq. (9) was set equal to unity. It may be seen from Eqs. (3) and (4) that both $(\rho c)_i$ and k_i are discontinuous at T = 273°K. In order to avoid this singularity, the melting temperature was assumed to be 272.9°K, which is realistic, as a residue of salt remains in the upper layers of the ice. The temperature at the underside of the ice was assumed to remain constant at the freezing point of sea water (271.2°K).

2.5 LIMITATIONS

There are a number of limitations that are inherent to, or implicit in, the proposed model. These shortcomings may be roughly divided into two groups: conceptual and physical. Conceptual limitations arise from a lack of theoretical understanding or the inability to model certain processes affecting the ice; physical limitations are due to uncertainties in the environmental data. The following discussion will outline these difficulties and attempt to evaluate the importance of each to the purpose of the present calculations.

2.5.1 Conceptual limitations

A basic shortcoming of the model is its inability to account for effects of mechanical stresses on the ice. Winds produce extensive deformation, as is evidenced by the occurrence of leads and pressure ridges. According to Wittmann and Schule (1966), up to 10 percent of the surface in the Central Arctic consists of open leads during all seasons. Untersteiner (1966), however, pointed out that this estimate is incompatible with several other estimates of the heat and ice budget and will require further investigation. Changes in the heat budget resulting from the variation of open water areas are not covered by the model.

Wittmann and Schule also report that 13 to 18 percent of the ice surveyed was made up of pressure ridges with a thickness of 20 to 30 meters. Often zones of several hundred square kilometers were more than 50 percent covered by "pressure ice." It has been stressed that this model computes ice thickness only as a result of thermodynamic processes. If mechanical deformation adds a significant contribution to the amount of ice stored in the Arctic, then the predictions from the model can be used in mass budget studies only in conjunction with suitable assumptions concerning the volume of ridged ice.

An indirect result of the prevailing wind patterns is the removal of large quantities of ice by surface currents. As mentioned in the introduction, an amount of ice roughly equivalent to a slab 30 cm thick and covering an area equal to the whole Arctic Ocean, is exported annually. It would be relatively simple to incorporate an export factor into the equations. However, the drift patterns indicate only a slight divergence in the Pacific Gyral, implying that most of the exported ice originates in the peripheral seas. Thus the contribution from the Central Arctic is probably small and has been neglected.

Another serious problem occurs in the treatment of the turbulent fluxes at the boundaries. In Eqs. (9) and (10), F_{ℓ}, F_{ℓ}, and F_{w} are assumed to be independent of growth rate and the physical state of the ice or snow at the boundaries. This assumption is not realistic

for thin or rapidly growing ice and, ideally, these fluxes should reflect conditions at both surfaces. But unless theoretical models of the atmosphere and ocean can be incorporated into the boundary conditions, the ice must remain isolated from its environment. Although the turbulent fluxes are small relative to the other energy fluxes, they are not small in comparison with the net energy balance at the surface. A series of experiments to be described in Section 4.3 demonstrates the extent to which these fluxes can influence ice thickness and temperature.

Other conceptual omissions include precise treatment of the downward heat transport from melting snow, the shape of the salinity profile for various ice conditions, and the heat storage by melt ponds. The techniques used to handle the first two problems have been previously discussed. No provision has been included to account for the heat released by freezing of the melt ponds in the autumn. The complete freezing of a 40-cm-deep melt pond releases nearly 3 $kcal/cm^2$. An addition of heat of this magnitude could significantly increase upper level temperatures, decrease bottom accretion, and prolong the period of bottom ablation; the extent of these effects would depend upon the length of time it takes for freezing to occur, along with the area covered by ponds and their depth at the onset of freeze-up.

Finally, it should be stressed that the model cannot predict whether the ice would return once it had vanished. In fact, results for pack ice thinner than 50 cm would probably be inaccurate, since such thin ice is mechanically weak and may show different drift and deformation patterns, along with a loss of horizontal uniformity. In addition, the assumptions regarding salinity and the turbulent fluxes are probably invalid for young, rapidly growing ice.

Although mechanical motions influence the volume of ice contained in the Arctic, they affect ice growth only indirectly. The factors of principal concern are those which directly influence the energy budget (turbulent fluxes, ponds, etc.). The consequences of these latter restrictions are examined in Chapters IV and V.

2.5.2 Physical limitations

The assumption of a constant oceanic heat flux is probably valid for the major part of the year; however the stable, low-salinity layer formed during the summer could considerably reduce F_w. Specifying F_w as a function of time, while retaining the same yearly total, could affect the monthly details of mass changes at the bottom, but it seems improbable that a time-dependent F_w would seriously change the mean ice thickness.

Another limitation arises from the coarseness of the input data. Energy-flux data are given as monthly averages, but integration of the model depends upon specifying these fluxes at daily or hourly intervals. The monthly averages must therefore be broken up into smaller increments by a smoothing process. Consequently the results will reflect the smoothing, and short-term trends or reversals will be absent. Although the model does predict temperature and thickness on a daily or hourly basis, only the monthly values can be accepted with any degree of confidence. The same is true with regard to albedo, although here the boundary condition has been constructed so that albedo values depend upon surface conditions to some degree. These limitations are not inherent in the model, and more detail can be incorporated when the empirical information becomes available.

III. METHODS OF SOLUTION

Solution of the theoretical model discussed in the previous chapter may be attempted by means of an analog computer. Much of the groundwork for such an approach has already been laid (Schwerdtfeger, 1964; U. S. Naval Civil Engineering Lab., 1965), but the expense of designing and constructing such a system has apparently prohibited further work. The alternative is to express the modeling equations in finite-difference form for solution on a high-speed digital computer (IBM 7090/7094). The latter method has been chosen for the present study.

3.1 DIFFUSION EQUATION

Because the heat-conduction equation is parabolic, its solution involves specifying a temperature profile at some initial time, $t = 0$, and values at both boundaries during each succeeding time step. The problem is then to predict future temperature profiles on the basis of this information. Initial-value problems of this sort are traditionally solved by either an explicit or implicit method. Unfortunately, implicit methods are inapplicable here because the equations require moving boundaries.

In choosing a method of solution, the prime consideration must be to minimize computer time, while making accurate approximations. Untersteiner (1964) solved Eq. (5) by employing the standard forward-difference method (Richtmyer, 1957; Forsythe, 1960), which required a time step (Δt) of one hour for a corresponding depth increment (Δz) of 10 cm; 45 minutes of computer (IBM 709) time were required for only one year of integration. The present model is much more complex and it is anticipated that 30 to 50 years of integration will be necessary for the ice to achieve equilibrium. These facts, combined with the need to integrate at least 25 separate cases, imply that the use of the forward-difference method would require an excessive amount of time on this computer.

Since 10 cm was deemed to be the minimum depth resolution necessary for meaningful results, various explicit schemes were studied

and tried, but with little success. Finally, a technique suggested by Sauliev (1957a, 1957b) was found to be a powerful method which combines some of the advantages of both implicit and explicit schemes, but is in fact explicit. Because it is unconditionally stable, the Sauliev method does not restrict the choice of grid spacing and is, in addition, ideally suited to handling nonlinear terms and moving boundaries.

The Sauliev method differs from other explicit methods by expressing the second-order differential in terms of values in two adjacent time levels. The scheme thus appears to be implicit; however the implicit terms are asymmetrically arranged so that, if solution is initiated at a known boundary value, each unknown can be obtained sequentially. Although the Sauliev method was originally designed to solve the one-dimensional diffusion equation, Larkin (1964) has successfully extended it to a two-dimensional case and it has been applied to other equations as well (Holton, 1967).

For the present case, let z and t space be subdivided into J and M subintervals of lengths Δz and Δt, respectively, containing points (z,t). Let us now consider Eq. (6) (neglecting the last term for reasons which will become obvious below). Applying the Sauliev method, Eq. (6) has the finite-difference form (see Fig. 4a):

$$(\rho c)_i \frac{\tilde{T}(z,t+\Delta t)-T(z,t)}{\Delta t} = \frac{k_i}{\Delta z}\left[\frac{T(z+\Delta z,t)-T(z,t)}{\Delta z} - \frac{\tilde{T}(z,t+\Delta t)-\tilde{T}(z-\Delta z,t+\Delta t)}{\Delta z}\right]$$

or

$$\tilde{T}(z,t+\Delta t) = \frac{1-\xi}{1+\xi} T(z,t) + \frac{\xi}{1+\xi}\left[T(z+\Delta z,t) + \tilde{T}(z-\Delta z,t+\Delta t)\right] , \quad (16)$$

where

$$\xi \equiv \frac{k_i \Delta t}{(\rho c)_i \Delta z^2}$$

Equation (16) may be solved only if $\tilde{T}(z-\Delta z,t+\Delta t)$ is known. If $z = 2$, then $T(z-\Delta z,t+\Delta t)$ is a boundary value and $\tilde{T}(2,t+\Delta t)$ may be evaluated, which in turn allows solution of $\tilde{T}(3,t+\Delta t)$ and so forth, as z ascends from 2 to J-1. The effect of a boundary value is thus propagated through the entire matrix at a given time level, which is not the case in other explicit methods. It may be noticed that all values of $\tilde{T}(z,t+\Delta t)$ may be determined from only one set of boundary values; however, equivalent values could have been determined from the other boundary ($z = J$). The formulation of this alternative estimate is completely analogous to (16):

$$\hat{T}(z,t+\Delta t) = \frac{1-\xi}{1+\xi} T(z,t) + \frac{\xi}{1+\xi} [\hat{T}(z+\Delta z,t+\Delta t) + T(z-\Delta z,t)] , \quad (17)$$

where $\hat{T}$ refers to values obtained as z descends from J-1 to 2 (see Fig. 4b). The Sauliev method is unique in that it offers two independent estimates of the temperature at $(z,t+\Delta t)$. This fact offers an opportunity to reduce one of the more serious limitations of the method.

Although it may easily be shown that (16) and (17) are stable regardless of the choice of Δt and Δz, the truncation error associated with the Sauliev method is an order of magnitude greater than with the forward-difference scheme. Taylor Series expansions may be used to determine truncation errors in (16) and (17) (Larkin, 1964). Examination of these expansions show that alternate terms in the two equations are equal and opposite, which immediately suggests the possibility of combining the expansions to reduce the truncation error. If (16) and (17) are averaged, we have:

$$\bar{T}(z,t+\Delta t) \equiv \frac{\tilde{T}(z,t+\Delta t) + \hat{T}(z,t+\Delta t)}{2} = \frac{1-\xi}{1+\xi} T(z,t) +$$

$$\frac{\xi}{2(1+\xi)} [\hat{T}(z+\Delta z,t+\Delta t) + T(z-\Delta z,t) + T(z+\Delta z,t) + \tilde{T}(z-\Delta z,t+\Delta t)] . \quad (18)$$

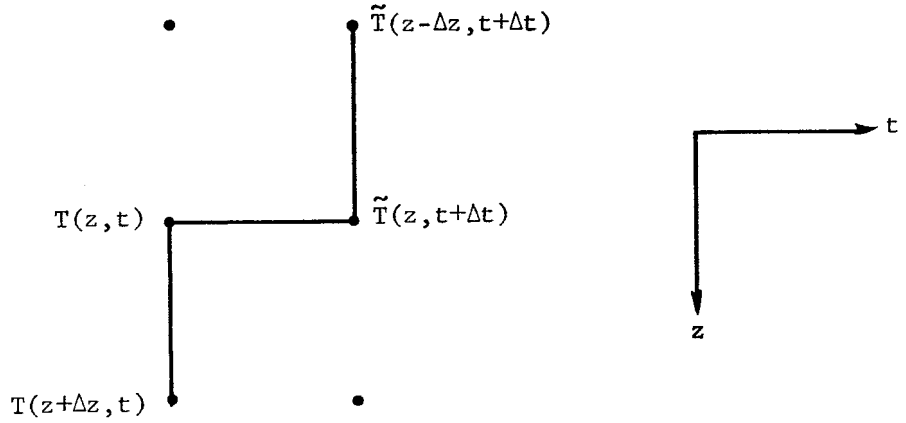

a. Calculation of $\tilde{T}(z,t+\Delta t)$

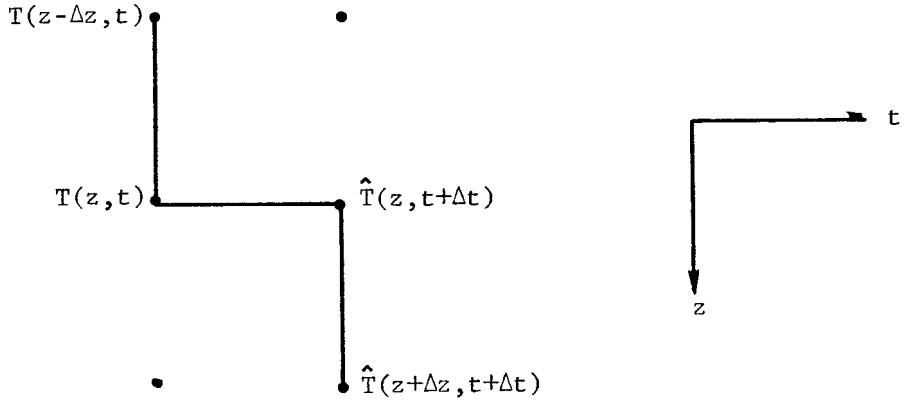

b. Calculation of $\hat{T}(z,t+\Delta t)$

Fig. 4 -- Calculations by the Sauliev Method.

The result of averaging $\hat{T}$ and $\tilde{T}$ is that two of the three largest error terms drop out, leaving a truncation error for $\bar{T}$ roughly proportional to Δt^2; this is comparable to other methods. The increase in accuracy justifies the added computer time necessary to evaluate $\bar{T}(z,t+\Delta t)$.

It is of interest to note that Eq. (18) has the exact form of the well known Crank-Nicholson method (Dingle, 1965). However, $\hat{T}(z+\Delta z,t+\Delta t)$ and $\tilde{T}(z-\Delta z,t+\Delta t)$ do not result from simultaneous solutions; rather they are approximated by the previously discussed methods. Equation (18) is thus an explicit approximation to an implicit scheme.

In dealing with the penetration of short-wave radiation, it is necessary to treat the I_o term in Eq. (6) as a forcing function because of the unique form of the Sauliev equations. Assume that $z = 1$ is the upper surface, and consider the situation at time t if the I_o term were included in (17). Absorption of solar energy would cause $\tilde{T}(2,t+\Delta t)$ to have a value higher than from pure conduction, but $\tilde{T}(2,t+\Delta t)$ is used to determine $\tilde{T}(3,t+\Delta t)$. $\tilde{T}(3,t+\Delta t)$ thus would feel the effect of solar heating at $\tilde{T}(2,t+\Delta t)$, in addition to direct penetration of short-wave radiation to this level. Since no conduction may occur during a particular instant of time, the described situation is opposed to reality and hence $\bar{T}$ must first be evaluated and the I_o term treated as a forcing function:

$$\bar{T}(z,t+\Delta t) = \frac{\tilde{T}(z,t+\Delta t) + \hat{T}(z,t+\Delta t)}{2} + \frac{\kappa_i I_o \Delta t}{(\rho c)_i} \exp(-\kappa_i z) \quad . \tag{19}$$

Equations (3), (4), (16), (17), and (19) are used to calculate temperatures within the ice. If snow is present, $I_o = 0$.

As a test of the Sauliev method, Untersteiner's (1964) experiment was repeated. Equation (6), the simplified form of Eq. (5), was integrated using the boundary values and grid spacing of Untersteiner. The maximum deviation of the results from those obtained by the forward-difference method was less than 0.05°K. This demonstrates the validity, not only of the technique, but also of the assumptions made to obtain (6).

The stability condition for the forward-difference method, $\xi_{max} \leq 1/2$, approximates the criteria for most of the other explicit schemes. Several cases, with various combinations of Δz and Δt, were solved in which ξ_{max} varied from one-half to 600. In all cases the method was stable, but for large values of ξ_{max} the truncation errors became large and the resulting temperature field lost most of its detail. On the basis of these experiments, it appears that truncation errors from the Sauliev method are unimportant if ξ_{max} is less than 8. For the initial test of the model, Δt = 12 hours and Δz = 10 cm ($\xi_{max} \simeq 6$) were chosen. With this choice of grid spacing, a yearly temperature field may be calculated from (6), with about 15 seconds of IBM 7094 computer time and a deviation from the forward-difference method of less than 0.1°K(0.05 percent).

3.2 BOUNDARY EQUATIONS

The balance-of-energy equations, together with the heat-conduction equation, give surface temperatures and mass changes at the boundaries. The greatest difficulty in a numerical solution to these equations is the moving boundaries. The coordinate system is fixed in space, but has two floating grid points located at the boundaries. As the ice grows and shrinks, the slab moves up and down through the grid system. Time and depth increments are constant, except for the space interval next to either boundary, which is some fraction of Δz. The only assumption necessary for this treatment is that the temperature profile is linear within $2\Delta z$ of the surfaces. This assumption is valid at the bottom, where the temperature gradient is nearly linear throughout the year, and likewise at the upper boundary during the ablation season. However the linear assumption must also be made during the first $2\Delta z$ of snow accumulation and this could lead in the model to heat losses slightly greater than reality.

3.2.1 Ice/water interface

The simplest situation exists at the bottom of the ice. Assume that, with some initial temperature profile at time t, the bottom of

the ice lies a distance $\Delta z'$ below the nearest grid point. At time $t + \Delta t$ there will exist a new profile and the bottom will have moved a distance $\Delta\varepsilon$ (see Fig. 5a). If a linear temperature is now assumed to exist between $T(J,t + \Delta t)$ and $\hat{T}(J - 2,t + \Delta t)$, then:

$$T(J-1,t+\Delta t) = T(J,t+\Delta t) + \frac{(\Delta z'+\Delta\varepsilon)}{\Delta z+\Delta z'+\Delta\varepsilon} [\hat{T}(J-2,t+\Delta t) - T(J,t+\Delta t)] \quad . \quad (20)$$

Applying Eq. (17) at $(J-2,t+\Delta t)$:

$$(1+\xi)\hat{T}(J-2,t+\Delta t) = (1-\xi)T(J-2,t) + \xi[T(J-1,t+\Delta t) + T(J-3,t)] \quad . \quad (21)$$

Substituting (20) into (21):

$$\hat{T}(J-2,t+\Delta t) = \frac{\xi\Delta zT(J,t+\Delta t)+(\Delta z+\Delta z'+\Delta\varepsilon)[(1-\xi)T(J-2,t)+\xi T(J-3,t)]}{(1+\xi)\Delta z + \Delta z' + \Delta\varepsilon} \quad . \quad (22)$$

Equation (6), the lower-boundary balance equation, has the finite-difference form:

$$F_w - \frac{k_i[T(J,t+\Delta t) - \hat{T}(J-2,t+\Delta t)]}{\Delta z + \Delta z' + \Delta\varepsilon} = -q_b \frac{\Delta\varepsilon}{\Delta t} \quad . \quad (23)$$

Incorporating (22) into (23) yields:

$$\frac{\Delta\varepsilon}{\Delta t} = -\frac{1}{2}\left[\frac{F_w}{q_b} + \frac{(1+\xi)\Delta z+\Delta z'}{\Delta t}\right] + \left\{\frac{1}{4}\left[\frac{(1+\xi)\Delta z+\Delta z'}{\Delta t} - \frac{F_w}{q_b}\right]^2 + \frac{k_i}{q_b\Delta t}[T(J,t+\Delta t) + (\xi-1)T(J-2,t) - \xi T(J-3,t)]\right\}^{\frac{1}{2}} \quad . \quad (24)$$

The right-hand side of Eq. (24) is written in terms of known quantities and we may now solve for $\Delta\varepsilon$. Knowing $\Delta\varepsilon$, it is then possible to solve for $\hat{T}(J-2,t+\Delta t)$ from (22) and for $T(J-1,t+\Delta t)$ from (20).

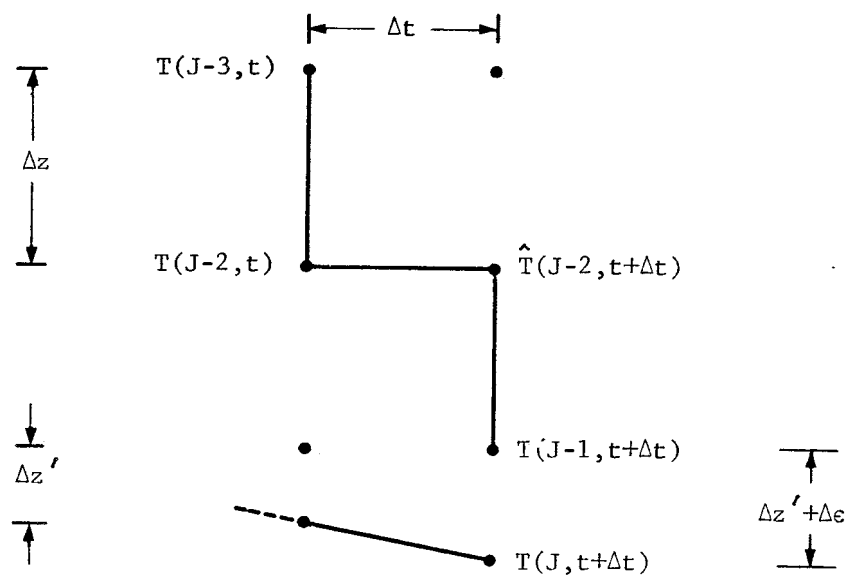

a. At the lower boundary

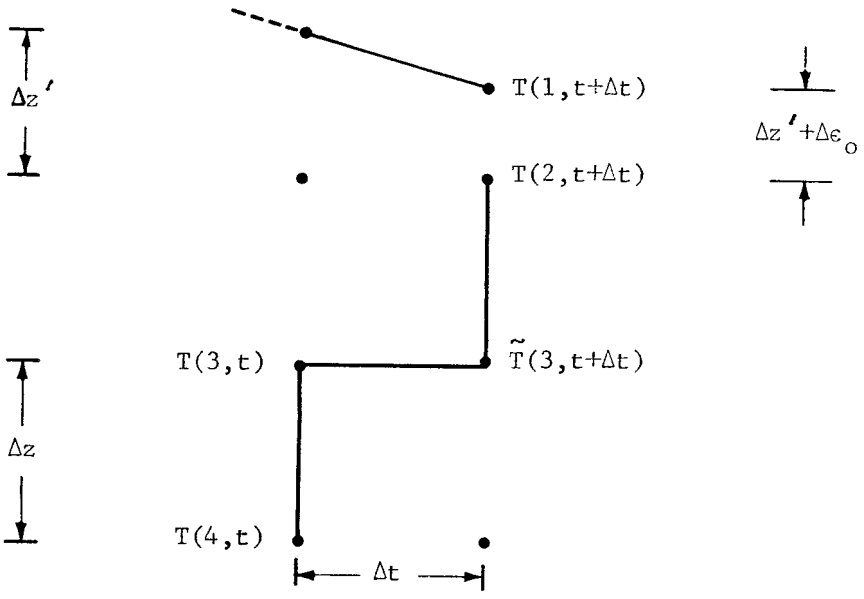

b. At the upper boundary during surface ablation

Fig. 5 -- Geometry of the grid system.

3.2.2 Upper surface

Because of the complexity of the balance equation and the many processes occurring, the solution of temperature and mass changes at the upper boundary offers more difficulties than at the lower. Assume that the upper surface is located at z = 1 and that no ablation or accretion is taking place, i.e., $T(1,t+\Delta t) < 272.9°K$. According to (16):

$$(1+\xi)\ \tilde{T}\ (2,t+\Delta t) = (1-\xi)\ T\ (2,t) + \xi[T(1,t+\Delta t) + T(3,t)]\ . \qquad (25)$$

Combining (25) with the finite-difference form of Eq. (8):

$$\varepsilon_L\ \sigma T(1,t+\Delta t)^4 + \frac{k_o}{(1+\xi)\Delta z}\ T(1,t+\Delta t) - \frac{k_o[(1-\xi)\ T\ (2,t) + \xi T(3,t)]}{(1+\xi)\ \Delta z} +$$

$$I_o - (1-\alpha)\ F_r - F_L - F_s - F_\ell = 0\ . \qquad (26)$$

Equation (26) is a 4th order equation in $T(1,t+\Delta t)$ and is solved by the Newton-Raphson iterative method, a recurrence formula (Hildebrand, 1956).

If the surface temperature, $T(1,t+\Delta t)$, is below the freezing point, Eq. (25) is solved and Eq. (19) is then used to obtain $\bar{T}(z,t+\Delta t)$. If, on the other hand, (26) predicts that the surface temperature is above the freezing point, then melting must occur and the boundary will move. Assuming a linear temperature profile within $2\Delta z$ of the surface and using the same notation as we did for the bottom of the ice (see Fig. 5b), we have:

$$T(2,t+\Delta t) = T(1,t+\Delta t) + \frac{\Delta z' + \Delta\varepsilon_o}{\Delta z+\Delta z'+\Delta\varepsilon_o}\ [\tilde{T}(3,t+\Delta t) - T(1,t+\Delta t)]\ . \qquad (27)$$

Applying (16) at $(3,t+\Delta t)$ and including (27):

$$\tilde{T}(3,t+\Delta t) = \frac{\xi\Delta z T(1,t+\Delta t) + (\Delta z+\Delta z'+\Delta\varepsilon_o)\,[(1-\xi)T(3,t)+\xi T(4,t)]}{(1+\xi)\Delta z = \Delta z' + \Delta\varepsilon_o} . \quad (28)$$

If $\Delta\varepsilon_o \neq 0$, Eqs. (8) and (28) give:

$$\varepsilon_L\sigma T(1,t+\Delta t)^4 + \frac{k_o}{(1+\xi)\Delta z+\Delta z'+\Delta\varepsilon_o}\,[T(1,t+\Delta t) + (\xi-1)T(3,t) - \xi T(4,t)]$$

$$+ I_o - (1-\alpha)\,F_r - F_L - F_s - F_\ell = q_o\,\frac{\Delta\varepsilon_o}{\Delta t} . \quad (29)$$

Solving (29) for $\Delta\varepsilon_o$:

$$\frac{\Delta\varepsilon_o}{\Delta t} = \frac{\varepsilon_L\sigma T(1,t+\Delta t)^4 + I_o - (1-\alpha)F_r - F_L - F_s - F_\ell}{2q_o} - \frac{1}{2\Delta t}\,[(1+\xi)\Delta z + \Delta z'] +$$

$$\left\{\frac{1}{4}\left[\frac{(1+\xi)\Delta z+\Delta z'}{\Delta t} + \frac{\varepsilon_L\sigma T(1,t+\Delta t)^4 + I_o - (1-\alpha)F_r - F_L - F_s - F_\ell}{q_o}\right]+\right.$$

$$\left.\frac{k_o}{q_o\Delta t}\,[T(1,t+\Delta t) + (\xi-1)T(3,t) - \xi T(4,t)]\right\}^{\frac{1}{2}} . \quad (30)$$

Since $\Delta\varepsilon_o \neq 0$, $T(1,t+\Delta t)$ is known to be at the freezing point of the ice or snow. If $\Delta\varepsilon_o$ is positive, then ablation has ceased and $T(1,t+\Delta t)$ is again determined from (26). After the snow has become isothermal, Eq. (30) reduces simply to:

$$\frac{\Delta\varepsilon_o}{\Delta t} = [\varepsilon_L\sigma T(1,t+\Delta t)^4 + I_o - (1-\alpha)F_r - F_L - F_s - F_\ell]/q_o . \quad (31)$$

Simultaneous solution of Eqs. (3), (4), (13), (16), (17), (20), (22), (24), (27), (28), and (30) or (26) allows the complete determination of $\tilde{T}(z,t+\Delta t)$, $\hat{T}(z,t+\Delta t)$ and any mass changes that may be taking place. Finally, $\bar{T}(z,t+\Delta t)$ is calculated from Eq. (19).

Actually, solution of the model is not quite this simple during the snow-accumulation period. If the snow depth is in excess of $2\Delta z$, then Eqs. (27), (28), and (29) may be applied, specifying that $\Delta\varepsilon_o = 0$. If the snow accumulation is less than $2\Delta z$, a linear temperature profile in the entire snow layer must be assumed and the ice/snow boundary condition incorporated into equations analogous to (27), (28), and (29). Because a second order differential cannot be accurately evaluated across dissimilar media, special techniques must be used to find the temperature at the ice/snow interface.[1] Using these methods, calculation of an annual temperature field and the associated thickness changes for 3-meter ice requires only 20 sec of IBM 7094 computer time per year of real time. Subroutine YARIT, a FORTRAN IV description of this integration, is presented in the appendix.

3.3 SMOOTHING THE INPUT ENERGY FLUXES

Since values of the energy fluxes are available only in the form of monthly averages, some method is needed to realistically divide them into increments corresponding to the chosen time steps. An analytic expression describing energy variations with time is the most convenient method. To attain smoothed values, it was assumed that the monthly averages were representative of the 15th day of the month. The monthly values were then divided by the number of time increments in a month and a curve of energy vs. time constructed. The irregularity of the curve precluded any attempt to describe the entire curve; however portions of it were approximated by polynomials. Since any

---

[1] Briefly, $\tilde{T}(z,t+\Delta t)$ is found in the snow and $\hat{T}(z,t+\Delta t)$ in the ice. Temperature at the interface is calculated from (12), which in turn allows us to determine $\tilde{T}(z,t+\Delta t)$ in the ice and $\hat{T}(z,t+\Delta t)$ in the snow. $\bar{T}(z,t+\Delta t)$ is then evaluated from (19).

n + 1 points determine an nth-order polynomial, four points on the curve were used to find a 3rd-order polynomial of the form

$$F(t) = A_1 t^3 + A_2 t^2 + A_3 t + A_4 \ . \tag{32}$$

The term F(t) directly gives the energy flux in a time step Δt, centered around time t. Values for F(t) are calculated only between the two central points on the energy vs. time curve, and smooth trends can be established from month to month. The constants in (32) are reevaluated each month to produce 12 different polynomials. This method has the disadvantage that the monthly sums of the flux increments may deviate from the specified amount by as much as 0.5 percent. Subroutine FLIP accomplishes this smoothing.

3.4 ANALYTIC EXPRESSION FOR ICE SALINITY

As discussed in Section 2.4.3, Schwarzacher's salinity profile may be approximated by an equation of the form:

$$S(z,t) = A + B \sin \left[C \left(\frac{z}{H} \right)^{n/[(\frac{z}{H})+m]} + D \right] . \tag{13}$$

The constants in (13) may be evaluated by imposing the following conditions: the salinity of ice at the boundaries z = 0 and z = H is fixed and has values $S(0,t) = S_o$ and $S(H,t) = S_H$; the slope of the profile is zero at both boundaries; and finally the salinity has values S_1 and S_2 at $z = z_1'$ and $z = z_2'$. Both z_1' and z_2' are some constant fraction of H; i.e., $z_1' = \eta_1 H$ and $z_2' = \eta_2 H$, where η_1 and η_2 are less than unity. Applying these constraints and solving for the constants, Eq. (13) becomes:

$$S(z,t) = \frac{S_o + S_H}{2} + \left(\frac{S_H - S_o}{2} \right) \sin \pi \left[\left(\frac{z}{H} \right)^{n/(\frac{z}{H}+m)} - \frac{1}{2} \right], \tag{33}$$

where

$$m = \left\{ \eta_2 \ell n \eta_1 \ell n \left[\frac{1}{2} + \frac{1}{\pi} \sin^{-1} \left(\frac{2S_2 - S_H - S_o}{S_H - S_o} \right) \right] - \eta_1 \ell n \eta_2 \ell n \left[\frac{1}{2} + \frac{1}{\pi} \sin^{-1} \left(\frac{2S_1 - S_H - S_o}{S_H - S_o} \right) \right] \right\}$$

$$\times \left\{ \eta_2 \ell n \left[\frac{1}{2} + \frac{1}{\pi} \sin^{-1} \left(\frac{2S_1 - S_H - S_o}{S_H - S_o} \right) \right] - \ell n \eta_1 \ell n \left[\frac{1}{2} + \frac{1}{\pi} \sin^{-1} \left(\frac{2S_1 - S_H - S_o}{S_H - S_o} \right) \right] \right\}^{-1}$$

and

$$n = \frac{\eta_1 + m}{\ell n \eta_1} \ell n \left[\frac{1}{2} + \frac{1}{\pi} \sin^{-1} \left(\frac{2S_1 - S_H - S_o}{S_H - S_o} \right) \right] .$$

How well (33) fits the observed profile depends upon the choice of η_1 and η_2. In the present case, $\eta_1 = 0.3$ and $\eta_2 = 0.6$ produced the best fit. Using these values, the maximum deviation of (13) from Schwarzacher's profile was less than 5 percent. Subroutine SALPR calculates the salinity profile in the program.

IV. RESULTS OF SELECTED INTEGRATIONS

Arbitrary initial conditions of temperature and ice thickness are imposed upon the equations, and integration proceeds until equilibrium is reached, that is, by our definition, when the annual bottom accretion is within 1 millimeter of the surface ice ablation. Steady-state solutions are generally reached after 30 to 100 years. Although there is a continuing output of data during the integration, usually only the steady-state annual patterns of temperature and thickness will be shown in the text. The isotherms are calculated by a contour plotting subroutine, and the temperature field is graphed by a Calcomp plotter. Each graph is accompanied by a table containing monthly averages and totals of various pertinent results.

4.1 INITIAL TESTS OF THE MODEL

To check the validity of the model and the numerical approximations employed, the best available estimates of the present energy fluxes were applied to the model. Assuming that arctic pack ice is in near-equilibrium, predictions of ice thickness and temperatures from this test were compared with Soviet and American observations. Investigations of response time and salinity effects were then conducted.

4.1.1 Heat budget of Fletcher

With the heat budget suggested by Fletcher (Table 1), with the other input data discussed in Chapter II, and with an initial thickness of 340 cm, equilibrium was reached after 38 years. Figure 6 illustrates the steady-state temperature and thickness patterns for this case. In Fig. 6, and all the similar plots that follow, time is graphed along the abscissa and thickness along the ordinate. The media (air, ice, and water) are distinguished by shading. Boundaries of the ice/snow slab appear as heavy black lines and isopleths of temperature as thin solid curves. The isotherms in the ice are labeled in negative degrees Celsius; isotherms in the snow (not labeled) are

drawn at 2°C intervals. Because hydrostatic adjustment of the ice has been removed from the equations, the upper and lower boundaries move independently of one another. Thus, instead of the upper boundary occupying a nearly constant level and the lower surface showing large changes in depth, the slab migrates downward with time. The advantage is that mass changes at each boundary are separately indicated, but it must be remembered that the depth indicated on the ordinate does not necessarily refer to ice thickness. Table 2 gives monthly and yearly values of ice thickness, surface temperatures, net radiative fluxes, and the conductive fluxes at both boundaries; also included in the table are values of the annual mass changes and associated dates.

From Table 2 and Fig. 6, it may be seen that the model predicts an average equilibrium thickness of 288 cm, with a maximum of 314 cm and a minimum of 271 cm. It is difficult to assess how representative these values are. Early submarine data (Lyon, 1961) indicate an average thickness of 4 to 5 meters, but this includes pressure ridges and may be biased by the location of the submarine's track. Later submarine observations (Wittmann and Schule, 1966) show 2 meters to be the most frequent ice thickness, but again, these data are regionally limited. Most of the drifting stations were established on pack ice, which averaged close to 3 meters in thickness (Petrov, 1954). Typical results are those of Untersteiner (1961) who found that thickness varied between 315 and 250 cm during the year. Considering that the input data are derived from these drifting stations, it is to be expected that the predicted thicknesses should agree most closely with their observations.

Perhaps more indicative is the pattern of mass changes predicted by the model. According to Soviet data (Yanes, 1966), average ablation on polar ice is 37 cm; snow melt begins in the first half of June and ablation generally ends between 10 and 23 August. An average from all U. S. drifting stations from 1957 to 1963 gives a surface ablation of 42 cm (Hanson, 1965). Table 2 shows a predicted ice ablation of 40 cm, starting on 29 June and terminating on 19 August. Snow melt begins on 8 June. All these features correspond closely with observations.

At the lower surface there are 45 cm of accretion and 5 cm of ablation. Unfortunately, mass changes at the bottom have never been well determined in the field. Yanes (op. cit.) feels that bottom ablation in equilibrium ice is small, if it occurs at all. Hanson (1965) measured a value of 10 cm, and Untersteiner (1961) observed 20 cm of ablation and 50 cm of accretion. In view of these uncertainties, the predicted values are not unreasonable, but lack of empirical data makes it impossible to evaluate the timing of these changes accurately.

Temperature profiles provide another basis for evaluating the theoretical results. An observed temperature field (Untersteiner, 1961) is reproduced in Fig. 7. Comparison of Figs. 6 and 7 shows good agreement throughout, except for fall temperatures within the ice. Smoothing of the input data is reflected in the results of Fig. 6 and the usual January warming trend (Laktionov, 1955; Hisdal, 1960) does not appear. Figure 7 suggests that ice temperatures in the theoretical model respond to surface conditions more rapidly than do the temperatures in real ice. Neglecting latent-heat release from surface melt ponds, underestimating I_o, specifying linear heat loss through the snow layer, or improper assumptions regarding the salinity profile could all contribute to this discrepancy.

Table 3 shows monthly surface temperatures from numerous drifting stations, averaged over 26 years of observations (A. Hanson, personal communication), and a comparison with the theoretical results. The annual averages are remarkably close, but temperatures predicted by the model are slightly colder in the fall and warmer in the spring than the observed ones. It should be remembered that the calculated temperatures apply for the surface and a comparison with observed air (screen) temperatures would have to take into account that, generally, a ground inversion prevails from September to April, whereas in May lapse conditions prevail. We suspect that the differences shown in Table 3 are more or less accidental, as some are positive and some are negative.

The net radiative fluxes calculated by the model also agree favorably with observations. According to Marshunova (1961) and Fletcher (1965), the net short-wave radiation ranges from 18.6 kcal/cm^2 year

Table 2. COMPUTED VALUES FOR EQUILIBRIUM CONDITIONS

Symbol	Variable	Jan	Feb	Mar	Apr
$T_{s,o}$	Mean snow surface temperature (^{o}C)	-30.98	-33.12	-31.85	-22.46
$T_{i,o}$	Mean ice surface temperature (^{o}C)	-17.95	-19.04	-19.18	-15.84
$\bar{H}$	Mean ice thickness (cm)	281.7	289.0	296.6	304.1
$F_{c,o}$	Heat flux through surface ($kcal/cm^2$)	0.781	0.823	0.716	0.355
$F_{c,h+H}$	Heat flux through bottom ($kcal/cm^2$)	-0.580	-0.605	-0.623	-0.574
$(1-\alpha)F_r$	Net short-wave radiation ($kcal/cm^2$)	0	0	0.406	1.893
$F_L-\sigma T_o^4$	Net long-wave radiation ($kcal/cm^2$)	-1.967	-1.562	-1.814	-2.451

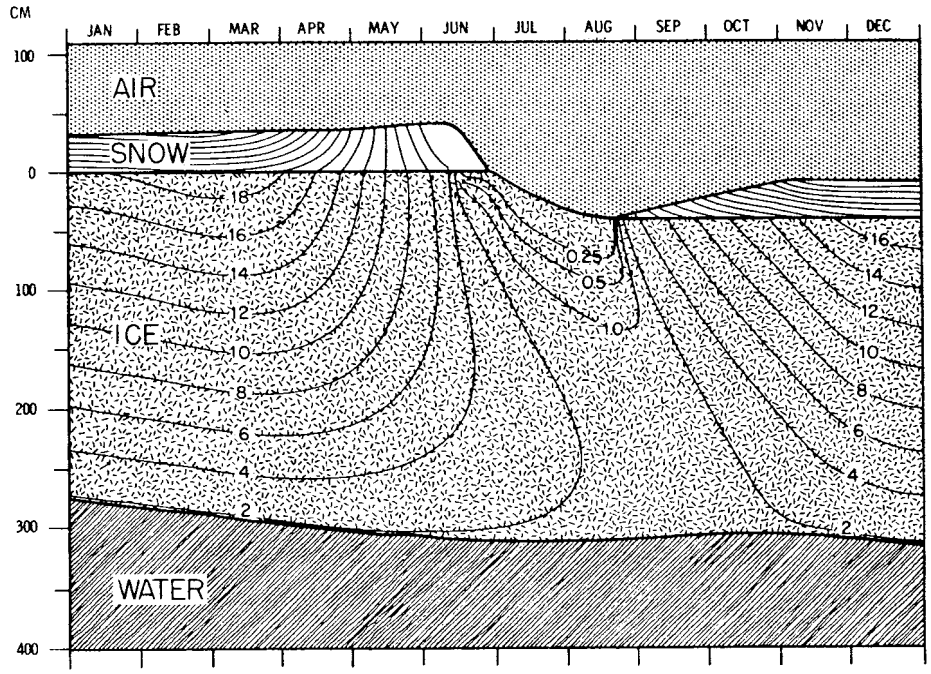

Fig. 6 -- Annual equilibrium temperature and thickness field for Case 1, Fletcher's heat budget.

IN CASE 1, FLETCHER'S HEAT BUDGET (SEE TABLE 1).

May	Jun	Jul	Aug	Sep	Oct	Nov	Dec	Year
-9.44	-0.33	-0.10	-1.12	-10.04	-20.37	-28.74	-30.28	-18.24
-9.71	-2.31	-0.10	-0.85	-6.24	-10.70	-14.84	-17.16	-11.16
310.3	314.0	296.1	278.1	272.8	270.8	270.7	275.0	288.3
-0.022	-0.119	-0.042	0.247	0.663	0.781	0.884	0.807	5.874
-0.448	-0.290	-0.135	-0.036	0.004	-0.015	-0.257	-0.510	-4.069
3.129	4.395	4.959	2.710	0.605	0.085	0	0	18.181
-2.200	-1.935	-0.903	-0.984	-0.712	-0.781	-1.438	-1.592	-18.339

Date	Onset	End
8 June	Snow ablation	
29 June	Ice ablation	
17 July		Bottom accretion
19 August		Surface ice ablation
4 November	Bottom accretion	

Other Data

Surface ice ablation*	40.1 cm
Bottom ablation	5.1 cm
Bottom accretion	45.2 cm
Short-wave radiation penetrating surface during snow-free period	1.291 kcal/cm^2

*Equals net bottom accretion.

Table 3. COMPARISON OF OBSERVED AND CALCULATED SURFACE TEMPERATURES (-°C) FOR SEA ICE OF EQUILIBRIUM THICKNESS.

Source	Jan	Feb	Mar	Apr	May	Jun	Jul	Aug	Sep	Oct	Nov	Dec	Year
Observed (screen height)	32.6	33.9	31.9	25.4	11.8	2.1	0.1	1.6	8.8	18.0	26.3	30.8	18.6
Calculated (surface)	31.0	33.1	31.9	22.5	9.4	0.3	0.1	1.1	10.0	20.4	28.7	30.2	18.2

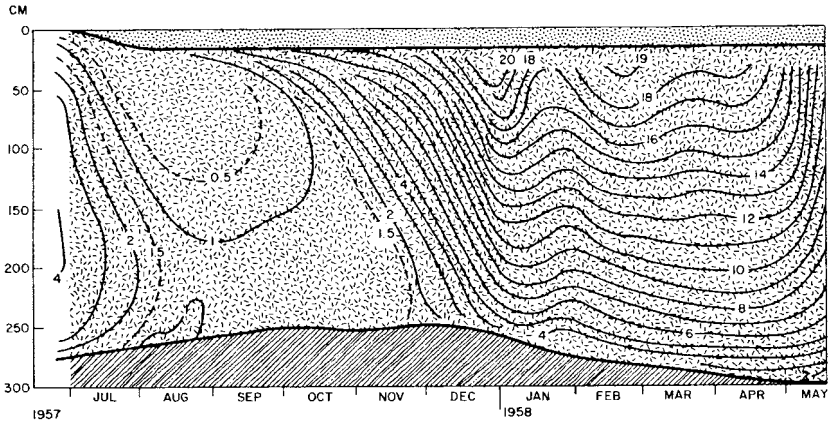

Fig. 7 -- Observed temperature of perennial ice at IGY Station Alpha, 1957-1958 (after Untersteiner, 1961).

at 75°N to 16.9 at 90°N, while net long-wave radiation ranges from -21 to -19.4 kcal/cm^2 year. Solar radiation absorbed by the surface in the model agrees closely with empirical data, implying that the albedo assumptions were adequate; however, the long-wave loss is smaller than observations indicate, primarily during the winter months. This smaller loss appears to arise from two causes. First, the model deals only with thick ice covered with a uniform blanket of snow; observations in the field are made over ice with variable thickness and snow cover. Second, necessary smoothing of the input functions removes short-term fluctuations in the surface temperature. Because of the nonlinear form of the Stefan-Boltzmann Law, this produces a bias toward lower surface temperatures and hence a smaller long-wave loss.

In a state of equilibrium, the sum of all energy fluxes into the ice should balance the sum of those leaving it. The results in Table 2 show that about 0.5 kcal/cm^2 year more energy leaves the slab than enters it. However, there are three energy sources which are not seen explicitly in the output data:

(a) Short-wave radiation that penetrates the ice and is not absorbed, passing instead through the ice and into the ocean. This flux is small for thick ice (25 cal/cm^2 year in the present case), but for thin ice it may reach values in excess of 25 percent of I_o.

(b) Latent heat released within the ice. As sea water freezes at the bottom of the ice, small pockets of brine are trapped. Continued accretion moves the older ice upward into regions of lower temperature, causing freezing in the brine pockets and a reduction in brine volume. The resulting heat release is accounted for by changes in $(\rho c)_i$ [see Eq. (3)].

(c) When the snow is saturated with melt water and is isothermal, no heat flows toward the surface. The ice/snow interface, however, remains at the freezing point, causing a large conductive flux into the ice. The sudden introduction of this flux is responsible for the step seen in the -1.0, -0.5, and -0.25 isotherms during June (Fig. 6).

When the effects of these energy sources are included, the energy balance for the entire slab presumably becomes zero and there is no contradiction.

Despite the many uncertainties in the input data, the picture presented by the model is surprisingly consistent with field observations. Thus the model and the various approximations appear to be valid and lend confidence to the model's application to other possible situations. To facilitate reference, all cases computed, and their characteristic difference for input data from Case 1, are listed in Table 29 on p. 130.

4.1.2 Response time

A study of the nonequilibrium behavior of sea ice offers insight into the nature of ice growth. To determine the response of ice thickness to a change of the external forcing, we assume that the ice is initially at equilibrium under the "standard" conditions of Case 1. A step change in F_w from 1.5 to 4.5 kcal/cm^2 year is then imposed. The thickness on 1 January for each succeeding year is graphed in Fig. 8. The exponential shape of this curve is typical of the manner in which both temperature and thickness approach equilibrium and is independent of the specified boundary conditions. The curve resembles that for the discharge rate of a simple capacitor. This similarity suggests that temperature and thickness response might be simulated by a relatively simple electrical analogy; for a given capacitor, the size of the initial charge would correspond to the deviation of temperature or thickness from equilibrium values. If this capacitor analogy is valid, the response time (period from change of input to achievement of equilibrium) of sea ice would be independent of the initial thickness. To check this, the experiment was repeated starting from initial thicknesses that differed by 10 to 400 cm from the equilibrium value. Results are shown in Fig. 9. There is little variation in response time between large deviations. However, when the initial thicknesses are close to the equilibrium value, there is a rapid variation in response time and the capacitor analogy breaks down. Although a

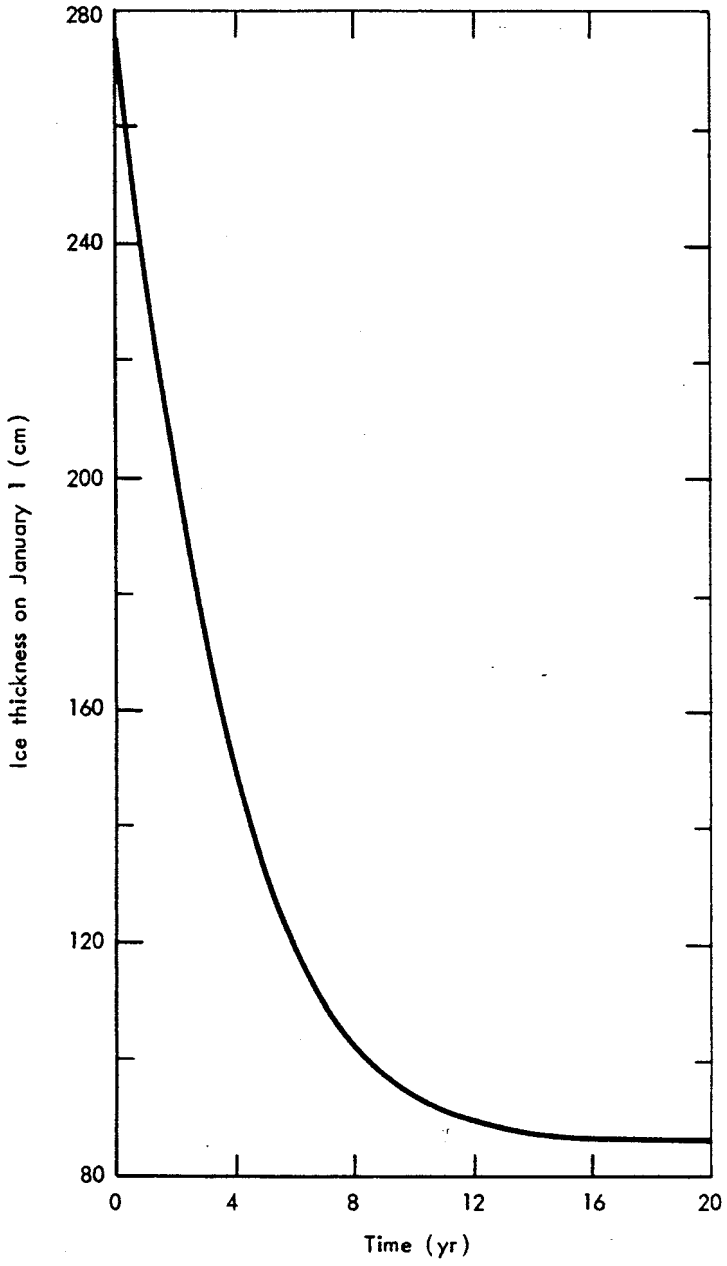

Fig. 8 -- Response time of sea ice as it approaches equilibrium after a step change in F_w from 1.5 to 4.5 kcal/cm^2 year.

comprehensive series of tests was not run for cases with greater equilibrium thicknesses, various isolated cases indicate that, as equilibrium thickness increases, the region of rapid variation in response time becomes smaller.

Despite the limited dependence on initial thickness, response time is determined primarily by the equilibrium thickness. As thickness increases, the ice responds more and more sluggishly to surface conditions. Mass and temperature changes at the upper boundary are not greatly influenced by temperature gradients within the ice and snow, but mass changes at the bottom are directly determined by the magnitude of these gradients. Therefore, even though surface ablation rapidly achieves a constant value, net bottom accretion continues to change slowly. It is clear from these considerations that the response time must increase with equilibrium thickness.

These results show that the response time is asymmetric. For example, when F_w is increased from 1.5 to 4.5 kcal/cm^2 year, the response time is about 20 years; if the ice is at equilibrium for an F_w of 4.5 kcal/cm^2 year and F_w is decreased to 1.5 kcal/cm^2 year, the response time is 44 years. An anomalous year will produce nonequilibrium conditions of several years duration, because of the exponential shape of the growth curve. Because response time is principally determined by the final thickness, the magnitude of the anomaly plays only a small part in determining the duration of the nonequilibrium conditions.

4.1.3 Effects of ice salinity

The salinity profile used in the model (Fig. 3) is probably characteristic of summer conditions only. However, it was assumed that any deviations from the profile were relatively unimportant during the winter when the thermal constants of the ice are nearly independent of salinity. In an attempt to verify this assumption and to define more precisely the effects of ice salinity, we have assumed in Case 2 that the salinity has a value of 0.09°/$_{oo}$ and is constant throughout the slab. Figure 10 shows the steady-state temperature

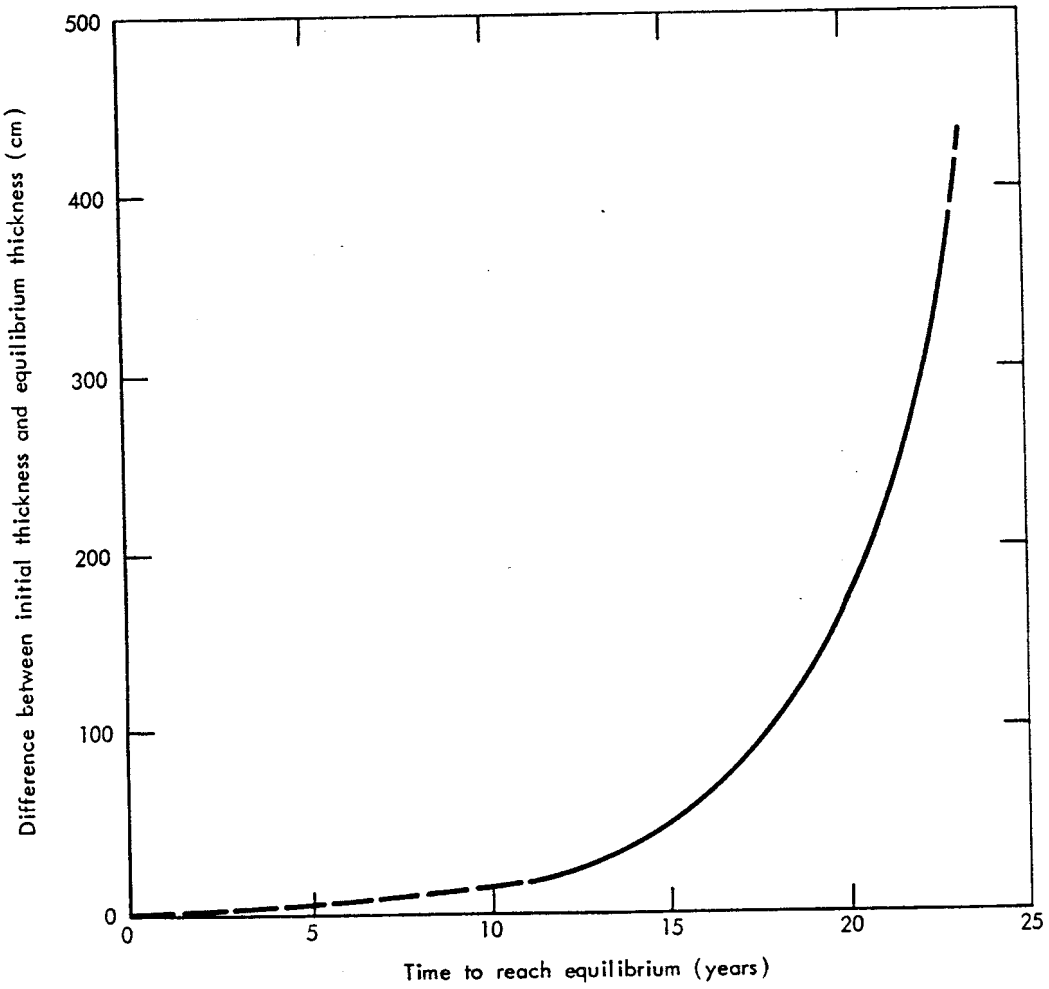

Fig. 9 -- Response time of sea ice as a function of the deviation of the initial thickness from equilibrium thickness, F_w = 4.5 kcal/cm^2 year.

Table 4. COMPUTED VALUES FOR EQUILIBRIUM CONDITIONS IN CASE 2,

Variable	Jan	Feb	Mar	Apr	May
Mean snow surface temperature (^{o}C)	-31.17	-33.30	-32.02	-22.60	-9.51
Mean ice surface temperature (^{o}C)	-18.80	-19.82	-19.95	-16.52	-10.10
Mean ice thickness (cm)	306.1	313.7	321.5	329.1	334.9
Heat flux through surface (kcal/cm^2)	0.742	0.788	0.682	0.325	-0.039
Heat flux through bottom (kcal/cm^2)	-0.666	-0.680	-0.692	-0.629	-0.454
Net short-wave radiation (kcal/cm^2)	0	0	0.406	1.893	3.129
Net long-wave radiation (kcal/cm^2)	-1.927	-1.526	-1.780	-2.420	-2.183

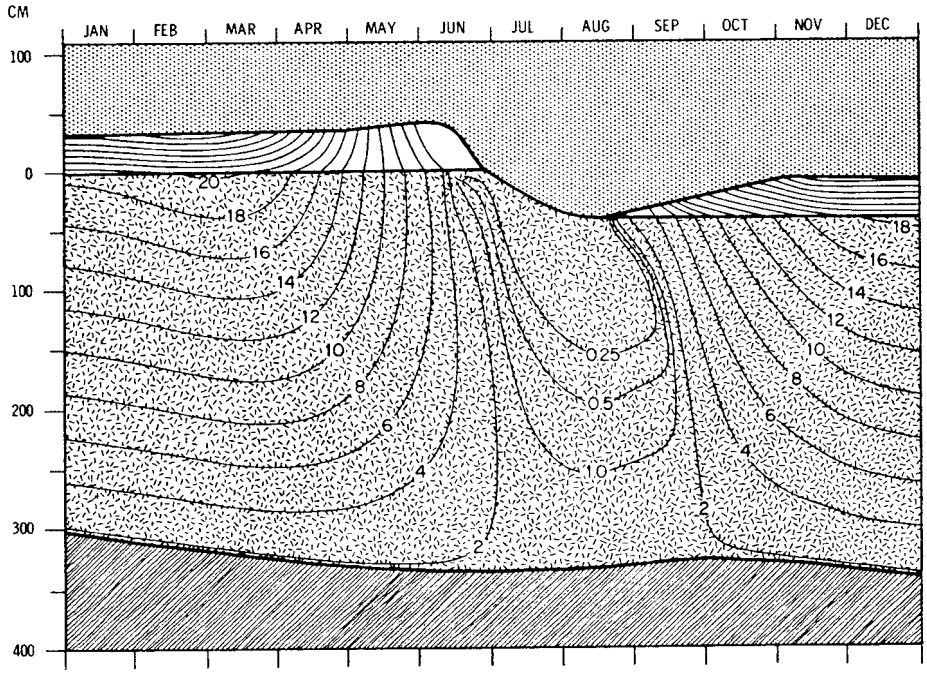

Fig. 10 -- Annual equilibrium temperature and thickness field for Case 2, constant salinity (0.09 °/$_{oo}$), F_w = 1.5 kcal/cm^2 year.

CONSTANT SALINITY (0.09 °/oo). ALL OTHER INPUT DATA AS IN CASE 1.

Jun	Jul	Aug	Sep	Oct	Nov	Dec	Year
-0.34	-0.10	-0.93	-9.62	-20.62	-29.06	-30.53	-18.32
-2.32	-0.10	-0.59	-5.35	-11.73	-16.21	-18.22	-11.64
337.8	317.3	294.7	289.1	288.4	292.3	298.8	310.3
-0.115	0.011	0.331	0.775	0.722	0.818	0.756	5.795
-0.212	0.051	0.127	0.082	-0.265	-0.515	-0.639	-4.491
4.395	4.959	2.710	0.605	0.085	0	0	18.181
-1.934	-0.903	-1.037	-0.825	-0.722	-1.372	-1.541	-18.170

Date	Onset	End
8 June	Snow ablation	
24 June		Bottom accretion
28 June	Ice ablation	
20 August		Surface ice ablation
4 October	Bottom accretion	

Other Data

Surface ice ablation*	41.5 cm
Bottom ablation	8.8 cm
Bottom accretion	50.3 cm
Short-wave radiation penetrating surface during snow-free period	1.291 kcal/cm^2

*Equals net bottom accretion.

and thickness patterns. Comparing these results with those from Case 1, we see that ice thickness is greater by 20 to 25 cm the year around, and that ice temperatures are 1 to 2°C lower during fall and winter. The greatest difference occurs, as expected, during the summer. Because of the negligible brine volume, summer heating (see -1°C isotherm) penetrates to much greater depths. The steepness of the -2°C isotherm shows that the entire slab responds rapidly to temperature changes at the surface.

The temperature pattern in Case 2 shows the extent to which the brine pockets store heat in the summer and retard heat transport between the boundaries. Reduction of salinity near the bottom of the ice allows heat to be more efficiently conducted upward into the ice and thus increases bottom accretion. At the same time, the larger conductive heat fluxes also cause slightly greater ice ablation at both boundaries. In this case, the increased bottom accretion is the dominant effect, producing the predicted thickening.

Case 3 is similar to Case 2, except that F_w was increased to 4.5 kcal/cm^2 year. Figure 11 and Table 5 give the results of the integration. Comparison of Cases 3 and 1 confirms the conclusions reached in Case 2 and also shows that the thickness of the ice does not appreciably change the effects of salinity.

The model may also be used to compare the growth of ice in fresh water and sea water. In Case 4, we have again assumed that the salinity is a constant 0.09°/$_{oo}$ and that the ice temperature at the lower boundary is -0.1°C; i.e., the slab is floating in essentially fresh water. All independent energy fluxes are the same as in Case 1. Results are presented in Fig. 12 and Table 6. The average equilibrium thickness is 348 cm, 60 cm greater than Case 1 and 40 cm greater than Case 2. The major difference between Cases 2 and 4 is the 50 percent less bottom ablation of Case 4. This is the result of the steeper temperature gradients near the bottom from September through March in Case 2 and is responsible for the predicted thickness increase. Although the assumption regarding heat flux in the water is certainly not characteristic of a fresh water body, Case 4 points out the main difference between the growth of sea ice and perennial lake ice; fresh

ice cannot store large amounts of heat and instead transfers it rapidly between the boundaries. Consequently, under similar conditions, fresh ice grows more rapidly and to a greater equilibrium thickness than does sea ice.

The results of Cases 2 to 4 indicate that the ice salinity has little influence on ice thickness but markedly influences summer temperature profiles. Therefore, since the winter temperature differences between Cases 1 and 2 appear to result solely from the slight thickness change, it may be assumed that reasonable ice temperatures can be obtained from the model knowing only the summer salinity profile.

4.1.4 Heat budget of Vowinckel and Orvig

An obvious application of the sea-ice model lies in its ability to evaluate the internal consistency of a given energy budget. We have seen in Section 4.1.1 that Fletcher's (1965) heat budget produces results in good agreement with observations; however, it seems likely that other combinations of input functions could produce equally acceptable results. A heat budget markedly different from that of Fletcher was presented by Vowinckel and Orvig (1966, 1967). Their values for F_L, F_r, F_S, F_ℓ, net short-wave radiation, and implied albedos are reproduced in Table 7. Their surface energy balance was determined according to the following equation (using our notation):

$$(1 - \alpha)F_r + F_L - \varepsilon_L \sigma T_o^4 + F_S + F_\ell + 0 = 0 \ , \qquad (34)$$

where 0 is the "heat exchange with deeper layers of the ocean." Obviously 0 is a residual term; it appears to include the effects of oceanic heat flux, penetration of short-wave radiation, heat conduction to the surface, surface ablation, and mass changes at the bottom of the ice. According to Vowinckel and Orvig, the annual sum of 0 (5.93 kcal/cm^2 year) corresponds to the oceanic heat flux (F_w), if the ice is in equilibrium. This is not strictly true because the energy lost at the surface through snow melt is not regained at the

Table 5. COMPUTED VALUES FOR EQUILIBRIUM CONDITIONS IN CASE 3, CONSTANT SALINITY

Variable	Jan	Feb	Mar	Apr	May
Mean snow surface temperature (^{o}C)	-29.31	-31.46	-30.26	-21.18	-8.66
Mean ice surface temperature (^{o}C)	-10.56	-11.65	-11.90	-9.38	-4.97
Mean ice thickness (cm)	100.0	110.0	119.9	127.7	130.3
Heat flux through surface (kcal/cm^2)	1.123	1.156	1.040	0.644	0.183
Heat flux through bottom (kcal/cm^2)	-1.085	-1.106	-1.054	-0.777	-0.350
Net short-wave radiation (kcal/cm^2)	0	0	0.406	1.893	3.129
Net long-wave radiation (kcal/cm^2)	-2.309	-1.895	-2.138	-2.740	-2.406

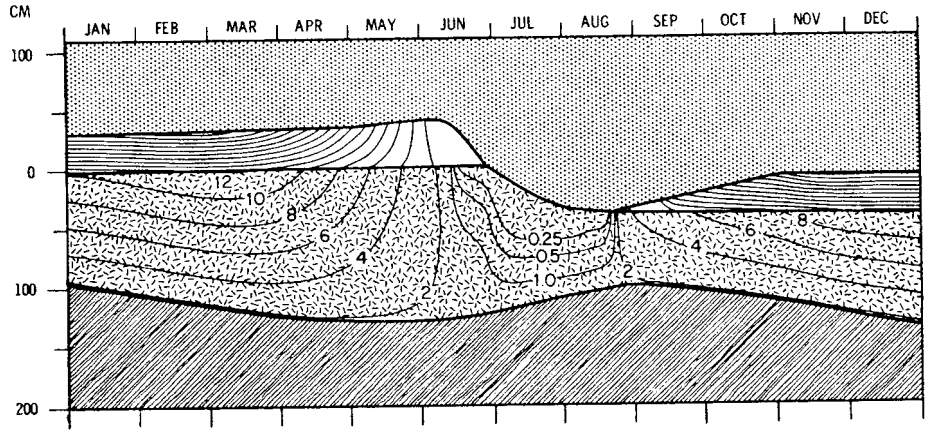

Fig. 11 -- Annual equilibrium temperature and thickness field for Case 3, constant salinity (0.09 °/$_{oo}$), F_w = 4.5 kcal/cm^2 year.

(0.09 °/oo), F_w = 4.5 kcal/cm^2 year. ALL OTHER INPUT DATA AS IN CASE 1.

Jun	Jul	Aug	Sep	Oct	Nov	Dec	Year
-0.23	-0.10	-1.36	-9.75	-19.47	-27.40	-28.63	-17.32
-0.84	-0.10	-1.16	-5.39	-7.19	-8.94	-9.92	-6.83
126.7	96.4	70.3	63.7	70.2	79.3	89.9	98.7
-0.046	0	0.116	0.737	0.990	1.169	1.149	8.262
0.064	0.417	0.252	-0.688	-0.949	-1.112	-1.125	-7.512
4.507	4.959	2.710	0.605	0.085	0	0	18.293
-1.966	-0.903	-0.916	-0.787	-0.989	-1.722	-1.934	-20.705

Date	Onset	End
13 May		Bottom accretion
6 June	Snow ablation	
27 June	Ice ablation	
17 August		Surface ice ablation
27 August	Bottom accretion	

Other Data

Surface ice ablation*	41.8 cm
Bottom ablation	26.7 cm
Bottom accretion	68.5 cm
Short-wave radiation penetrating surface during snow-free period	1.326 kcal/cm^2

*Equals net bottom accretion.

Table 6. COMPUTED VALUES FOR EQUILIBRIUM CONDITIONS IN CASE 4, CONSTANT SALINITY

Variable	Jan	Feb	Mar	Apr	May
Mean snow surface temperature (^{o}C)	-31.16	-33.31	-32.04	-22.62	-9.51
Mean ice surface temperature (^{o}C)	-18.75	-19.87	-20.05	-16.62	-10.14
Mean ice thickness (cm)	343.3	350.4	357.8	365.1	371.1
Heat flux through surface (kcal/cm^2)	0.744	0.785	0.678	0.321	-0.041
Heat flux through bottom (kcal/cm^2)	-0.623	-0.647	-0.665	-0.623	-0.478
Net short-wave radiation (kcal/cm^2)	0	0	0.406	1.893	3.129
Net long-wave radiation (kcal/cm^2)	-1.930	-1.524	-1.775	-2.416	-2.181

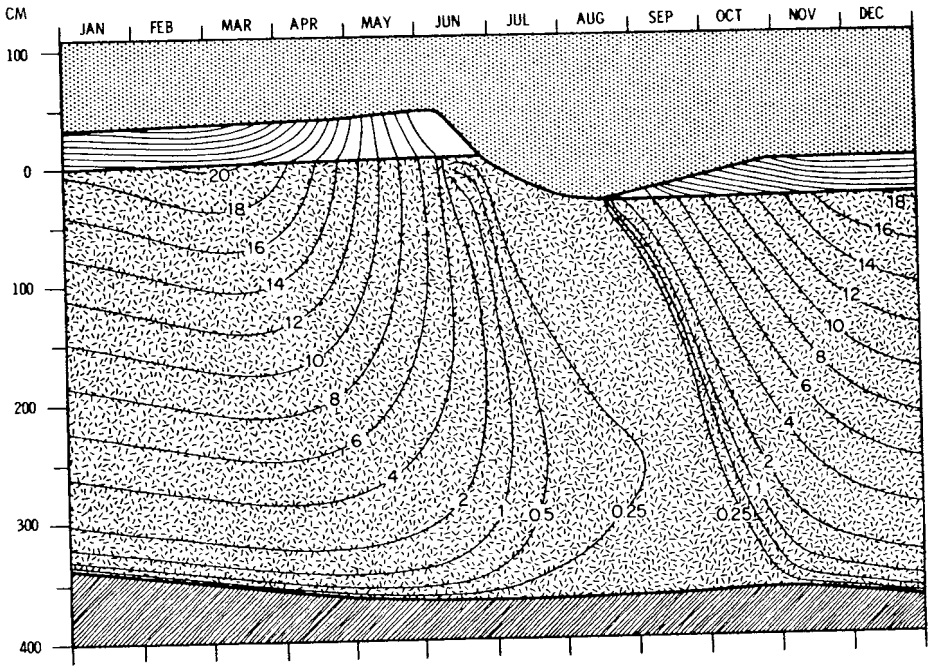

Fig. 12 -- Annual equilibrium temperature and thickness field for Case 4, constant salinity (0.09 °/$_{oo}$), F_w = 1.5 kcal/cm^2 year, bottom temperature = 0.1^{o}C.

(0.09 °/oo), BOTTOM TEMPERATURE = -0.1 °C. ALL OTHER INPUT DATA AS IN CASE 1.

Jun	Jul	Aug	Sep	Oct	Nov	Dec	Year
-0.33	-0.10	-0.93	-9.45	-20.30	-28.87	-30.45	-18.26
-2.30	-0.10	-0.58	-4.87	-10.49	-15.38	-17.91	-11.42
374.6	355.7	335.5	331.9	330.6	331.4	336.6	348.6
-0.113	0.013	0.332	0.820	0.797	0.858	0.771	5.965
-0.285	-0.106	-0.045	-0.029	-0.033	-0.379	-0.577	-4.491
4.396	4.959	2.710	0.605	0.085	0	0	18.182
-1.934	-0.903	-1.038	-0.870	-0.797	-1.413	-1.556	-18.338

Date	Onset	End
8 June	Snow ablation	
28 June	Ice ablation	
9 July		Bottom accretion
20 August		Surface ice ablation
29 October	Bottom accretion	

Other Data

Surface ice ablation*	41.5 cm
Bottom ablation	4.1 cm
Bottom accretion	45.6 cm
Short-wave radiation penetrating surface during snow-free period	1.291 kcal/cm^2

*Equals net bottom accretion.

underside of the ice. Thus their value for F_w is closer to 6.6 kcal/cm^2 year. As will be seen in Section 4.2.2, an F_w of this magnitude causes the ice to vanish. To test the heat budget of Vowinckel and Orvig it was therefore necessary to assume a smaller value for F_w. Likewise, it is not possible to estimate from their data how much short-wave radiation penetrates to deeper layers of the ice. In the following case, F_w and I_o were assumed to be as in Case 1 (F_w = 1.5 kcal/cm^2 year, I_o = 17 percent.

With these values, and the surface heat budget of Vowinckel and Orvig, the model predicts 115 cm of surface-ice ablation and complete melting of ice during the fifth summer. Comparison of Tables 1 and 7 shows that Vowinckel and Orvig assume albedos that are up to 20 percent lower than Marshunova's; consequently, the net short-wave radiation is 12 kcal/cm^2 year larger. Even increasing I_o to an unrealistically large 50 percent would result in 60 to 70 cm of surface-ice ablation and an equilibrium thickness of roughly 1.0 to 1.5 meters.

The greatest discrepancy between Fletcher's budget and that of Vowinckel and Orvig is in the amount of absorbed short-wave radiation. As is pointed out in Section 2.4.5, the average heat exchange over a large area cannot be used to determine ice growth. If albedos representative of the ice and snow alone are substituted, Vowinckel and Orvig's heat budget should be applicable to the present sea-ice model. We therefore repeated the experiment using the albedos suggested by Marshunova (Table 1) and the incoming energy fluxes (F_L, F_r, F_s, F_ℓ) given in Table 7. The results of this case (6) are shown in Table 8. Case 6 was integrated for a 40-year period, during which the ice grew to 540 cm. Although the ice has not strictly achieved equilibrium, the initial 1.5 cm difference between surface ablation and net bottom accretion would cause the ice to grow only another 20 cm during the subsequent 60 years (see Section 4.1.3). The calculated energy fluxes and temperatures would not be changed significantly.

The differences between Case 6 and Case 1 are the result of markedly different assumptions regarding the turbulent fluxes and incoming

Table 7. AVERAGE MONTHLY VALUES FOR THE INPUT DATA AT THE UPPER BOUNDARY ACCORDING TO VOWINCKEL AND ORVIG (1966, 1967).

Input	Jan	Feb	Mar	Apr	May	Jun	Jul	Aug	Sep	Oct	Nov	Dec	Year
Incoming short-wave radiation ($kcal/cm^2$)	0	0	1.8	8.6	15.9	16.9	13.4	8.4	2.6	0.2	0	0	67.8
Net short-wave radiation ($kcal/cm^2$)	0	0	0.6	2.3	5.6	7.7	7.7	4.6	1.2	0.06	0	0	29.7
Implied surface albedo	...	...	0.67	0.73	0.65	0.54	0.43	0.46	0.54	0.63	...	...	...
Incoming long-wave radiation ($kcal/cm^2$)	10.1	9.0	9.7	11.0	15.1	17.2	19.2	18.8	16.4	14.5	11.1	10.4	162.4
Flux of sensible heat ($kcal/cm^2$)	0.12	0.06	0.06	-0.90	-1.00	-0.65	0.04	-0.56	-1.00	0	0.06	0.06	-3.71
Flux of latent heat ($kcal/cm^2$)	0.09	0	0	-0.07	-0.50	-0.44	-0.16	-0.66	-0.69	-0.09	0.09	0	-2.43

solar energy. Vowinckel and Orvig assume a sensible heat loss at the surface 6 $kcal/cm^2$ year greater than Doronin (Table 1) and a latent heat loss that is 0.8 $kcal/cm^2$ year less. Surface ablation in Case 6 is 75 percent of Case 1 because they assume a smaller F_r and also specify smaller turbulent heat losses during the summer. Although decreased surface ablation accounts for part of the predicted thickening, the greater part is a result of the extremely low winter temperatures at the surface. These temperatures are lower than in Case 1 because Vowinckel and Orvig assume that almost no sensible heat reaches the surface during this time. In July, on the other hand, they assume that the heat loss by F_s and F_ℓ is less than Doronin's estimate by 0.8 $kcal/cm^2$ year. During September they estimate that the sum of F_s and F_ℓ is -1.7 $kcal/cm^2$, which causes the ice to cool so rapidly that, in contrast to observations, the net long-wave radiation balance becomes positive.

The above discussion has shown that none of the values suggested by Vowinckel and Orvig for the oceanic heat flux, surface albedo, or

Table 8. COMPUTED VALUES FOR CASE 6, INCOMING ENERGY FLUXES AT THE UPPER
ALL OTHER INPUT DATA AS IN CASE 1. AS DESCRIBED IN

Variable	Jan	Feb	Mar	Apr	May
Mean snow surface temperature (^{o}C)	-37.95	-42.49	-39.45	-31.24	-14.45
Mean ice surface temperature (^{o}C)	-24.53	-27.44	-27.78	-25.06	-17.60
Mean ice thickness (cm)	532.9	535.5	539.3	544.1	549.3
Heat flux through surface (kcal/cm^2)	0.807	0.881	0.659	0.330	-0.172
Heat flux through bottom (kcal/cm^2)	-0.245	-0.335	-0.407	-0.449	-0.453
Net short-wave radiation (kcal/cm^2)	0	0	0.368	1.664	2.794
Net long-wave radiation (kcal/cm^2)	-1.016	-0.941	-1.090	-1.030	-1.125

BOUNDARY FROM VOWINCKEL AND ORVIG (TABLE 7), ALBEDOS FROM MARSHUNOVA (TABLE 1). SECTION 4.1.4, THE ICE IS NOT STRICTLY IN EQUILIBRIUM.

Jun	Jul	Aug	Sep	Oct	Nov	Dec	Year
-2.75	-0.10	-1.74	-14.21	-20.27	-31.18	-36.06	-22.66
-9.85	-0.10	-1.41	-10.47	-13.44	-18.10	-22.38	-16.51
554.0	551.2	538.4	532.8	533.0	532.9	533.2	539.7
-0.361	-0.103	0.288	0.683	0.550	0.838	0.843	5.244
-0.403	-0.327	-0.235	-0.162	-0.122	-0.123	-0.164	-3.423
3.336	4.216	2.555	0.449	0.040	0	0	15.423
-1.792	-1.081	-0.726	-0.558	-0.499	-0.985	-0.904	-10.633

Date	Onset	End
23 June	Snow ablation	
12 July	Ice ablation	
16 August		Surface ice ablation
10 October		Bottom accretion
20 November	Bottom accretion	

Other Data

Surface ice ablation*	28.5 cm
Bottom ablation	0.2 cm
Bottom accretion	30.2 cm
Short-wave radiation penetrating surface during snow-free period	0.820 kcal/cm^2

*Equals net bottom accretion.

the turbulent fluxes can be considered representative of conditions over the bare ice, although they may be correct in terms of a large-scale average. Since ice thickness is not directly a function of energy transfer over leads and melt ponds, the heat budget of Vowinckel and Orvig cannot be used for realistic calculations of ice growth. Likewise, because of a lack of detail in Eq. (34), the sea-ice model cannot be used for an explicit evaluation of their assumed energy budget. If Vowinckel and Orvig had estimated the separate contributions to the O term and the effects of leads on the turbulent fluxes, it might have been possible to obtain an independent evaluation of their large-scale heat budget, assuming that the parameters specified in Case 1 are characteristic of the bare ice.

4.2 ANALYSIS OF FURTHER CASES

The effects of a certain parameter on sea ice may be investigated by varying this parameter, while holding all others constant. Since the results of Case 1 are compatible with observations, the input data for this case have been adopted as the "standard conditions." The experiments discussed in this section define how penetrating short-wave radiation, oceanic heat flux, and the snow cover influence the growth and temperature regime of sea ice.

4.2.1 Penetration of short-wave radiation

The amount of short-wave radiation which penetrates the ice (I_o) has been inferred from temperature profiles (Untersteiner, 1961), but may be in error by as much as a factor of two. Untersteiner (1964) has theoretically investigated the effect of I_o on internal ice temperatures, but no previous work has related I_o to equilibrium thickness. The experiments described in this section will expand upon Untersteiner's work and define the role which I_o plays in annual mass changes.

It was assumed in Case 1 that 17 percent (about 1.2 kcal/cm^2 year) of the net short-wave radiation penetrates the ice during the snow-free period. In cases 7 to 10 we have specified that I_o is 0, 8.5,

25.5, and 34 percent of the net short-wave radiation, respectively. All other input data are unchanged from Case 1. The results of these experiments are given in Figs. 13 to 17 and Tables 9 to 12.

Contrary to what might be expected, equilibrium thickness actually increases as more radiation penetrates the ice (Fig. 17). Because the net short-wave radiation remains constant and a greater percentage of it is absorbed within the ice, less energy is available for melting at the surface. The additional energy absorbed within the ice causes slight additional warming in the slab, but it is, for the most part, stored as heat of fusion within the diluted brine. Since there is little temperature change, the conductive heat flux to the surface remains almost unchanged during the ablation season. Tables 9 to 12 show that, as I_o increases from 0 to 34 percent, surface ablation decreases from 52.3 to 24.7 cm/year. Less surface ablation means that the ice must thicken to slow bottom accretion and maintain equilibrium.

Temperatures change surprisingly little as I_o varies. As I_o increases from 0 to 2.5 kcal/cm^2 year, the annual surface temperature decreases by only 0.1°C, while the average temperature at the ice/snow interface decreases by 1°C. The maximum temperature change within the ice is 3°C. Intuitively, it could be argued that an increased energy input of 2.5 kcal/cm^2 year into the ice should cause average temperatures to rise, despite an increase in thickness. An examination of Tables 9 to 12 shows that, although downward heat input into the ice has increased by 2.5 kcal/cm^2 year, the upward heat flux at the surface has increased by only 0.4 kcal/cm^2 year. This seeming contradiction is explained by the 28-cm decrease in bottom accretion, which reduces the heat conducted into the ice by about 2.0 kcal/cm^2 year. Thus the net energy input is only 20 percent of the increase in I_o and, except during the summer and fall, ice thickness determines the temperature profiles.

The date of the onset of ice and snow ablation does not vary, and the duration of surface ablation is nearly the same. As the ice thickens from 240 to 370 cm, bottom ablation starts about a half-month later and is extended by about 2 months. Comparison with cases of equivalent

Table 9. COMPUTED VALUES FOR EQUILIBRIUM CONDITIONS

Variable	Jan	Feb	Mar	Apr	May
Mean snow surface temperature (^{o}C)	-30.73	-32.85	-31.58	-22.23	-9.28
Mean ice surface temperature (^{o}C)	-16.76	-17.75	-17.87	-14.62	-8.74
Mean ice thickness (cm)	238.3	246.7	255.3	263.4	269.7
Heat flux through surface (kcal/cm^2)	0.832	0.876	0.770	0.408	0.020
Heat flux through bottom (kcal/cm^2)	-0.658	-0.668	-0.675	-0.602	-0.442
Net short-wave radiation (kcal/cm^2)	0	0	0.406	1.893	3.129
Net long-wave radiation (kcal/cm^2)	-2.017	-1.615	-1.868	-2.503	-2.242

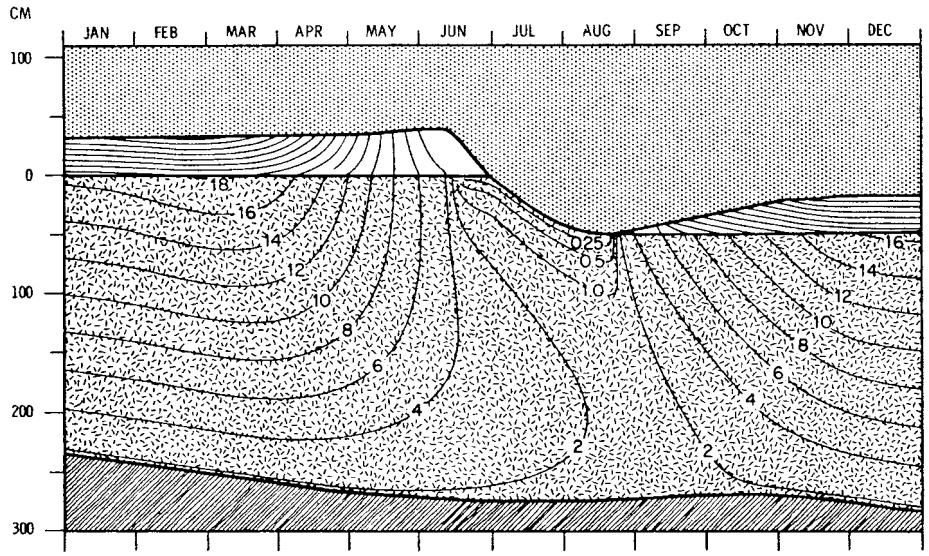

Fig. 13 -- Annual equilibrium temperature and thickness field for Case 7, $I_o = 0$.

IN CASE 7, I_o = 0. ALL OTHER INPUT DATA AS IN CASE 1.

Jun	Jul	Aug	Sep	Oct	Nov	Dec	Year
-0.29	-0.10	-1.14	-10.19	-20.43	-28.71	-30.10	-18.14
-2.02	-0.10	-0.97	-6.69	-10.91	-14.59	-16.28	-10.61
272.3	250.2	224.5	219.5	219.1	222.9	230.0	242.6
-0.102	-0.329	-0.004	0.623	0.768	0.891	0.843	5.595
-0.263	-0.120	-0.040	-0.013	-0.222	-0.503	-0.641	-4.846
4.435	4.959	2.789	0.605	0.085	0	0	18.300
-1.947	-0.903	-0.979	-0.672	-0.767	-1.445	-1.628	-18.587

Date	Onset	End
7 June	Snow ablation	
28 June	Ice ablation	
13 July		Bottom accretion
22 August		Surface ice ablation
7 October	Bottom accretion	

Other Data

Surface ice ablation*	52.3 cm
Bottom ablation	3.4 cm
Bottom accretion	55.7 cm
Short-wave radiation penetrating surface during snow-free period	0

*Equals net bottom accretion.

Table 10. COMPUTED VALUES FOR EQUILIBRIUM CONDITIONS IN

Variable	Jan	Feb	Mar	Apr	May
Mean snow surface temperature (^{o}C)	-30.85	-32.98	-31.71	-22.33	-9.35
Mean ice surface temperature (^{o}C)	-17.31	-18.32	-18.44	-15.15	-9.16
Mean ice thickness (cm)	256.9	264.8	272.9	280.8	287.0
Heat flux through surface (kcal/cm^2)	0.806	0.851	0.745	0.384	0.002
Heat flux through bottom (kcal/cm^2)	-0.629	-0.638	-0.648	-0.592	-0.447
Net short-wave radiation (kcal/cm^2)	0	0	0.406	1.893	3.129
Net long-wave radiation (kcal/cm^2)	-1.992	-1.590	-1.843	-2.480	-2.224

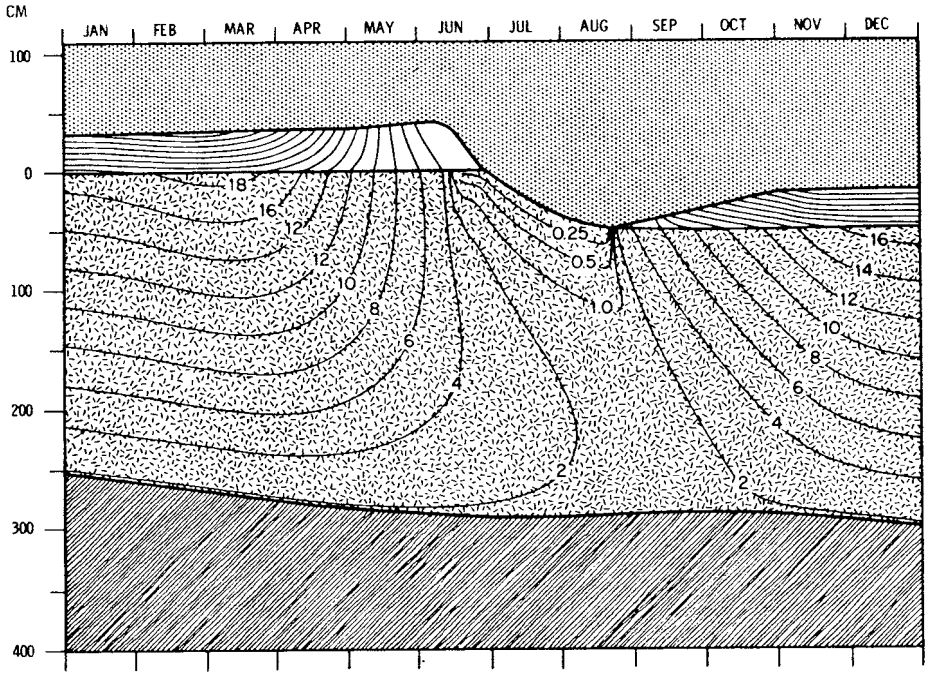

Fig. 14 -- Annual equilibrium temperature and thickness field for Case 8, I_o = 8.5 percent.

CASE 8, I_o = 8.5%. ALL OTHER INPUT DATA AS IN CASE 1.

Jun	Jul	Aug	Sep	Oct	Nov	Dec	Year
-0.30	-0.10	-1.19	-10.14	-20.41	-28.75	-30.20	-18.19
-2.16	-0.10	-0.97	-6.49	-10.81	-14.76	-16.72	-10.87
289.9	270.4	247.2	242.6	241.1	243.1	249.2	262.0
-0.101	-0.158	0.131	0.635	0.772	0.883	0.823	5.773
-0.276	-0.121	-0.028	0.007	-0.099	-0.408	-0.592	-4.470
4.433	4.959	2.737	0.605	0.085	0	0	18.246
-1.945	-0.903	-0.966	-0.685	-0.771	-1.437	-1.608	-18.443

Date	Onset	End
7 June	Snow ablation	
28 June	Ice ablation	
14 July		Bottom accretion
21 August		Surface ice ablation
19 October	Bottom accretion	

Other Data

Surface ice ablation*	46.5 cm
Bottom ablation	4.5 cm
Bottom accretion	51.0 cm
Short-wave radiation penetrating surface during snow-free period	0.658 kcal/cm^2

*Equals net bottom accretion.

Table 11. COMPUTED VALUES FOR EQUILIBRIUM CONDITIONS

Variable	Jan	Feb	Mar	Apr	May
Mean snow surface temperature (°C)	-31.10	-33.29	-32.03	-22.62	-9.56
Mean ice surface temperature (°C)	-18.50	-19.78	-20.01	-16.66	-10.42
Mean ice thickness (cm)	316.4	322.7	329.6	336.5	342.4
Heat flux through surface ($kcal/cm^2$)	0.756	0.789	0.679	0.319	-0.052
Heat flux through bottom ($kcal/cm^2$)	-0.504	-0.546	-0.576	-0.554	-0.445
Net short-wave radiation ($kcal/cm^2$)	0	0	0.406	1.893	3.129
Net long-wave radiation ($kcal/cm^2$)	-1.942	-1.528	-1.777	-2.414	-2.169

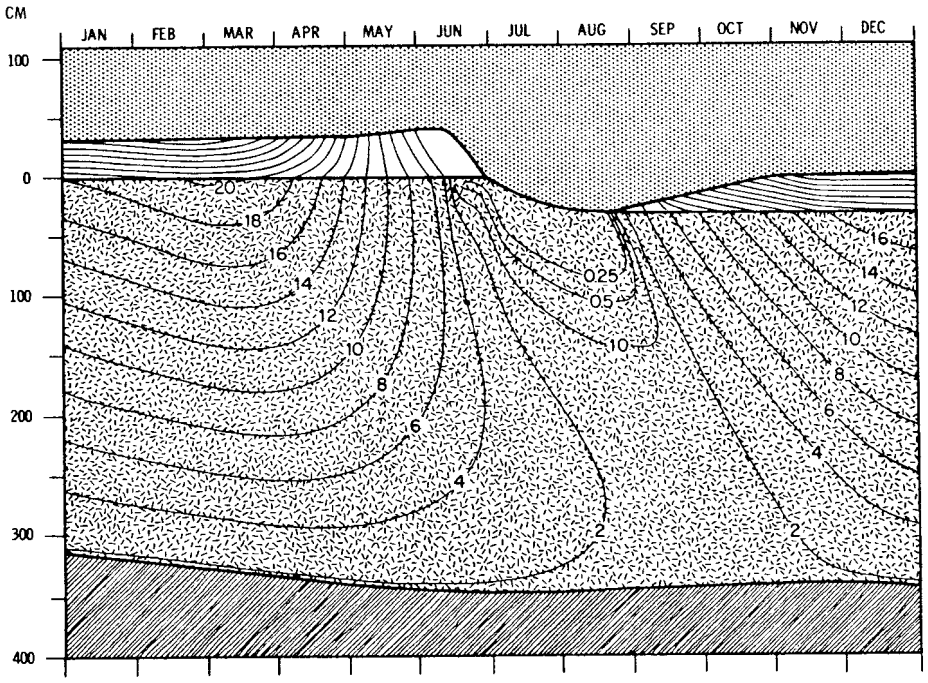

Fig. 15 -- Annual equilibrium temperature and thickness field for Case 9, I_o = 25.5 percent.

IN CASE 9, I_o = 25.5%. ALL OTHER INPUT DATA AS IN CASE 1.

Jun	Jul	Aug	Sep	Oct	Nov	Dec	Year
-0.35	-0.10	-0.95	-9.80	-20.31	-28.72	-30.32	-18.26
-2.63	-0.10	-0.61	-5.71	-10.50	-14.75	-17.35	-11.42
345.8	332.4	316.5	313.6	311.6	310.1	311.6	324.1
-0.130	0.014	0.325	0.726	0.794	0.888	0.798	5.906
-0.308	-0.159	-0.056	-0.012	0.005	-0.090	-0.351	-3.596
4.359	4.959	2.710	0.605	0.085	0	0	18.145
-1.929	-0.903	-1.030	-0.776	-0.794	-1.442	-1.583	-18.288

Date	Onset	End
8 June	Snow ablation	
29 June	Ice ablation	
22 July		Bottom accretion
17 August		Surface ice ablation
21 November	Bottom accretion	

Other Data

Surface ice ablation*	32.8 cm
Bottom ablation	5.8 cm
Bottom accretion	38.6 cm
Short-wave radiation penetrating surface during snow-free period	1.910 kcal/cm^2

*Equals net bottom accretion.

Table 12. COMPUTED VALUES FOR EQUILIBRIUM CONDITIONS

Variable	Jan	Feb	Mar	Apr	May
Mean snow surface temperature (^{o}C)	-31.15	-33.41	-32.20	-22.79	-9.68
Mean ice surface temperature (^{o}C)	-18.72	-20.33	-20.76	-17.48	-11.19
Mean ice thickness (cm)	359.8	364.3	370.0	376.1	381.7
Heat flux through surface (kcal/cm^2)	0.746	0.765	0.647	0.282	-0.085
Heat flux through bottom (kcal/cm^2)	-0.360	-0.462	-0.513	-0.516	-0.438
Net short-wave radiation (kcal/cm^2)	0	0	0.406	1.893	3.129
Net long-wave radiation (kcal/cm^2)	-1.932	-1.504	-1.744	-2.378	-2.136

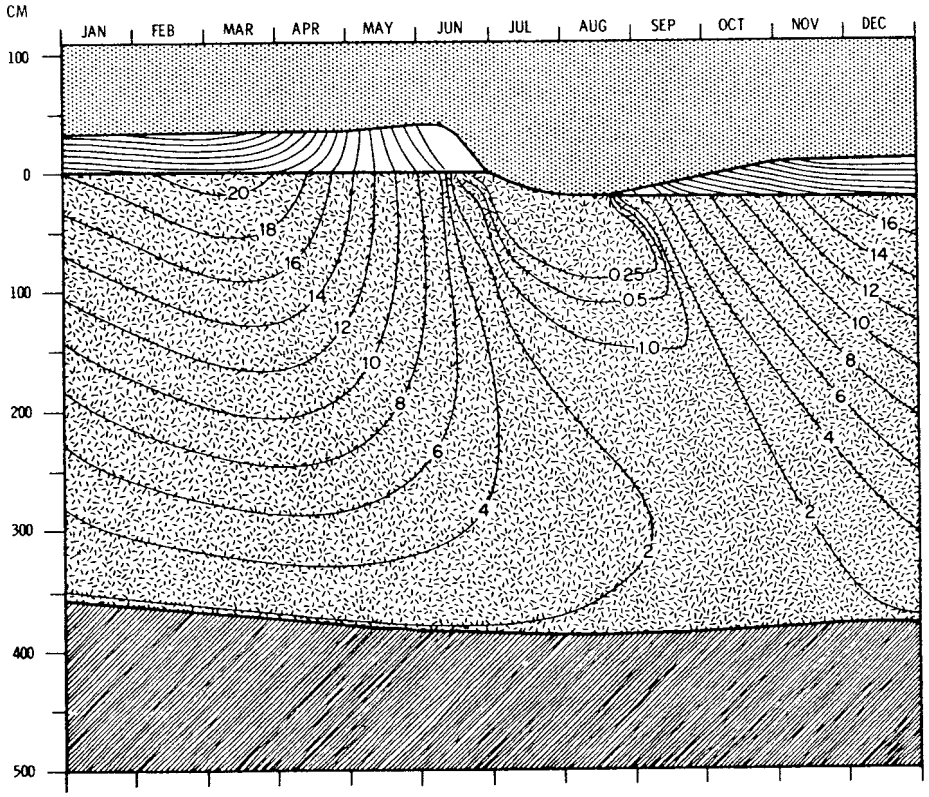

Fig. 16 -- Annual equilibrium temperature and thickness field for Case 10, I_o = 34 percent.

IN CASE 10, I_o = 34%. ALL OTHER INPUT DATA AS IN CASE 1.

Jun	Jul	Aug	Sep	Oct	Nov	Dec	Year
-0.38	-0.10	-0.87	-9.26	-20.16	-28.66	-30.30	-18.25
-2.92	-0.10	-0.50	-4.45	-9.95	-14.50	-17.26	-11.51
385.4	375.6	364.1	362.3	360.6	358.8	357.8	368.1
-0.141	0.037	0.355	0.870	0.829	0.901	0.802	6.006
-0.323	-0.187	-0.082	-0.035	-0.010	-0.009	-0.144	-3.080
4.354	4.959	2.710	0.605	0.085	0	0	18.140
-1.922	-0.903	-1.043	-0.920	-0.828	-1.455	-1.588	-18.354

Date	Onset	End
8 June	Snow ablation	
29 June	Ice ablation	
1 August		Bottom accretion
14 August		Surface ice ablation
14 December	Bottom accretion	

Other Data

Surface ice ablation*	24.7 cm
Bottom ablation	6.0 cm
Bottom accretion	30.7 cm
Short-wave radiation penetrating surface during snow-free period	2.547 kcal/cm^2

*Equals net bottom accretion.

thicknesses (e.g., Case 13) shows that bottom accretion is initiated approximately a month later for a large I_o.

As was pointed out in Section 4.1.1, the model predicts more rapid cooling in the fall than observations indicate. One possible reason for this is that we have underestimated I_o. Comparison of Figs. 6, 7, and 16 shows that, when I_o is 34 percent (Case 10), the fall temperatures are in much better agreement with empirical data than in Case 1; however, ice ablation at the surface is too small.

It is possible to increase surface ablation, while maintaining a large I_o simply by decreasing the albedo of the melting ice (α_i); α_i is sufficiently in doubt that a small percentage change is acceptable. In Case 11, α_i has been reduced from 0.64 to 0.58 and I_o specified as 34 percent. Results are given in Table 13 and Fig. 18. A comparison of Cases 1 and 11 shows nearly the same surface ablation,

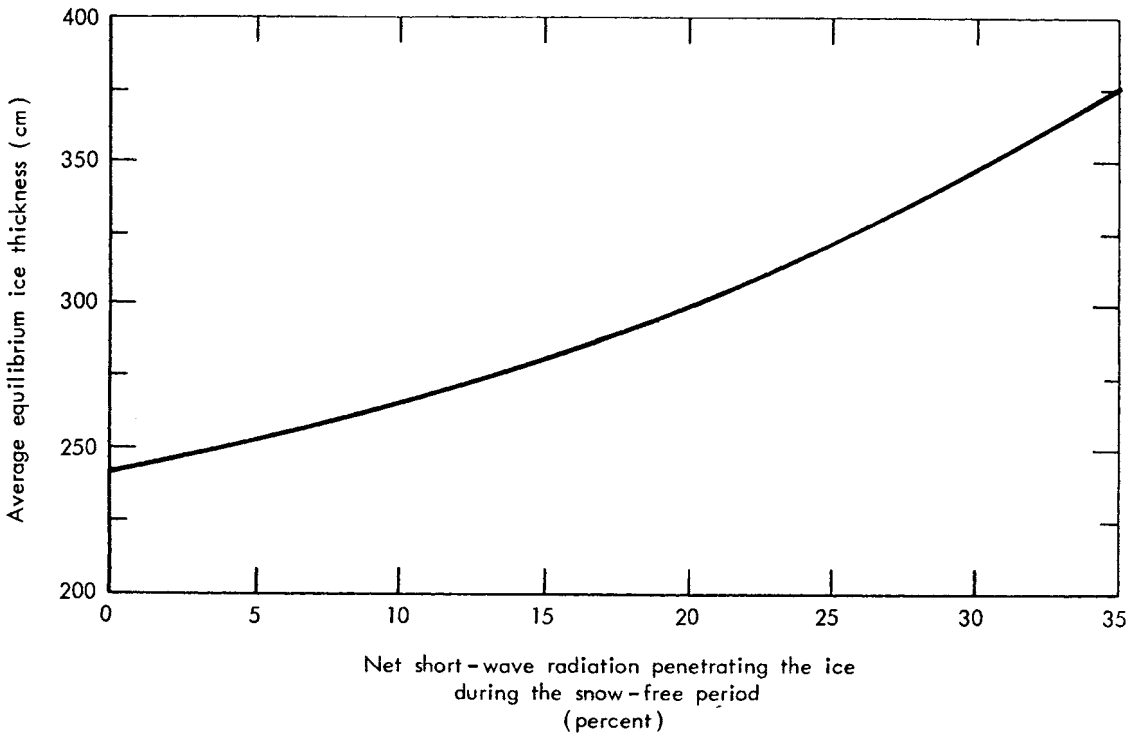

Fig. 17 -- Average equilibrium thickness as a function of the percentage of net short-wave radiation which penetrates the ice during the snow-free period.

but solar energy absorbed within the ice is greater by 1.9 kcal/cm^2 yr. Since mass changes at the surface have been separated from I_o, it now becomes possible to define how the ice responds to I_o alone. Even though surface ablation remains nearly constant, bottom ablation in Case 11 is more than double that of Case 1. To maintain equilibrium, bottom accretion must therefore increase, but this may occur only if the ice thins. Average thickness in Case 11 is 229 cm, that is, 60 cm less thickness for an annual energy greater by only 1.9 kcal/cm^2. Figure 23 shows that an equivalent increase in F_w would cause the equilibrium thickness to decrease from 288 cm to 140 cm, illustrating the greater efficiency of heat addition from the ocean.

In Case 11 the rate of cooling within the ice in autumn is considerably less than in Case 1. Surface temperatures are higher in the winter, but this is due to thinner ice. Fall temperature patterns in Fig. 18 are similar to the observed ones (Fig. 7); however, the cooling rate in the upper meter of the ice is still too high September through December. It does not appear that a further increase in I_o would be able to duplicate the pattern of Fig. 7. Because the greatest discrepancy now occurs in the upper portion of the ice, the most likely explanation for the slower cooling in autumn is the latent-heat release from freezing melt ponds, possibly combined with an underestimation of I_o.

Although Untersteiner (1961) calculated an I_o of 34 percent during the height of the melt season and Chernigovskii (1963) appears to have measured an I_o of 47 percent, there are several objections to values this large. When I_o is large, the combination of a thickness of 300 cm and a surface ablation of 40 cm is impossible. If we accept less ice ablation, it is possible to have a reasonable ice thickness and a large I_o. Untersteiner, for example, measured only 32 cm of ice melt, which is consistent with his ice thickness and I_o measurements. Ablation during the following year was 53 cm, but no I_o calculations were reported.

These considerations demonstrate the need for careful studies of the relationship between I_o, net short-wave radiation, and surface ablation. Observations of melt ponds after the fall freeze-up would

Table 13. COMPUTED VALUES FOR EQUILIBRIUM CONDITIONS IN CASE 11,

Variable	Jan	Feb	Mar	Apr	May
Mean snow surface temperature (^{o}C)	-30.58	-32.71	-31.20	-22.13	-9.22
Mean ice surface temperature (^{o}C)	-16.18	-17.23	-17.37	-14.15	-8.36
Mean ice thickness (cm)	221.8	230.6	239.6	248.2	254.6
Heat flux through surface (kcal/cm^2)	0.863	0.905	0.796	0.431	0.036
Heat flux through bottom (kcal/cm^2)	-0.683	-0.696	-0.703	-0.622	-0.440
Net short-wave radiation (kcal/cm^2)	0	0	0.406	1.893	3.129
Net long-wave radiation (kcal/cm^2)	-2.048	-1.643	-1.894	-2.526	-2.258

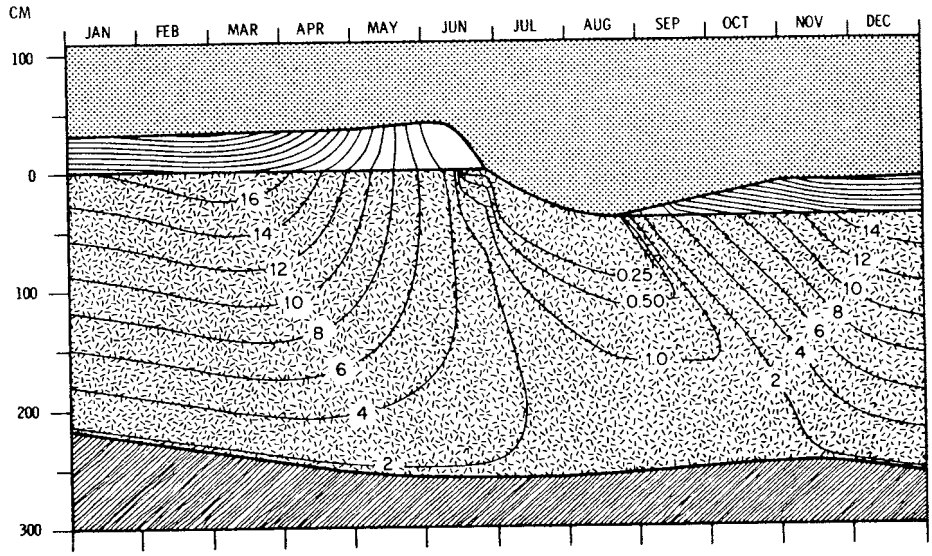

Fig. 18 -- Annual equilibrium temperature and thickness field for Case 11, I_o = 34 percent, surface ice albedo = 0.58.

I_o = 34%, ICE ALBEDO = 0.58. ALL OTHER INPUT DATA AS IN CASE 1.

Jun	Jul	Aug	Sep	Oct	Nov	Dec	Year
-0.30	-0.10	-0.86	-9.21	-19.80	-28.30	-29.90	-17.88
-'.84	-0.10	-0.48	-4.26	-8.53	-12.92	-15.47	-9.74
257.4	236.8	217.2	212.6	209.1	207.6	213.2	229.1
-0.091	0.040	0.364	0.881	0.914	0.977	0.886	7.003
-0.250	-0.034	0.082	0.100	0.096	-0.249	-0.632	-4.032
4.817	5.785	3.098	0.605	0.085	0	0	19.818
-1.944	-0.903	-1.057	-0.931	-0.914	-1.532	-1.671	-19.322

Date	Onset	End
7 June	Snow ablation	
26 June	Ice ablation	
3 July		Bottom accretion
18 August		Surface ice ablation
10 November	Bottom accretion	

Other Data

Surface ice ablation*	39.6 cm
Bottom ablation	12.1 cm
Bottom accretion	51.7 cm
Short-wave radiation penetrating surface during snow-free period	3.176 kcal/cm^2

*Equals net bottom accretion.

also be useful. Because it is still impossible to say which combination of I_o and surface ablation is truly representative, the succeeding cases were integrated with an I_o of 17 percent, conceding, however, that I_o may be larger.

4.2.2 Oceanic heat flux

Since the pioneering work of Malmgren (1927), the turbulent transfer of heat from the ocean to the ice has been subject to numerous estimates and speculations (see Chapters I and II). Wide variations in F_w are an integral part of several theories of the ice ages, and numerous schemes for artificially influencing the extent of the pack ice depend upon changing F_w (Toporkov, 1963; Fletcher, 1965). The feasibility of any of these proposals is difficult to establish because of a lack of quantitative knowledge regarding the sensitivity of ice response to F_w. It is not known how large the heat flux must become before the ice would vanish, and disagreement still exists as to the present magnitude of F_w. In this section an attempt will be made first to describe the total response of the ice to changes in F_w, then to determine an upper limit for F_w, and finally to define a range of conditions under which the ice could currently exist.

Five cases were integrated using annual values for F_w of 0, 0.75, 3.0, 4.5, and 6.0 kcal/cm^2 year (Cases 12 to 16, respectively). Because no obvious inconsistencies had resulted from assuming that F_w remained constant throughout the year in Case 1, the other cases were computed under the same assumption. All other fluxes were left unchanged. The temperature fields and monthly averages for Cases 12 to 15 appear in Figs. 19 to 22 and Tables 14 to 17. When F_w = 6.0 kcal/cm^2 year, the ice vanishes before equilibrium is established and consequently no other results are presented for this case.

Figure 23 shows a graph of equilibrium thickness vs. F_w; curves for seasonal maximum and minimum thickness and average thickness are drawn. When the ice is thicker, the average value is closer to the minimum, reflecting the decrease in bottom ablation. Under present

surface conditions, the theoretical thermodynamic limit of ice thickness is about 560 cm, whereas the ice should vanish if F_w increases to five or six kcal/cm^2 year.

An examination of surface conditions shows that variations in oceanic heat flux have relatively little direct influence on processes occurring at the upper boundary. The surface temperature of ice 90 cm thick is up to 12°C higher than the surface temperature of 560-cm ice, but because the snow is an effective thermal insulator, average snow surface temperatures are only two or three degrees higher. Likewise, because of the snow cover, the onset of snow and ice ablation changes by only three days. A somewhat surprising result is that the upper surface ice ablation varies by only a few centimeters. Tables 2 and 14 to 17 show that the quantity of heat conducted to the surface during the snow-free period is similar in all cases, indicating that temperature gradients during the summer are generally determined by the penetrating short-wave radiation, rather than by the ice thickness.

Figure 24 shows cumulative bottom accretion vs. time and illustrates the earlier onset of, and greater amount of, bottom ablation associated with higher F_w. Bottom accretion, unexpectedly, also begins earlier in the fall when F_w is larger. Examination of the temperature fields verifies that, in thin ice, the lower portion responds more rapidly to temperature changes at the surface. Thus the steeper temperature gradients within the ice outweigh the effects of a higher F_w and result in earlier bottom accretion.

Most field observations indicate an average ice thickness between 250 and 350 cm, which corresponds in Fig. 23 to values of F_w between 1.0 and 2.0 kcal/cm^2 year. These values refer to an "effective" F_w. It is probable that more heat is carried into the basin but is lost through leads. Because uncertainties that could also affect thickness exist in the other input data, it is not possible to assign a specific value to F_w. However, on the basis of the temperature results, it is unlikely that errors in the energy fluxes at the upper surface could modify the thickness results by more than ± 0.5 m. This being the case, the estimates of oceanic heat flux by Crary, Badgley, and Untersteiner must be very close to reality and the earlier ones considerably in error.

Table 14. COMPUTED VALUES FOR EQUILIBRIUM CONDITIONS IN

Variable	Jan	Feb	Mar	Apr	May
Mean snow surface temperature (°C)	-31.64	-33.90	-32.70	-23.27	-10.09
Mean ice surface temperature (°C)	-20.88	-22.47	-23.05	-19.94	-13.67
Mean ice thickness (cm)	557.0	560.0	564.0	568.8	574.0
Heat flux through surface (kcal/cm^2)	0.646	0.669	0.545	0.173	-0.191
Heat flux through bottom (kcal/cm^2)	-0.156	-0.225	-0.283	-0.326	-0.334
Net short-wave radiation (kcal/cm^2)	0	0	0.406	1.893	3.129
Net long-wave radiation (kcal/cm^2)	-1.832	-1.408	-1.643	-2.268	-2.030

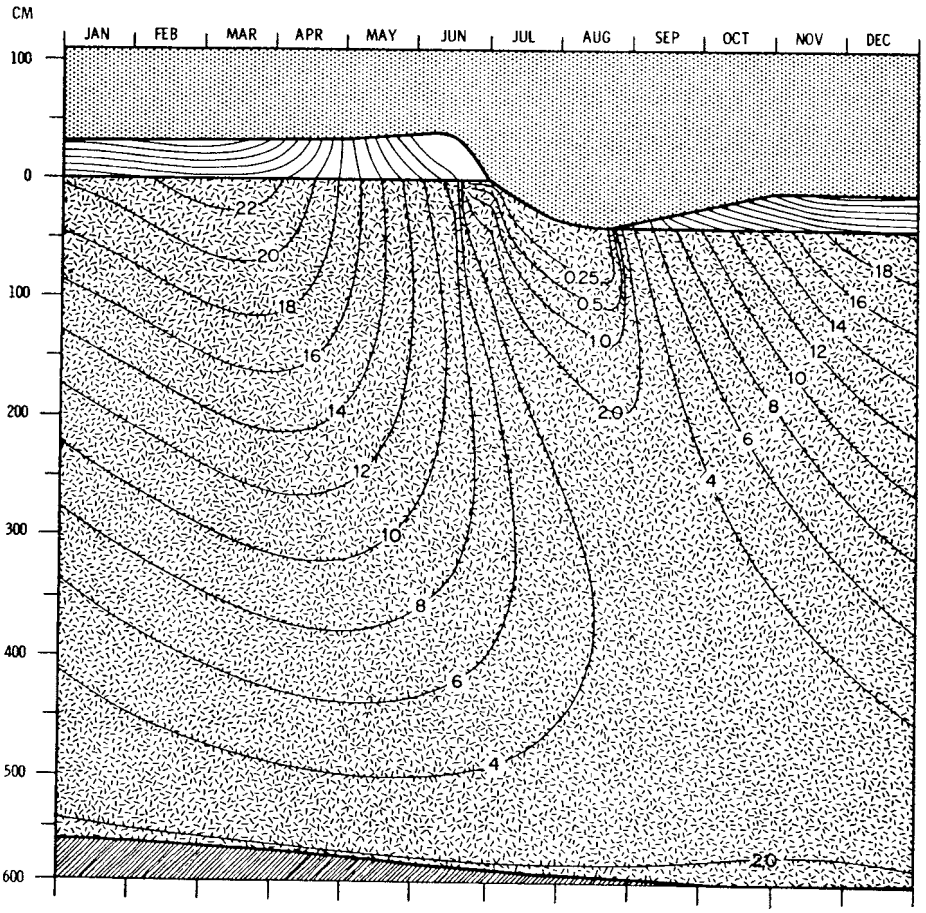

Fig. 19 -- Annual equilibrium temperature and thickness field for Case 12, $F_w = 0$.

CASE 12, F_w = 0. ALL OTHER INPUT DATA AS IN CASE 1.

Jun	Jul	Aug	Sep	Oct	Nov	Dec	Year
-0.47	-0.10	-1.09	-10.47	-20.86	-29.26	-30.85	-18.73
-4.33	-0.10	-0.81	-7.31	-12.58	-17.08	-19.64	-13.49
579.0	565.8	551.1	550.6	552.4	553.8	555.1	561.0
-0.196	-0.072	0.266	0.553	0.668	0.776	0.689	4.525
-0.309	-0.252	-0.185	-0.131	-0.097	-0.083	-0.100	-2.478
4.237	4.959	2.710	0.605	0.085	0	0	18.023
-1.895	-0.904	-0.994	-0.602	-0.668	-1.330	-1.475	-17.048

Date	Onset	End
9 June	Snow ablation	
1 July	Ice ablation	
...		Bottom accretion
19 August		Surface ice ablation
...	Bottom accretion	

Other Data

Surface ice ablation*	38.7 cm
Bottom ablation	0
Bottom accretion	38.7 cm
Short-wave radiation penetrating surface during snow-free period	1.222 kcal/cm^2

*Equals net bottom accretion.

Table 15. COMPUTED VALUES FOR EQUILIBRIUM CONDITIONS IN CASE 13,

Variable	Jan	Feb	Mar	Apr	May
Mean snow surface temperature (°C)	-31.33	-33.55	-32.32	-22.89	-9.77
Mean ice surface temperature (°C)	-19.50	-20.95	-21.31	-18.01	-11.68
Mean ice thickness (cm)	384.5	390.0	396.4	403.1	409.3
Heat flux through surface (kcal/cm^2)	0.709	0.737	0.622	0.259	-0.106
Heat flux through bottom (kcal/cm^2)	-0.380	-0.449	-0.489	-0.486	-0.430
Net short-wave radiation (kcal/cm^2)	0	0	0.406	1.893	3.129
Net long-wave radiation (kcal/cm^2)	-1.895	-1.476	-1.720	-2.354	-2.115

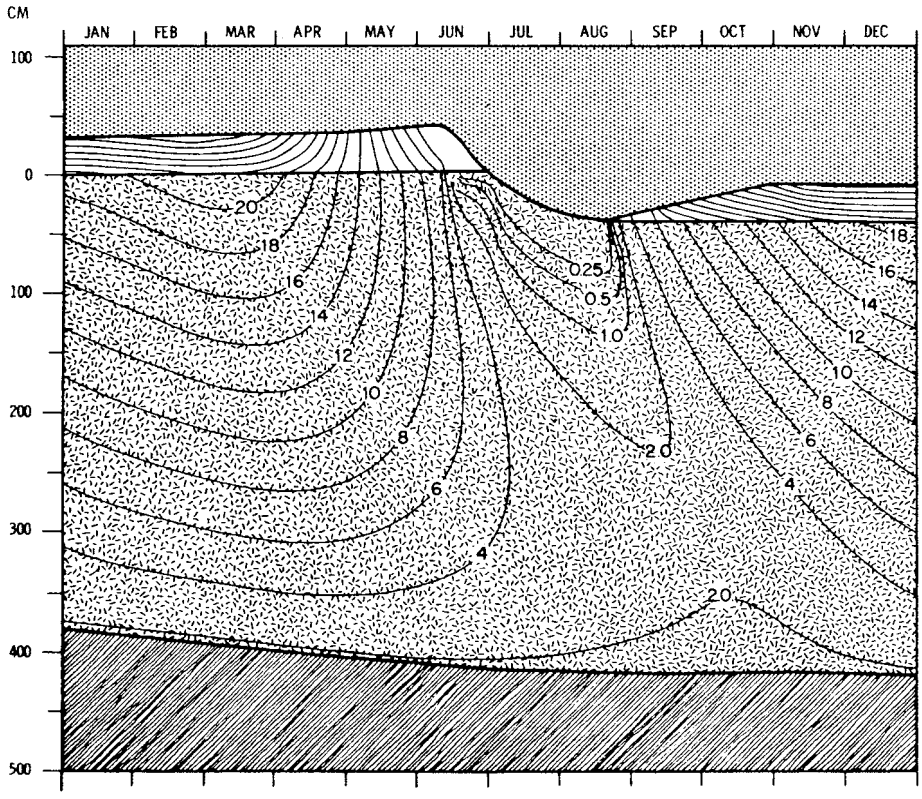

Fig. 20 -- Annual equilibrium temperature and thickness field for Case 13, F_w = 0.75 kcal/cm^2 year.

F_w = 0.75 kcal/cm² year. ALL OTHER INPUT DATA AS IN CASE 1.

Jun	Jul	Aug	Sep	Oct	Nov	Dec	Year
-0.39	-0.10	-1.08	-10.23	-20.59	-28.97	-30.55	-18.48
-3.20	-0.10	-0.80	-6.72	-11.56	-15.81	-18.31	-12.33
413.8	399.4	381.4	379.5	379.3	379.2	380.6	391.3
-0.156	-0.042	0.270	0.614	0.730	0.837	0.752	5.225
-0.325	-0.208	-0.113	-0.061	-0.039	-0.084	-0.237	-3.302
4.319	4.959	2.710	0.605	0.085	0	0	18.105
-1.918	-0.903	-0.996	-0.663	-0.730	-1.391	-1.538	-17.699

Date	Onset	End
8 June	Snow ablation	
29 June	Ice ablation	
19 August		Surface ice ablation
13 September		Bottom accretion
10 November	Bottom accretion	

Other Data

Surface ice ablation*	39.9 cm
Bottom ablation	0.5 cm
Bottom accretion	40.4 cm
Short-wave radiation penetrating surface during snow-free period	1.256 kcal/cm²

*Equals net bottom accretion.

Table 16. COMPUTED VALUES FOR EQUILIBRIUM CONDITIONS IN CASE 14,

Variable	Jan	Feb	Mar	Apr	May
Mean snow surface temperature (^{o}C)	-30.03	-32.15	-30.90	-21.68	-8.95
Mean ice surface temperature (^{o}C)	-13.73	-14.73	-14.86	-11.90	-6.74
Mean ice thickness (cm)	159.3	168.0	177.0	184.8	189.5
Heat flux through surface (kcal/cm^2)	0.976	1.017	0.908	0.532	0.107
Heat flux through bottom (kcal/cm^2)	-0.808	-0.821	-0.814	-0.670	-0.425
Net short-wave radiation (kcal/cm^2)	0	0	0.406	1.893	3.129
Net long-wave radiation (kcal/cm^2)	-2.162	-1.756	-2.006	-2.627	-2.329

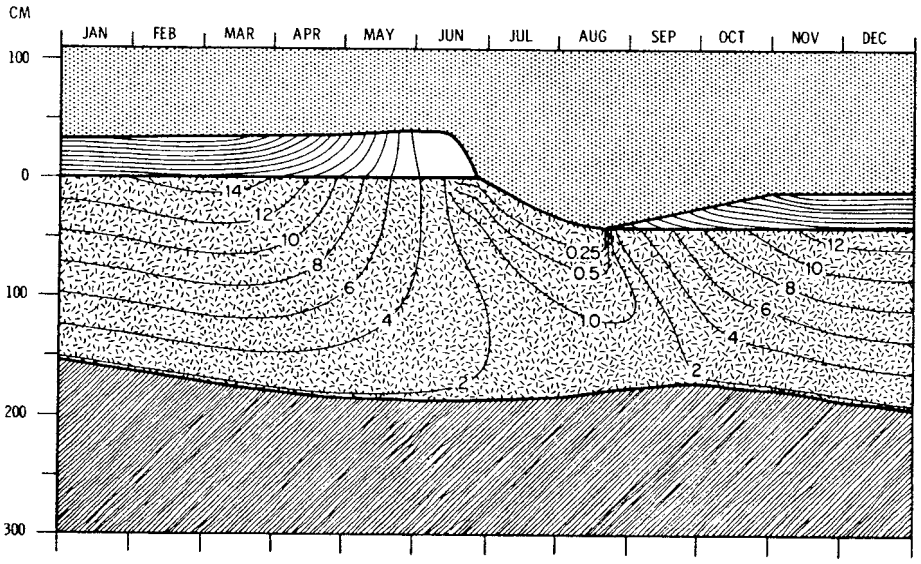

Fig. 21 -- Annual equilibrium temperature and thickness field for Case 14, F_w = 3.0 kcal/cm^2 year.

F_w = 3.0 kcal/cm^2 year. ALL OTHER INPUT DATA AS IN CASE 1.

Jun	Jul	Aug	Sep	Oct	Nov	Dec	Year
-0.26	-0.10	-1.11	-9.69	-20.06	-28.15	-29.41	-17.71
-1.37	-0.10	-0.83	-5.39	-9.50	-12.23	-13.32	-8.72
189.4	168.1	144.2	136.2	135.3	141.6	150.3	161.9
-0.079	-0.098	0.206	0.753	0.853	1.010	0.988	7.172
-0.194	0.027	0.145	0.093	-0.504	-0.766	-0.830	-5.566
4.469	4.959	2.710	0.605	0.085	0	0	18.255
-1.956	-0.903	-0.986	-0.803	-0.852	-1.563	-1.772	-19.714

Date	Onset	End
7 June	Snow ablation	
7 June		Bottom accretion
28 June	Ice ablation	
18 August		Surface ice ablation
3 October	Bottom accretion	

Other Data

Surface ice ablation*	40.1 cm
Bottom ablation	16.7 cm
Bottom accretion	56.7 cm
Short-wave radiation penetrating surface during snow-free period	1.308 kcal/cm^2

*Equals net bottom accretion.

Table 17. COMPUTED VALUES FOR EQUILIBRIUM CONDITIONS IN CASE 15,

Variable	Jan	Feb	Mar	Apr	May
Mean snow surface temperature (°C)	-29.21	-31.35	-30.15	-21.12	-8.66
Mean ice surface temperature (°C)	-10.11	-11.17	-11.42	-9.07	-5.01
Mean ice thickness (cm)	93.8	103.3	112.8	120.2	123.0
Heat flux through surface (kcal/cm^2)	1.144	1.178	1.061	0.658	0.182
Heat flux through bottom (kcal/cm^2)	-0.976	-0.993	-0.952	-0.724	-0.389
Net short-wave radiation (kcal/cm^2)	0	0	0.406	1.893	3.129
Net long-wave radiation (kcal/cm^2)	-2.330	-1.917	-2.159	-2.755	-2.405

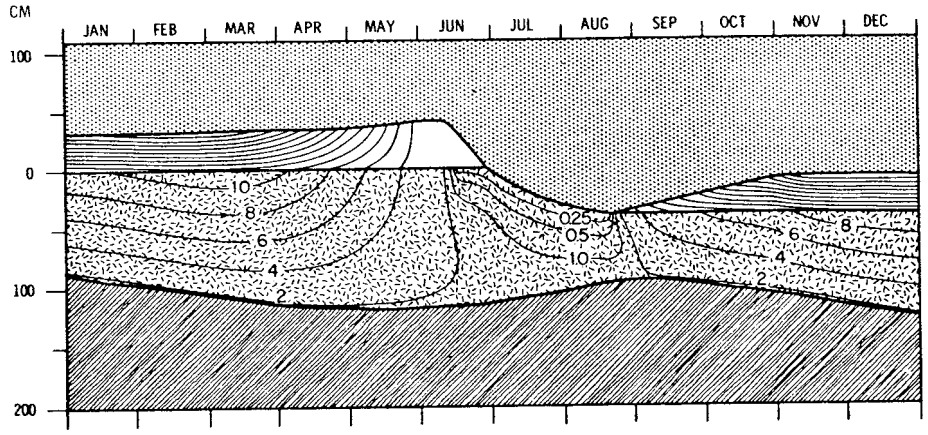

Fig. 22 -- Annual equilibrium temperature and thickness field for Case 15, F_w = 4.5 kcal/cm^2 year.

F_w = 4.5 kcal/cm^2 year. ALL OTHER INPUT DATA AS IN CASE 1.

Jun	Jul	Aug	Sep	Oct	Nov	Dec	Year
-0.23	-0.10	-1.09	-9.58	-19.39	-27.31	-28.54	-17.23
-0.98	-0.10	-0.80	-5.05	-6.89	-8.54	-9.49	-6.55
120.0	95.0	67.2	60.0	65.4	74.0	84.1	93.2
-0.069	-0.195	0.134	0.781	1.008	1.189	1.169	8.241
-0.095	0.218	0.381	-0.517	-0.858	-0.999	-1.015	-6.919
4.503	4.959	2.710	0.605	0.085	0	0	18.289
-1.964	-0.903	-0.991	-0.830	-1.007	-1.741	-1.954	-20.957

Date	Onset	End
16 May		Bottom accretion
6 June	Snow ablation	
27 June	Ice ablation	
17 August		Surface ice ablation
7 September	Bottom accretion	

Other Data

Surface ice ablation*	37.8 cm
Bottom ablation	25.5 cm
Bottom accretion	63.3 cm
Short-wave radiation penetrating surface during snow-free period	1.326 kcal/cm^2

*Equals net bottom accretion.

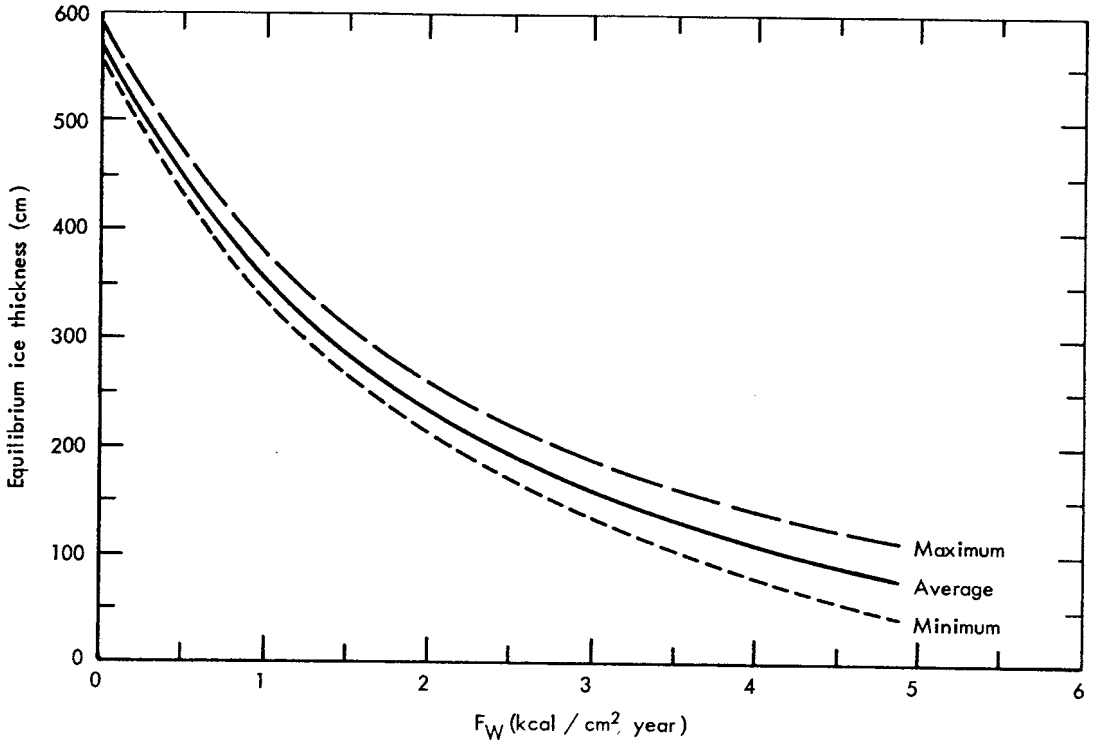

Fig. 23 -- Equilibrium ice thickness as a function of the oceanic heat flux.

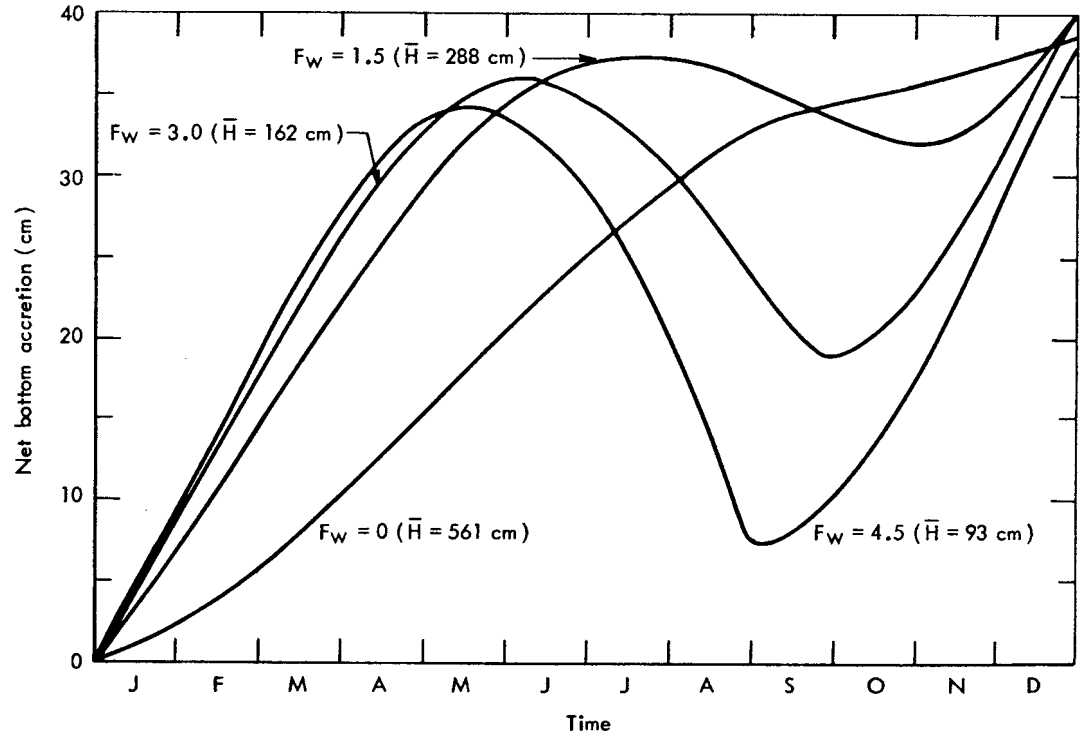

Fig. 24 -- Net bottom accretion as a function of time for equilibrium ice with various oceanic heat fluxes (F_w).

4.2.3 Snow cover

A snow cover insulates the ice from the cold air and reflects much of the incoming short-wave radiation. The effects of snow on surface ablation and ice temperatures suggest that small changes in snow thickness might result in significant changes in equilibrium thickness. The series of experiments described in this section indicates that this is not the case.

It was assumed in Case 1 that the maximum snow depth under present conditions is 40 cm. To investigate the effects of variable snow thickness, six cases were integrated specifying maximum snow depths of 0, 20, 60, 80, 100, and 120 cm. Snow was added in increments as described in 2.4.4, except that each accumulation increment was multiplied by a constant factor (0.5, 1.5, etc.) to bring the final snow depth up to the desired total. Except for the no-snow Case (17), all assumptions were consistent with Case 1. When the snow was absent during the entire year, it was assumed that $\alpha_i = 0.75$ if the surface temperature was below freezing and 0.64 during periods of surface melting. Figures 25 to 30 and Tables 18 to 23 present the results of these experiments.

Figure 30 shows the average equilibrium thickness as a function of maximum annual snow depth. It is surprising that, for snow depths between 0 and 70 cm, the average ice thickness remains almost unchanged; above 70 cm, the thickness increases rapidly. To explain the unusual shape of this curve, it is necessary to examine the three major variables which are influenced by the amount of snow: ice temperature, surface ice ablation, and I_o. A thinner snow cover allows greater cooling of the ice during the winter, promoting bottom accretion. If ice ablation at the surface remained constant, greater bottom accretion would lead to thicker equilibrium ice. However, when the maximum snow depth is less, the snow cover is removed earlier, thereby decreasing the average albedo and prolonging the period of ice ablation. Also, less energy is required to remove the thinner snow cover. With these effects ice ablation is greater and more short-wave radiation is absorbed within the ice. Greater ice ablation

at the surface tends to thin the ice but, as we saw in Section 4.2.1, I_o interacts with the ice in a more complex manner. Greater I_o causes more bottom ablation, tending to thin the ice, while simultaneously depriving the surface of energy which could otherwise be used for melting. Thus there are four opposing effects: two which promote thickening and two which promote thinning. Figure 30 results from the balance of these effects. When maximum snow depth lies between 0 and 70 cm, there is a mutual compensation between the thickening effects and the thinning effects; when the annual snow depth exceeds 70 cm, decreasing ice ablation and a smaller I_o dominate the balance and the ice thickens to maintain the balance.

These points are illustrated by the contrast between Case 1 and Case 17, the no-snow case. Ice surface temperatures in Case 17 are consistently lower, the maximum difference being about 10°C, while the annual average differs by 5°C. As may be seen from Fig. 25, temperature gradients within the ice are very steep during the winter months, resulting in 30 cm more bottom accretion than in Case 1. Because there is no snow to melt and because α_i is smaller than α_s, surface ice ablation is greater by 28 cm. Although net short-wave radiation is 4.5 kcal/cm^2 year higher, 2.6 kcal/cm^2 year of this excess is absorbed within the ice, producing slightly more bottom ablation. Ice thickness during the spring is somewhat greater than in Case 1, but in the fall and early winter it is appreciably less. Thus, despite large differences in the mass changes at the boundaries, the annual energy balance and thickness of the slab are only slightly affected. A similar analysis of Cases 20 to 22 shows how less net short-wave radiation and the greater snow cover combine to check surface-ice ablation and I_o. The smaller energy input to the slab rapidly becomes the dominant influence and results in the predicted thickening of the ice.

Under the assumed energy input, the maximum snow depth which may occur, without producing an annual surplus, is 120 cm. If snow accumulation exceeds this amount, equilibrium ice will grow from above and ablate from below. The metamorphism of snow into ice cannot be handled by the present model. From this series of experiments, it appears that present variations in annual snowfall over the Central Arctic have little effect on average ice thickness.

4.3 EVALUATION OF METHODS TO INFLUENCE THE ICE COVER ARTIFICIALLY

Man may be able to induce large-scale changes in climate by artificially altering the horizontal extent of pack ice in the Arctic. Although the exact climatic consequences of such changes are unknown, quantitative results from the sea-ice model may be used to evaluate the feasibility of various schemes to accomplish these changes.

Barring changes in the energy balance at the surface, the effective oceanic heat flux must be increased by nearly 400 percent (see Section 4.2.2) if the ice in the Central Arctic is to vanish. It has been proposed that, by pumping water out of the Arctic Ocean across a dam at Bering Straits, the increased inflow of Atlantic water could dissipate the ice cover (Toporkov, 1963). As Badgley (1961) has pointed out, even doubling the heat flux by this method is beyond current technological capabilities. Another scheme suggests covering the Norwegian Sea with chemicals to retard cooling, thereby producing a temperature increase of 3 to 4°C in the entering Atlantic waters (Makarova et al., 1962). This might remove ice in the peripheral seas, at least, but as the area of open water increases, more and more heat will be lost. Unless chemicals are spread across these areas also, it seems unlikely that this method can seriously affect the central basin. The conclusion must be that it is not currently feasible to remove the pack ice by artificially changing F_w. It is beyond the scope of this paper to try to estimate the necessary rise in sea level required for a four-fold increase in F_w; this estimate should be made, however, since the ice-age theories of Ewing and Donn (1956, 1958, 1966) rest on the assumption that the pack ice vanished in response to a natural rise in sea level.

It is clear from Cases 17 to 22 that artificial suppression of snowfall would be an ineffective means of decreasing the ice pack because of the compensating increase in winter bottom accretion. Early removal of the snow, perhaps by annual flooding of the floes with sea water in May or early June, offers the only possibility of using the snow to decrease ice thickness.

Table 18. COMPUTED VALUES FOR EQUILIBRIUM CONDITIONS IN SURFACE TEMPERATURE IS LESS THAN 272.9 °K.

Variable	Jan	Feb	Mar	Apr	May
Mean snow surface temperature (°C)	...	...	...	...	...
Mean ice surface temperature (°C)	-28.86	-30.80	-29.79	-21.01	-7.48
Mean ice thickness (cm)	300.2	312.7	325.4	337.1	345.2
Heat flux through surface (kcal/cm^2)	1.220	1.291	1.076	0.667	0.301
Heat flux through bottom (kcal/cm^2)	-0.930	-0.936	-0.930	-0.783	-0.496
Net short-wave radiation (kcal/cm^2)	0	0	0.597	2.490	4.346
Net long-wave radiation (kcal/cm^2)	-2.404	-2.029	-2.235	-2.781	-2.722

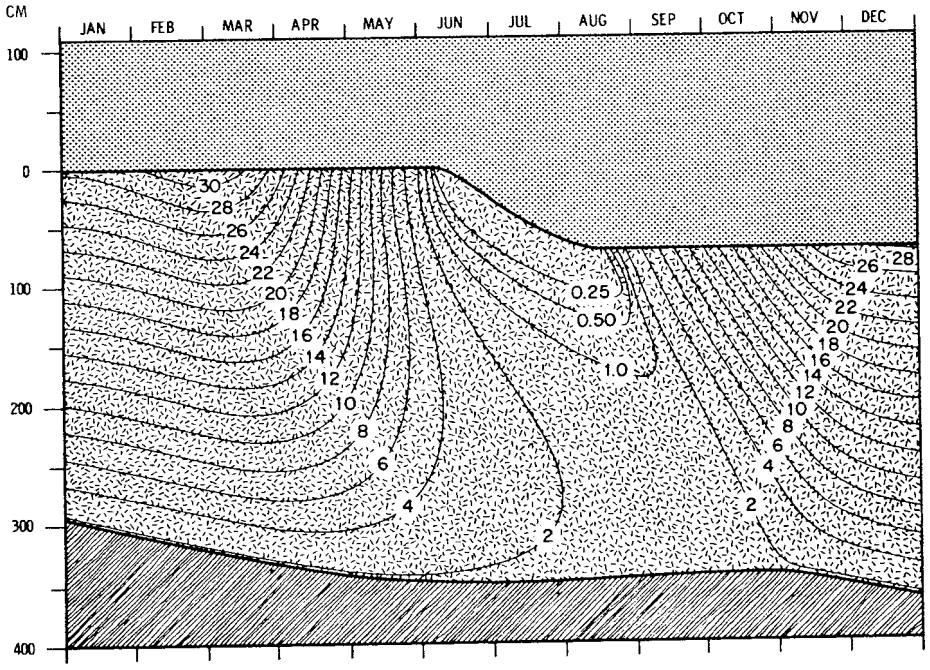

Fig. 25 -- Annual equilibrium temperature and thickness field for Case 17, maximum snow depth = 0.

CASE 17, MAXIMUM SNOW DEPTH = 0, ICE ALBEDO = 0.75 IF THE
ALL OTHER INPUT DATA AS IN CASE 1.

Jun	Jul	Aug	Sep	Oct	Nov	Dec	Year
...	...	...	...	...	...	...	...
-0.22	-0.10	-0.72	-7.89	-17.52	-25.86	-28.15	-16.53
337.3	301.9	280.9	277.3	275.0	277.2	287.7	304.8
-0.027	0.008	0.305	1.134	1.438	1.495	1.246	10.154
-0.232	-0.084	-0.013	0.020	-0.013	-0.583	-0.910	-5.889
6.313	4.959	2.909	0.945	0.142	0	0	22.700
-1.954	-0.903	-1.098	-1.279	-1.451	-2.054	-2.036	-22.946

Date	Onset	End
...	Snow ablation	
6 June	Ice ablation	
3 July		Bottom accretion
19 August		Surface ice ablation
28 October	Bottom accretion	

Other Data

Surface ice ablation*	68.5 cm
Bottom ablation	6.4 cm
Bottom accretion	74.9 cm
Short-wave radiation penetrating surface during snow-free period	3.859 kcal/cm^2

*Equals net bottom accretion.

Table 19. COMPUTED VALUES FOR EQUILIBRIUM CONDITIONS IN CASE 18,

Variable	Jan	Feb	Mar	Apr	May
Mean snow surface temperature (^{o}C)	-30.32	-32.39	-31.34	-22.51	-9.84
Mean ice surface temperature (^{o}C)	-22.67	-24.08	-24.10	-19.33	-11.04
Mean ice thickness (cm)	312.3	320.9	329.8	338.6	345.9
Heat flux through surface (kcal/cm^2)	0.916	0.969	0.821	0.347	-0.125
Heat flux through bottom (kcal/cm^2)	-0.663	-0.684	-0.701	-0.657	-0.515
Net short-wave radiation (kcal/cm^2)	0	0	0.406	1.892	3.129
Net long-wave radiation (kcal/cm^2)	-2.101	-1.708	-1.917	-2.439	-2.095

MAXIMUM SNOW DEPTH = 20 cm. ALL OTHER INPUT DATA AS IN CASE 1.

Jun	Jul	Aug	Sep	Oct	Nov	Dec	Year
-0.48	-0.10	-1.05	-9.65	-19.57	-27.78	-29.57	-17.88
-2.25	-0.10	-0.91	-7.46	-13.59	-19.19	-21.81	-13.88
348.9	324.0	303.8	300.8	299.0	299.2	304.5	319.0
-0.225	-0.007	0.287	0.763	0.966	1.087	0.954	6.753
-0.334	-0.164	-0.060	-0.016	-0.028	-0.298	-0.585	-4.705
4.851	4.959	2.710	0.605	0.085	0	0	18.637
-1.886	-0.903	-1.006	-0.813	-0.966	-1.642	-1.738	-19.214

Date	Onset	End
9 June	Snow ablation	
21 June	Ice ablation	
23 July		Bottom accretion
20 August		Surface ice ablation
2 November	Bottom accretion	

Other Data

Surface ice ablation*	50.1 cm
Bottom ablation	4.3 cm
Bottom accretion	54.4 cm
Short-wave radiation penetrating surface during snow-free period	1.557 kcal/cm^2

*Equals net bottom accretion.

Table 20. COMPUTED VALUES FOR EQUILIBRIUM CONDITIONS IN CASE 19,

Variable	Jan	Feb	Mar	Apr	May
Mean snow surface temperature (^{o}C)	-31.57	-33.77	-32.41	-22.70	-9.39
Mean ice surface temperature (^{o}C)	-15.06	-15.98	-16.19	-13.69	-8.88
Mean ice thickness (cm)	276.8	282.6	288.7	294.9	300.0
Heat flux through surface (kcal/cm^2)	0.661	0.694	0.603	0.302	-0.007
Heat flux through bottom (kcal/cm^2)	-0.483	-0.505	-0.528	-0.498	-0.399
Net short-wave radiation (kcal/cm^2)	0	0	0.406	1.893	3.129
Net long-wave radiation (kcal/cm^2)	-1.846	-1.433	-1.701	-2.398	-2.215

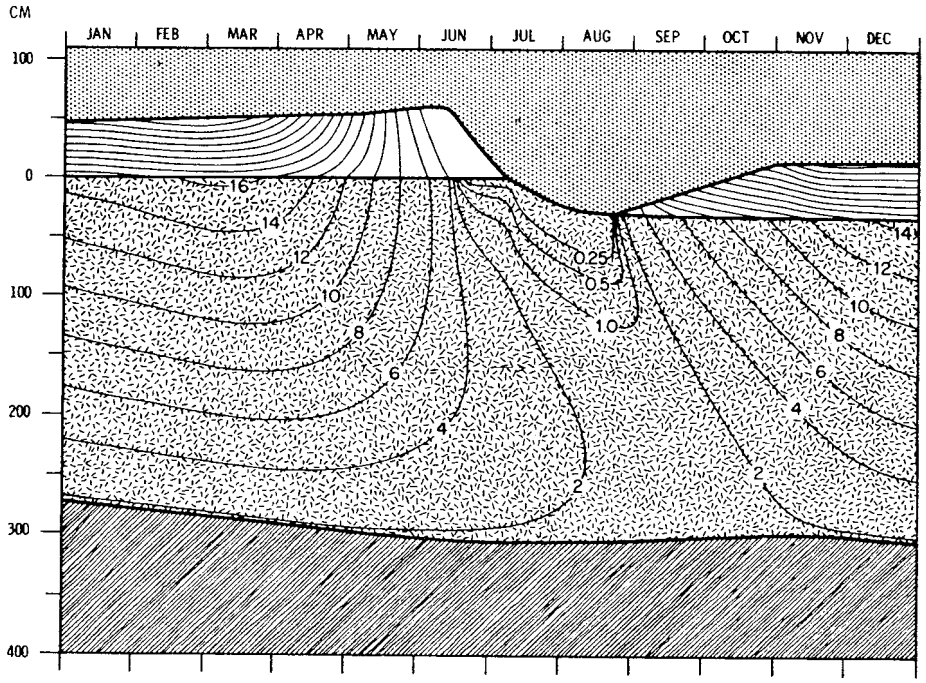

Fig. 26 -- Annual equilibrium temperature and thickness field for Case 19, maximum snow depth = 60 cm.

MAXIMUM SNOW DEPTH = 60 cm. ALL OTHER INPUT DATA AS IN CASE 1.

Jun	Jul	Aug	Sep	Oct	Nov	Dec	Year
-0.29	-0.10	-1.18	-10.39	-20.94	-29.46	-30.89	-18.59
-2.42	-0.10	-0.81	-5.51	-8.97	-12.17	-14.24	-9.50
303.2	294.1	277.9	271.7	269.6	269.0	271.7	283.3
-0.081	-0.052	0.226	0.572	0.650	0.735	0.682	4.984
-0.267	-0.133	-0.037	0.004	-0.008	-0.185	-0.391	-3.429
4.087	4.839	2.710	0.605	0.085	0	0	17.752
-1.948	-0.909	-0.967	-0.621	-0.649	-1.290	-1.467	-17.455

Date	Onset	End
7 June	Snow ablation	
6 July	Ice ablation	
17 July		Bottom accretion
19 August		Surface ice ablation
9 November	Bottom accretion	

Other Data

Surface ice ablation*	30.2 cm
Bottom ablation	5.5 cm
Bottom accretion	35.7 cm
Short-wave radiation penetrating surface during snow-free period	1.042 kcal/cm^2

*Equals net bottom accretion.

Table 21. COMPUTED VALUES FOR EQUILIBRIUM CONDITIONS IN CASE 20,

Variable	Jan	Feb	Mar	Apr	May
Mean snow surface temperature (^{o}C)	-32.08	-34.34	-32.93	-22.96	-9.47
Mean ice surface temperature (^{o}C)	-13.55	-14.51	-14.84	-12.91	-8.94
Mean ice thickness (cm)	310.3	314.1	318.6	323.3	327.4
Heat flux through surface (kcal/cm^2)	0.558	0.583	0.502	0.247	-0.028
Heat flux through bottom (kcal/cm^2)	-0.344	-0.393	-0.425	-0.416	-0.360
Net short-wave radiation (kcal/cm^2)	0	0	0.406	1.893	3.129
Net long-wave radiation (kcal/cm^2)	-1.744	-1.322	-1.599	-2.341	-2.194

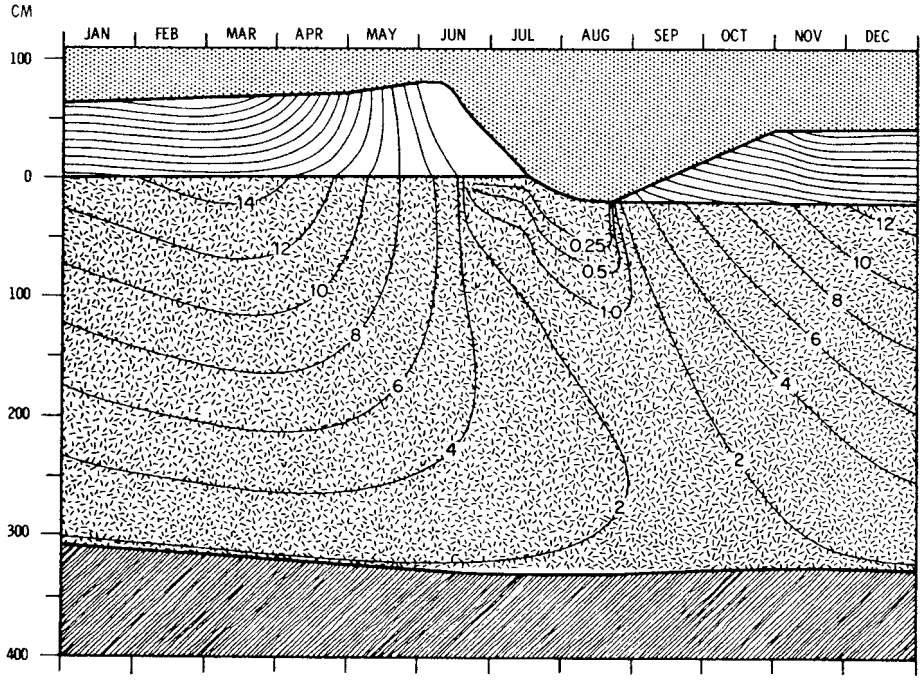

Fig. 27 -- Annual equilibrium temperature and thickness field for Case 20, maximum snow depth = 80 cm.

MAXIMUM SNOW DEPTH = 80 cm. ALL OTHER INPUT DATA AS IN CASE 1.

Jun	Jul	Aug	Sep	Oct	Nov	Dec	Year
-0.28	-0.10	-1.23	-10.71	-21.40	-30.00	-31.41	-18.91
-2.92	-0.10	-0.77	-5.19	-8.12	-10.72	-12.62	-8.77
330.4	328.0	316.7	310.0	308.3	306.9	307.5	316.8
-0.083	-0.040	0.213	0.489	0.543	0.624	0.577	4.186
-0.265	-0.157	-0.069	-0.025	-0.013	-0.085	-0.238	-2.790
3.940	4.516	2.710	0.605	0.085	0	0	17.282
-1.949	-0.918	-0.954	-0.538	-0.543	-1.177	-1.362	-16.642

Date	Onset	End
7 June	Snow ablation	
15 July	Ice ablation	
24 July		Bottom accretion
19 August		Surface ice ablation
24 November	Bottom accretion	

Other Data

Surface ice ablation*	20.2 cm
Bottom ablation	4.8 cm
Bottom accretion	25.0 cm
Short-wave radiation penetrating surface during snow-free period	0.775 kcal/cm^2

*Equals net bottom accretion.

Table 22. COMPUTED VALUES FOR EQUILIBRIUM CONDITIONS IN CASE 21,

Variable	Jan	Feb	Mar	Apr	May
Mean snow surface temperature (^{o}C)	-32.51	-34.81	-33.40	-23.29	-9.60
Mean ice surface temperature (^{o}C)	-13.00	-14.02	-14.61	-13.27	-9.96
Mean ice thickness (cm)	406.2	407.5	409.7	412.4	415.3
Heat flux through surface (kcal/cm^2)	0.473	0.492	0.409	0.174	-0.061
Heat flux through bottom (kcal/cm^2)	-0.176	-0.241	-0.285	-0.308	-0.303
Net short-wave radiation (kcal/cm^2)	0	0	0.406	1.893	3.129
Net long-wave radiation (kcal/cm^2)	-1.658	-1.231	-1.506	-2.267	-2.160

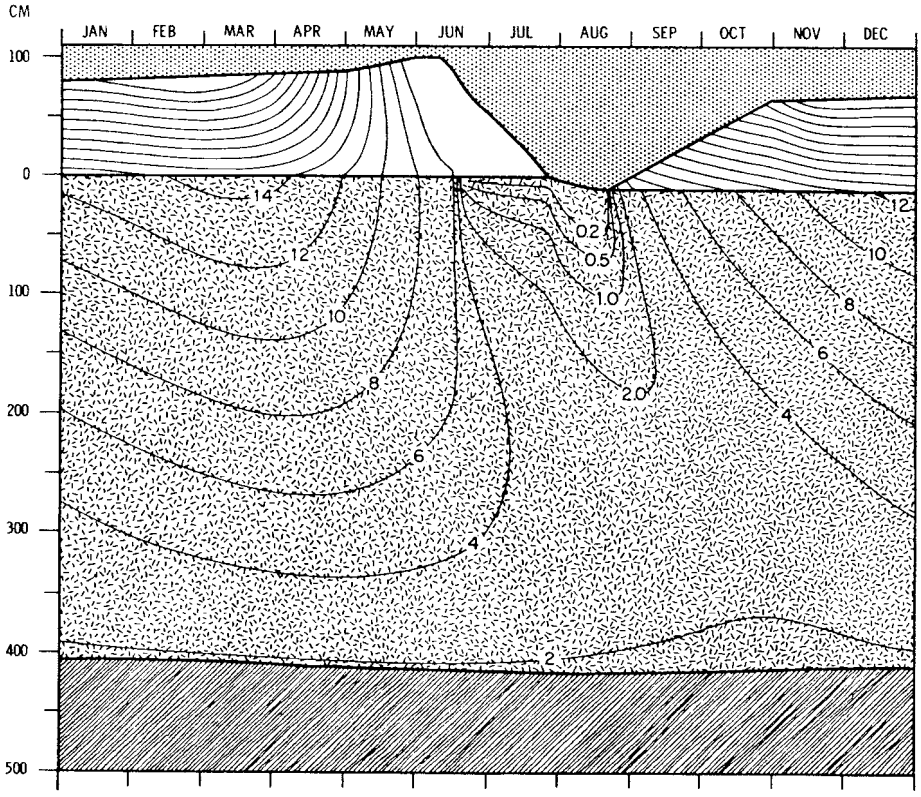

Fig. 28 -- Annual equilibrium temperature and thickness field for Case 21, maximum snow depth = 100 cm.

MAXIMUM SNOW DEPTH = 100 cm. ALL OTHER INPUT DATA AS IN CASE 1.

Jun	Jul	Aug	Sep	Oct	Nov	Dec	Year
-0.29	-0.10	-1.28	-11.02	-21.80	-30.48	-31.85	-19.20
-3.82	-0.10	-0.76	-5.27	-8.06	-10.36	-12.07	-8.78
417.8	419.0	415.8	409.0	408.0	406.8	406.1	411.1
-0.094	-0.023	0.188	0.410	0.453	0.524	0.487	3.432
-0.262	-0.194	-0.124	-0.077	-0.052	-0.056	-0.101	-2.179
3.874	4.140	2.710	0.605	0.085	0	0	16.841
-1.946	-0.928	-0.940	-0.459	-0.453	-1.079	-1.271	-15.898

Date	Onset	End
7 June	Snow ablation	
25 July	Ice ablation	
14 August		Bottom accretion
19 August		Surface ice ablation
26 December	Bottom accretion	

Other Data

Surface ice ablation*	10.6 cm
Bottom ablation	3.4 cm
Bottom accretion	14.0 cm
Short-wave radiation penetrating surface during snow-free period	0.502 kcal/cm^2

*Equals net bottom accretion.

Table 23. COMPUTED VALUES FOR EQUILIBRIUM CONDITIONS IN CASE 22,

Variable	Jan	Feb	Mar	Apr	May
Mean snow surface temperature (°C)	-32.97	-35.29	-33.84	-23.59	-9.70
Mean ice surface temperature (°C)	-14.08	-15.07	-15.73	-14.74	-11.91
Mean ice thickness (cm)	702.0	701.5	701.2	701.2	701.4
Heat flux through surface (kcal/cm^2)	0.381	0.398	0.323	0.108	-0.085
Heat flux through bottom (kcal/cm^2)	-0.092	-0.099	-0.113	-0.131	-0.151
Net short-wave radiation (kcal/cm^2)	0	0	0.406	1.893	3.129
Net long-wave radiation (kcal/cm^2)	-1.567	-1.137	-1.419	-2.200	-2.134

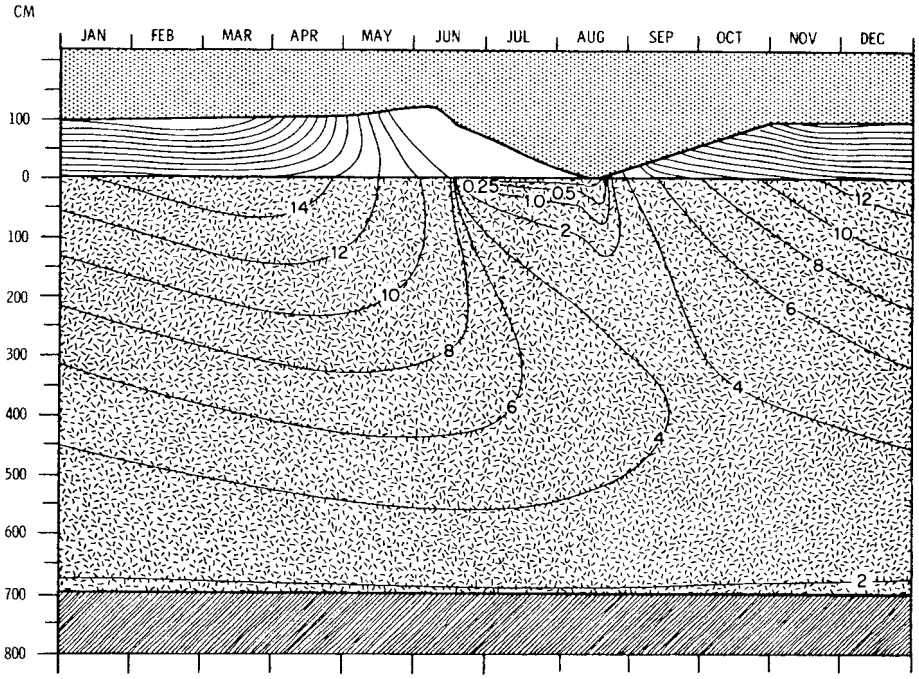

Fig. 29 -- Annual equilibrium temperature and thickness field for Case 22, maximum snow depth = 120 cm. The scale is not suitable for comparison with Fig. 6.

MAXIMUM SNOW DEPTH = 120 cm. ALL OTHER INPUT DATA AS IN CASE 1.

Jun	Jul	Aug	Sep	Oct	Nov	Dec	Year
-0.29	-0.10	-1.50	-11.42	-22.21	-30.96	-32.32	-19.52
-5.44	-0.10	-1.07	-6.21	-9.12	-11.43	-13.15	-9.84
701.9	702.6	702.9	703.0	703.0	702.8	702.3	702.2
-0.108	0	0.111	0.306	0.360	0.426	0.394	2.614
-0.165	-0.170	-0.160	-0.138	-0.117	-0.101	-0.092	-1.531
3.827	3.750	2.643	0.605	0.085	0	0	16.338
-1.944	-0.932	-0.890	-0.356	-0.360	-0.981	-1.178	-15.097

Date	Onset	End
5 April	Bottom accretion	
7 June	Snow ablation	
12 August	Ice ablation	
18 August		Surface ice ablation
4 October		Bottom accretion

Other Data

Surface ice ablation*	0.5 cm
Bottom ablation	2.1 cm
Bottom accretion	2.6 cm
Short-wave radiation penetrating surface during snow-free period	0.143 kcal/cm^2

*Equals net bottom accretion.

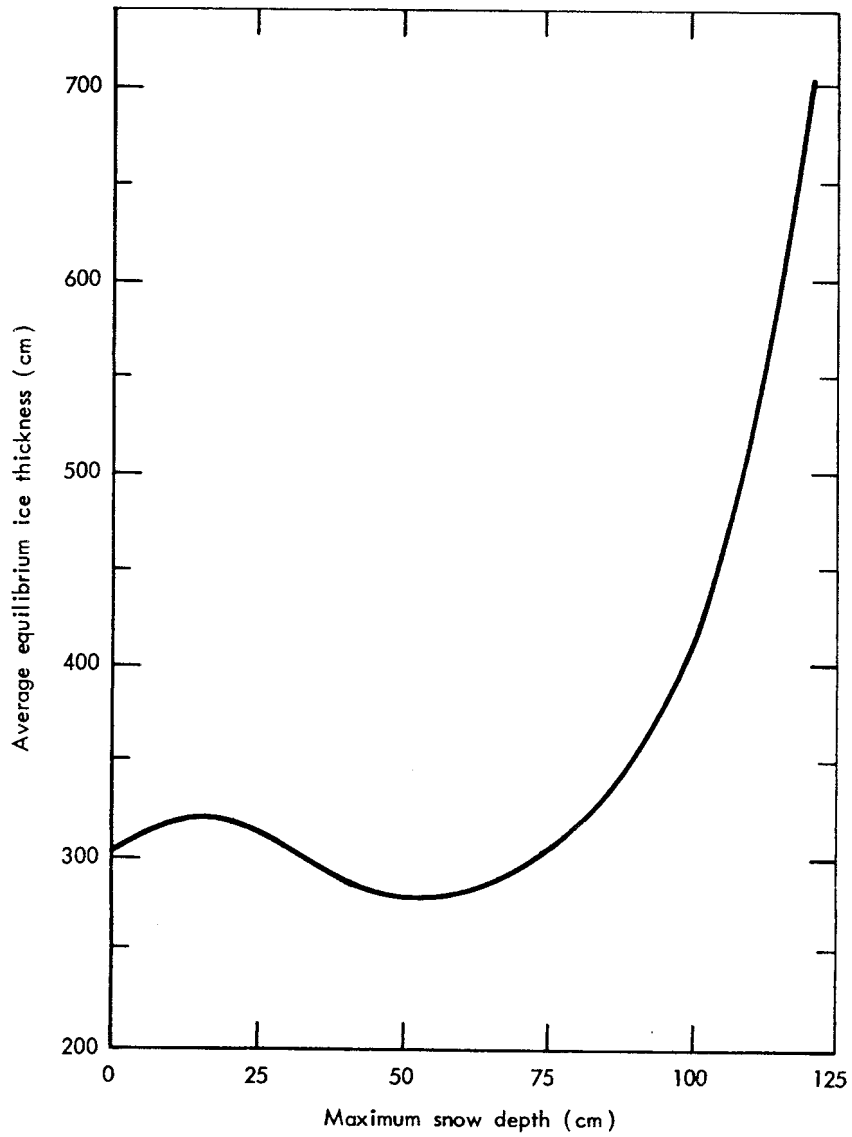

Fig. 30 -- Average equilibrium thickness of ice as a function of maximum annual snow depth.

In addition to the previously discussed possibilities, the energy balance could be influenced by artificial modification of surface albedo, long-wave emissivity, incoming long-wave and short-wave radiation, or the turbulent fluxes. In the remainder of this section we shall examine these approaches.

4.3.1 Influencing the turbulent heat fluxes

Although the flux of latent heat (F_ℓ) and the flux of sensible heat (F_s) are small compared with the radiative fluxes, they are not negligible when compared with the net energy balance at the surface. According to Doronin (see Table 1), the annual sum of F_s and F_ℓ is only -0.5 kcal/cm^2 year. At first it appears unlikely that this small amount of energy could significantly influence ice thickness; however, closer scrutiny reveals that variations in F_s and F_ℓ can play a large part in determining surface conditions, particularly during the ablation period. Case 23 illustrates these points by arbitrarily assuming that $F_s = F_\ell = 0$ during the entire year. The results are given in Table 24 and Fig. 31.

Because the sensible heat flux normally supplies about 0.75 kcal/cm^2 month to the surface during the winter, surface temperatures during this time are 2 to 3°C lower in Case 23 than Case 1; the annual average temperature remains unchanged. Over 3 kcal/cm^2 is presently lost by the surface during the ablation season by means of the turbulent fluxes. Eliminating this loss results in 85 cm of ice ablation and an equilibrium thickness of 107 cm. This is roughly the same thickness change that was achieved when F_w was increased to 4.5 kcal/cm^2 year (Case 15) or when α_i is reduced by 10 percent (Case 26). The ice would have been even thinner in Case 23 if F_s and F_ℓ had been set to zero during the melt period only. However, in interpreting this experiment, it should be borne in mind that the input data for the turbulent fluxes in the air boundary layer are not only the least reliable (Fletcher, 1965; Vowinckel and Taylor, 1964), but also the most sensitive to those feedback effects that are not accounted for in the model.

Although there appears to be no direct way of appreciably influencing F_s, the flux of latent heat could be lessened by reducing evaporation during the summer. If evaporation could be completely eliminated between June and August, an additional 20 to 25 cm of ice ablation would occur, reducing equilibrium thickness to between 150 and 175 cm. This suggests that, at least for the Central Arctic, ice thickness might more effectively be reduced by retarding evaporation from the ice, rather than from the Norwegian Sea.

4.3.2 Influencing the incoming radiative fluxes

The current advances being made in weather modification offer hope that cloudiness may be controlled to some extent in the future. Cloudiness plays the major role in determining the amount of long-wave and short-wave radiation reaching the surface. Without specifying what cloud conditions would be required, two cases involving increases in the incoming radiation fluxes were investigated.

In Case 24 the incoming short-wave radiation (F_r) is made greater by 10 percent, or 7.5 kcal/cm^2 year, while all other assumptions are unchanged from Case 1. Figure 32 and Table 25 show the results. The net short-wave radiation increases by only 1.6 kcal/cm^2 year, because of the high albedo of the surface. Snow melt begins earlier and I_o is only 0.4 kcal/cm^2 year greater. Thus the solar energy available for melting and heating at the surface is only about 1.2 kcal/cm^2 year greater than in Case 1. Ice ablation is 19 cm more at the surface and 5 cm more at the bottom, resulting in 120 cm less in the average equilibrium thickness. The greater surface temperatures are due primarily to the lesser ice thickness.

For Case 25 the incoming long-wave radiation (F_L) has been increased by 10 percent from October through April, simulating a greater winter cloudiness than in Case 1. Table 26 and Fig. 33 show the results of this integration. Surface temperatures for October through April are about 5°C higher, but they remain relatively unchanged during the rest of the year. Net long-wave radiation is also the same since adjustments in the surface temperatures compensate for a greater F_L.

Surface ablation is unchanged, but bottom ablation is greater by 60 percent. The greater bottom ablation is then responsible for an 85-cm decrease in equilibrium thickness.

Although it is not clear to what extent artificial cloud modification could influence F_r or F_L, the changes assumed in Cases 24 and 25 are probably within the range of natural variations. It seems unlikely that artificial changes would be much greater. Controlling cloudiness thus appears to be one of the less promising avenues to ice control.

4.3.3 Modifying the surface

Because of the magnitude of the incoming solar radiation, a small reduction in surface albedo would provide a large increase in available energy at the surface. Dispersal of some dark substance, such as coal dust, over the surface might accomplish this reduction. A more feasible method might be to introduce snow lichen, which could then propagate itself naturally (Fletcher, 1965). In Case 26 it has been assumed that, by some unspecified means, the albedo has been reduced by 10 percent from 1 June until the onset of snow accumulation. Albedos during the rest of the year are assumed to be the same as in Case 1. Results of the integration are given in Fig. 34 and Table 27. Comparison with Case 1 shows an excess of net short-wave radiation of 4 kcal/cm^2 year, with an attendant deficiency in average equilibrium thickness of nearly 200 cm. Surface ablation has doubled, bottom ablation tripled, and I_o is 1 kcal/cm^2 year greater. Temperatures and the dependent fluxes behave as would be expected for ice of 100 cm thickness.

When summer albedo was decreased by 20 percent (Case 27), the ice vanished during the summer of the third year, before equilibrium could be established.

If the experiments suggested in Cases 26 and 27 were actually carried out, it is probable that the resulting thickness changes would be even greater than predicted. The dispersal of any dark substance on the surface would naturally reduce I_o. If I_o were reduced by one-half, an additional 15 cm of surface ice ablation would occur, enough to reduce the equilibrium thickness in Case 26 to less than 50 cm.

Table 24. COMPUTED VALUES FOR EQUILIBRIUM CONDITIONS IN

Variable	Jan	Feb	Mar	Apr	May
Mean snow surface temperature (^{o}C)	-34.01	-35.00	-33.25	-21.97	-6.08
Mean ice surface temperature (^{o}C)	-12.43	-13.53	-13.79	-10.70	-5.05
Mean ice thickness (cm)	108.6	123.0	136.7	148.2	154.8
Heat flux through surface (kcal/cm^2)	1.283	1.244	1.094	0.608	0.045
Heat flux through bottom (kcal/cm^2)	-1.055	-1.034	-0.957	-0.728	-0.372
Net short-wave radiation (kcal/cm^2)	0	0	0.406	1.893	3.129
Net long-wave radiation (kcal/cm^2)	-1.283	-1.244	-1.504	-2.507	-3.179

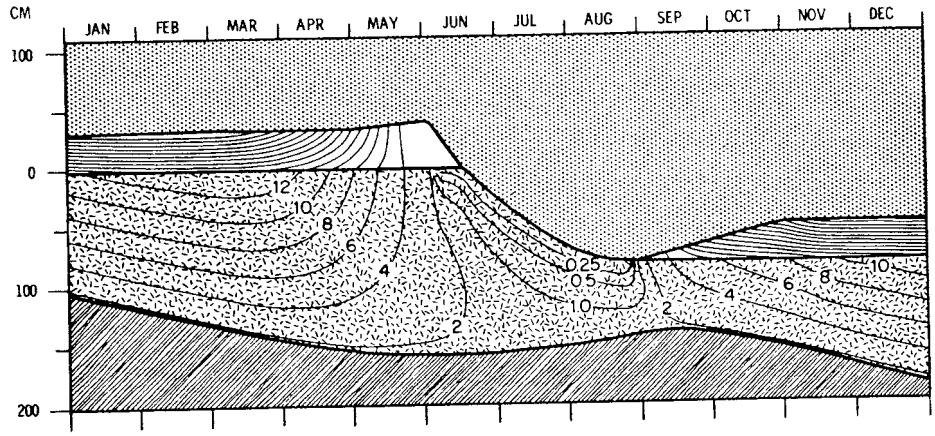

Fig. 31 -- Annual equilibrium temperature and thickness field for Case 23, $F_s = F_\ell = 0$.

CASE 23, $F_s = F_\ell = 0$. ALL OTHER INPUT DATA AS IN CASE 1.

Jun	Jul	Aug	Sep	Oct	Nov	Dec	Year
-0.10	-0.10	-0.33	-7.79	-19.19	-29.43	-32.01	-18.27
-0.27	-0.10	-0.28	-4.24	-6.89	-9.34	-11.03	-7.30
149.0	103.0	66.6	58.4	66.6	79.2	93.9	107.3
-0.099	-0.187	-0.127	0.693	1.002	1.265	1.280	8.102
-0.065	0.203	0.340	-0.317	-0.822	-1.026	-1.074	-6.907
5.678	4.959	2.987	0.605	0.085	0	0	19.740
-2.015	-0.865	-1.267	-1.297	-1.086	-1.262	-1.281	-18.790

Date	Onset	End
1 June	Snow ablation	
10 June		Bottom accretion
14 June	Ice ablation	
26 August		Surface ice ablation
9 September	Bottom accretion	

Other Data

Surface ice ablation*	84.5 cm
Bottom ablation	15.0 cm
Bottom accretion	99.5 cm
Short-wave radiation penetrating surface during snow-free period	1.896 kcal/cm^2

*Equals net bottom accretion.

Table 25. COMPUTED VALUES FOR EQUILIBRIUM CONDITIONS IN CASE 24, 10% INCREASE IN

Variable	Jan	Feb	Mar	Apr	May
Mean snow surface temperature (^{o}C)	-30.11	-32.24	-30.85	-21.06	-7.95
Mean ice surface temperature (^{o}C)	-13.99	-15.05	-15.20	-12.04	-6.63
Mean ice thickness (cm)	166.7	177.0	187.3	196.7	202.9
Heat flux through surface (kcal/cm^2)	0.959	0.998	0.880	0.486	0.060
Heat flux through bottom (kcal/cm^2)	-0.779	-0.786	-0.778	-0.644	-0.402
Net short-wave radiation (kcal/cm^2)	0	0	0.447	2.082	3.442
Net long-wave radiation (kcal/cm^2)	-2.145	-1.736	-2.018	-2.771	-2.596

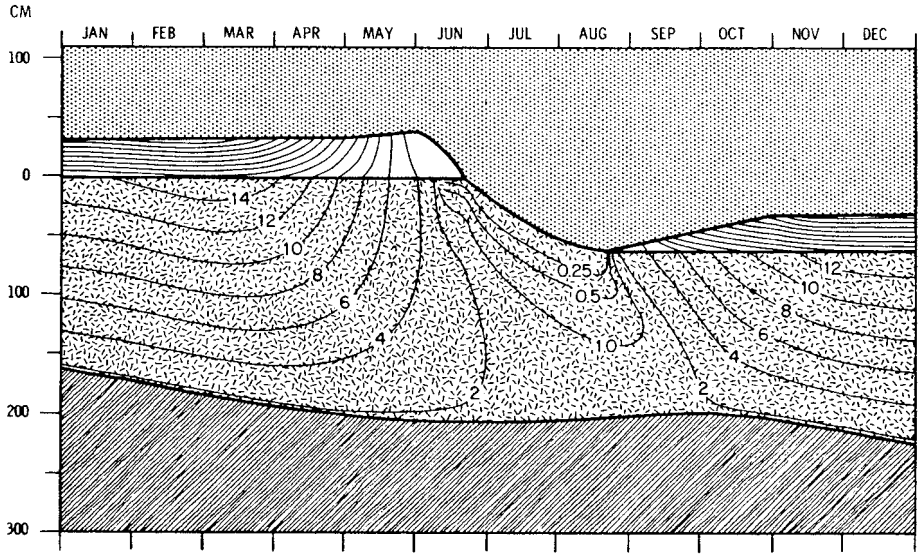

Fig. 32 -- Annual equilibrium temperature and thickness field for Case 24, 10 percent increase in the amount of incoming short-wave radiation.

THE AMOUNT OF INCOMING SHORT-WAVE RADIATION. ALL OTHER INPUT DATA AS IN CASE 1.

Jun	Jul	Aug	Sep	Oct	Nov	Dec	Year
-0.10	-0.10	-0.94	-9.45	-20.02	-28.20	-29.48	-17.54
-0.95	-0.10	-0.70	-5.20	-9.44	-12.34	-13.52	-8.76
203.2	170.6	144.0	137.6	138.0	145.9	156.3	168.9
-0.076	-0.073	0.179	0.757	0.853	0.999	0.973	6.994
-0.180	0.041	0.150	0.109	-0.460	-0.741	-0.802	-5.271
5.520	5.455	3.039	0.665	0.094	0	0	20.742
-2.000	-0.903	-1.037	-0.867	-0.861	-1.552	-1.758	-20.243

Date	Onset	End
2 June	Snow ablation	
21 June	Ice ablation	
23 June		Bottom accretion
21 August		Surface ice ablation
1 October	Bottom accretion	

Other Data

Surface ice ablation*	58.9 cm
Bottom ablation	10.7 cm
Bottom accretion	69.6 cm
Short-wave radiation penetrating surface during snow-free period	1.715 kcal/cm^2

*Equals net bottom accretion.

Table 26. COMPUTED VALUES FOR EQUILIBRIUM CONDITIONS IN CASE 25, THROUGH APRIL. ALL OTHER

Variable	Jan	Feb	Mar	Apr	May
Mean snow surface temperature (^{o}C)	-26.08	-28.15	-26.78	-17.95	-8.61
Mean ice surface temperature (^{o}C)	-13.31	-14.25	-14.30	-11.18	-6.93
Mean ice thickness (cm)	198.5	206.2	214.2	221.6	226.7
Heat flux through surface (kcal/cm^2)	0.766	0.812	0.705	0.366	0.081
Heat flux through bottom (kcal/cm^2)	-0.615	-0.631	-0.633	-0.539	-0.371
Net short-wave radiation (kcal/cm^2)	0	0	0.406	1.893	3.129
Net long-wave radiation (kcal/cm^2)	-1.951	-1.551	-1.803	-2.460	-2.303

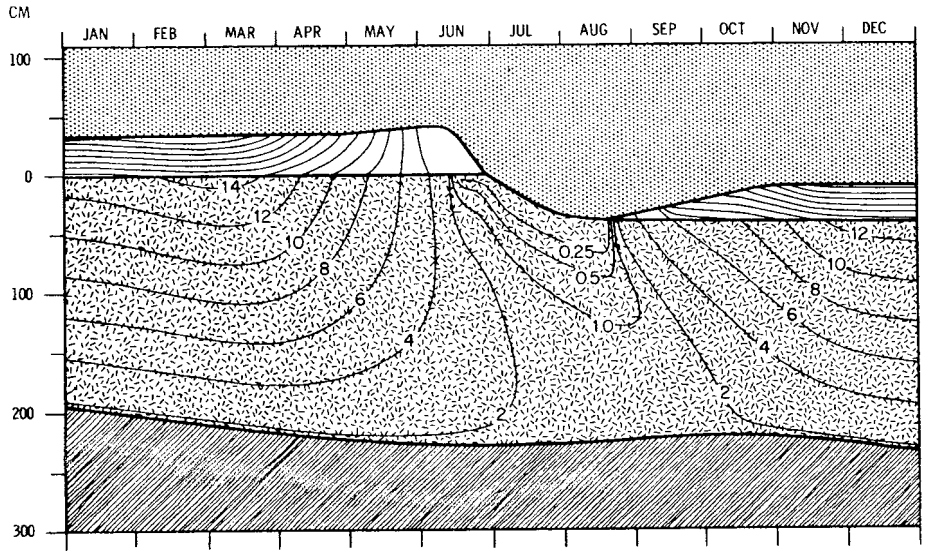

Fig. 33 -- Annual equilibrium temperature and thickness field for Case 25, 10 percent increase in the amount of incoming long-wave radiation during October-April.

10% INCREASE IN THE AMOUNT OF INCOMING LONG-WAVE RADIATION OCTOBER
INPUT DATA AS IN CASE 1.

Jun	Jul	Aug	Sep	Oct	Nov	Dec	Year
-0.32	-0.10	-1.23	-9.41	-15.81	-23.76	-25.36	-15.30
-1.58	-0.10	-0.96	-5.62	-8.09	-11.29	-12.87	-8.37
229.1	208.7	190.2	183.0	181.1	184.1	190.8	202.8
-0.083	-0.069	0.213	0.678	0.624	0.794	0.767	5.653
-0.209	-0.032	0.068	0.083	-0.150	-0.460	-0.603	-4.091
4.431	4.959	2.710	0.605	0.085	0	0	18.217
-1.960	-0.903	-0.978	-0.728	-0.624	-1.347	-1.552	-18.160

Date	Onset	End
7 June	Snow ablation	
28 June	Ice ablation	
1 July		Bottom accretion
18 August		Surface ice ablation
13 October	Bottom accretion	

Other Data

Surface ice ablation*	40.6 cm
Bottom ablation	8.2 cm
Bottom accretion	48.8 cm
Short-wave radiation penetrating surface during snow-free period	1.291 kcal/cm^2

*Equals net bottom accretion.

Another possibility is that long-wave emissivity (ε_L) and absorptivity might also be reduced. Since outgoing long-wave radiation is considerably greater than incoming, a decrease in ε_L would reduce the net heat loss from the surface. It is not obvious, however, to what extent the resulting temperature increase would affect ice thickness. In Case 28, all external parameters are the same as in Case 1, with the exception that ε_L has been specified as 0.8, a reduction of 20 percent. The equilibrium temperature field is shown in Fig. 35. The average surface temperature (Table 28) is 2°C higher than in Case 1, and monthly temperatures at the ice/snow interface are up to 7°C higher. Surface ice ablation has increased by one-third, and the average equilibrium thickness decreased to slightly more than 50 percent of Case 1. The net short-wave radiation has increased by 1 kcal/cm^2 year because of the shorter time required to melt the snow and the resulting lower albedo. The net long-wave radiation actually becomes slightly more negative because of the higher surface temperatures.

The thickness decrease in Case 28 can be attributed to two factors: higher temperatures and increased surface ablation. The increased ablation is due to greater net short-wave radiation and a less negative net long-wave balance during the melt season; the higher temperatures are a result of the thinner ice and the smaller amount of upward long-wave radiation. Although it is not possible to separate these effects, a general idea of the efficiency of each may be obtained by a comparison with other cases. The ice ablation and surface temperatures in Case 7 ($I_o = 0$) were roughly the same as in Case 28, but the thickness decreased by only 45 cm as compared to 130 cm in the present case. During the first year that ε_L was decreased, monthly surface temperatures increased by about 1.5°C in the fall and winter. Since the ice thickness was still about 275 cm, this increase must result from the change in ε_L alone and not from a thickness decrease. Thus raising the surface temperature by only 1.5°C caused roughly an additional 85 cm decrease in the equilibrium thickness. Although we have shown that ice thickness is quite sensitive to surface temperature, this temperature should be distinguished from the air (screen) temperature, about which no statement may be made at this stage.

The cases discussed in this section suggest that modification of the snow or ice surface is the most effective means of large-scale ice removal. Ideally, the surface should be covered with a substance that reduces not only the albedo and I_o, but evaporation and long-wave emissivity as well. However, in addition to the logistical problems involved in such a project, it may be difficult to find a material with a long-wave emissivity substantially less than one. Furthermore, a finely distributed dark solid, like coal dust, would rapidly melt into the ice and lose its effectiveness. The ideal material would be dark, nontoxic, lighter than water, slowly soluble in water, and have a low emissivity. A systematic search should be made to find a substance with an optimal combination of these properties.

Table 27. COMPUTED VALUES FOR EQUILIBRIUM CONDITIONS IN CASE 26, 10% REDUCTION

Variable	Jan	Feb	Mar	Apr	May
Mean snow surface temperature (^{o}C)	-29.41	-31.58	-30.40	-21.32	-8.77
Mean ice surface temperature (^{o}C)	-10.86	-12.08	-12.45	-10.01	-5.62
Mean ice thickness (cm)	107.1	119.5	131.8	142.3	148.8
Heat flux through surface (kcal/cm^2)	1.104	1.131	1.010	0.613	0.154
Heat flux through bottom (kcal/cm^2)	-0.914	-0.923	-0.888	-0.687	-0.392
Net short-wave radiation (kcal/cm^2)	0	0	0.406	1.893	3.129
Net long-wave radiation (kcal/cm^2)	-2.289	-1.870	-2.108	-2.709	-2.377

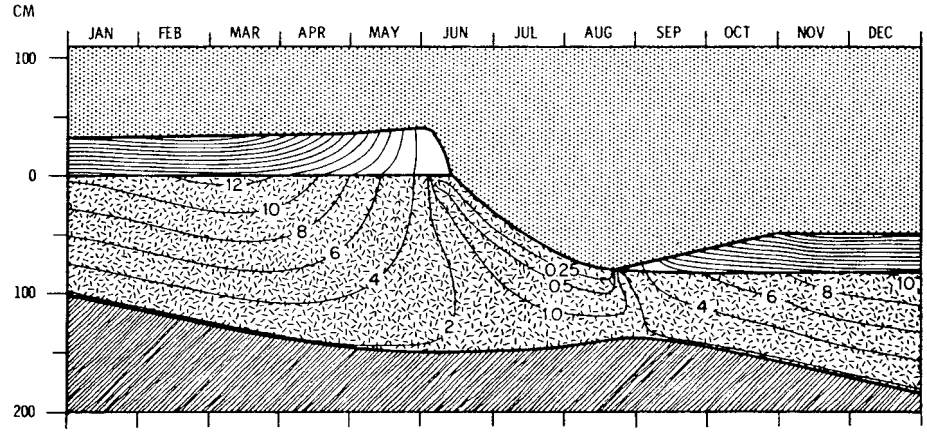

Fig. 34 -- Annual equilibrium temperature and thickness field for Case 26, 10 percent reduction in the surface albedo during June-August.

IN THE SURFACE ALBEDO JUNE THROUGH AUGUST. ALL OTHER INPUT DATA AS IN CASE 1.

Jun	Jul	Aug	Sep	Oct	Nov	Dec	Year
-0.10	-0.10	-0.99	-9.57	-19.45	-27.43	-28.70	-17.32
-0.26	-0.10	-0.73	-5.10	-7.07	-8.95	-10.10	-6.94
141.8	95.7	63.6	59.7	69.1	81.1	94.4	104.6
-0.103	-0.172	0.098	0.785	0.995	1.163	1.135	7.913
-0.058	0.240	0.381	-0.524	-0.827	-0.955	-0.964	-6.510
7.138	5.841	3.194	0.605	0.085	0	0	22.290
-1.999	-0.903	-1.022	-0.834	-0.994	-1.716	-1.920	-20.742

Date	Onset	End
1 June	Snow ablation	
12 June	Ice ablation	
12 June		Bottom accretion
21 August		Surface ice ablation
3 September	Bottom accretion	

Other Data

Surface ice ablation*	78.3 cm
Bottom ablation	15.1 cm
Bottom accretion	93.4 cm
Short-wave radiation penetrating surface during snow-free period	2.245 kcal/cm^2

*Equals net bottom accretion.

Table 28. COMPUTED VALUES FOR EQUILIBRIUM CONDITIONS IN CASE 28, 20%

Variable	Jan	Feb	Mar	Apr	May
Mean snow surface temperature (^{o}C)	-27.97	-30.31	-28.93	-19.34	-6.98
Mean ice surface temperature (^{o}C)	-12.78	-13.85	-14.01	-10.93	-5.92
Mean ice thickness (cm)	158.9	168.6	178.6	187.5	193.2
Heat flux through surface (kcal/cm^2)	0.903	0.955	0.839	0.452	0.048
Heat flux through bottom (kcal/cm^2)	-0.746	-0.757	-0.753	-0.612	-0.372
Net short-wave radiation (kcal/cm^2)	0	0	0.406	1.892	3.129
Net long-wave radiation (kcal/cm^2)	-2.089	-1.693	-1.936	-2.548	-2.270

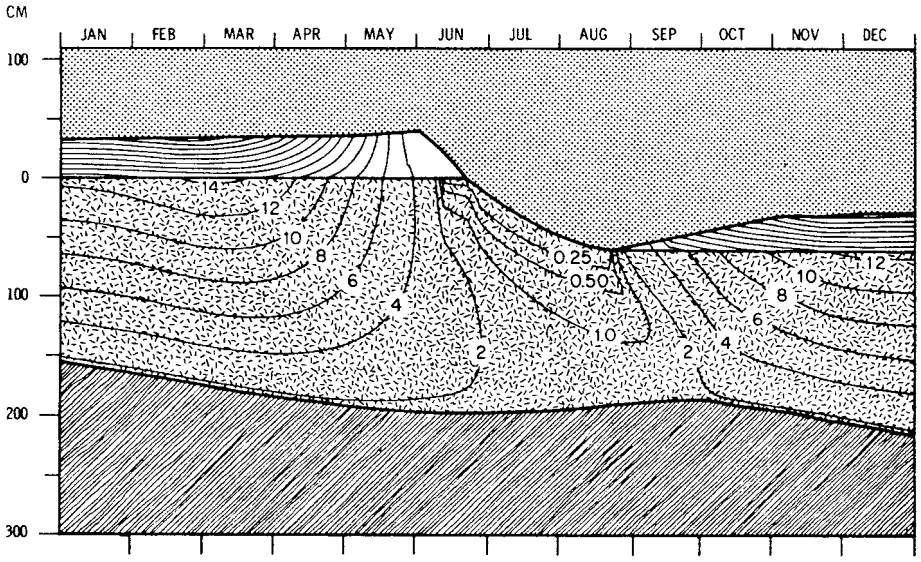

Fig. 35 -- Annual equilibrium temperature and thickness field for Case 28, 20 percent reduction in the long-wave emissivity.

REDUCTION IN THE LONG-WAVE EMISSIVITY. ALL OTHER INPUT DATA AS IN CASE 1.

Jun	Jul	Aug	Sep	Oct	Nov	Dec	Year
-0.08	-0.10	-0.84	-9.03	-19.25	-26.67	-27.63	-16.43
-0.67	-0.10	-0.63	-4.96	-9.00	-11.50	-12.47	-8.07
192.6	161.1	136.5	130.1	130.9	138.9	148.9	160.5
-0.072	-0.086	0.141	0.734	0.827	0.955	0.924	6.620
-0.151	0.065	0.164	0.105	-0.480	-0.729	-0.777	-5.045
5.166	4.959	2.789	0.605	0.085	0	0	19.031
-1.603	-0.731	-0.841	-0.784	-0.827	-1.509	-1.709	-18.540

Date	Onset	End
1 June	Snow ablation	
20 June	Ice ablation	
20 June		Bottom accretion
22 August		Surface ice ablation
29 September	Bottom accretion	

Other Data

Surface ice ablation*	55.4 cm
Bottom ablation	11.4 cm
Bottom accretion	66.8 cm
Short-wave radiation penetrating surface during snow-free period	1.605 kcal/cm^2

*Equals net bottom accretion.

Table 29. SUMMARY OF CASES COMPUTED

[The "Standard Case" is based on Fletcher's data (Table 1, p. 27). For all subsequent cases, only the deviations from the input data of Case 1 are listed.]

Case	Table	Page	Mean Annual Ice Thickness (cm)	Characteristics
1	2	54	288	Fletcher's heat budget and F_w = 1.5 kcal/cm^2 year (The "standard case")
2	4	62	310	Uniform, low ice salinity (0.09 °/oo)
3	5	66	99	Uniform, low ice salinity (0.09 °/oo) and F_w = 4.5 kcal/cm^2 year
4	6	68	349	Uniform, low ice salinity (0.09 °/oo) and near-fresh water (-0.1°C) below the ice
5	...	...	no ice	Vowinckel/Orvig heat budget (Table 7, p. 71)
6	8	72	~560	Vowinckel/Orvig heat budget (Table 7) and albedo of Marshunova (Table 1)
7	9	76	243	I_o = 0% of F_r. No fraction of the short-wave radiation penetrating the ice surface
8	10	78	262	I_o = 8.5% of F_r during snow-free period
9	11	80	324	I_o = 25.5% of F_r during snow-free period
10	12	82	368	I_o = 34.0% of F_r during snow-free period
11	13	86	229	I_o = 34.0% of F_r during snow-free period and ice albedo lowered to 0.58
12	14	90	561	F_w = 0. No heat flux in the ocean
13	15	92	391	F_w = 0.75 kcal/cm^2 year
14	16	94	162	F_w = 3.0 kcal/cm^2 year
15	17	96	93	F_w = 4.5 kcal/cm^2 year
16	...	...	no ice	F_w = 6.0 kcal/cm^2 year
17	18	102	305	No snow (h_{max} = 0). Ice albedo = 0.75 if below 272.9°K surface temperature
18	19	104	319	h_{max} = 20 cm
19	20	106	283	h_{max} = 60 cm
20	21	108	317	h_{max} = 80 cm
21	22	110	411	h_{max} = 100 cm
22	23	112	702	h_{max} = 120 cm
23	24	118	107	F_s = F_ℓ = 0. No flux of sensible or latent heat
24	25	120	169	F_r increased by 10%
25	26	122	203	F_L (incoming long-wave) increased by 10% during October-April
26	27	126	105	Albedo reduced by 0.1 during June-August
27	...	...	no ice	Albedo reduced by 0.2 during June-August
28	28	128	160	Long-wave emissivity reduced from 1.0 to 0.8

V. DISCUSSION AND SUGGESTIONS FOR FUTURE RESEARCH

To assist the reader in making his own comparisons among the 28 cases, Table 29 displays, in briefest form, the parameters varied for each case and the resulting equilibrium thickness for each. Also, inside the back cover is an overlay that permits direct visual comparison of Case 1 with any other.

Numerical integration of the sea-ice model has shown that it is internally consistent, and, within its inherent limitations, capable of predicting the behavior of sea ice under a variety of postulated conditions. The experiments described in the previous chapter have afforded an insight into the complex relationship between ice thickness and both the dependent and independent energy fluxes. Besides the information generated internally by varying the model, there are areas of consistency or inconsistency between the model and field observation that merit discussion. The performance of the model has been examined for varying values of the input parameters, and the results compared with present observations. In this way, it has been possible to suggest probable values for many of the external parameters. Analysis of the results has also pointed out features of the energy budget that deserve priority in future field studies.

Wittmann and Schule (1966) believe that open leads are so extensive in the Arctic that most of the heat transfer between the ocean and the atmosphere would occur in these areas. The results of Cases 1 and 12 to 16 indicate that 1 to 2 kcal/cm^2 year must be supplied to the ice by the ocean. It is estimated from sparse oceanographic data that only 2.0 to 2.5 kcal/cm^2 year are advected into the central Arctic Ocean (Crary, 1960). If the model is correct, it is not possible to reconcile Wittmann and Schule's observations and the oceanographic information with the present ice thickness. Further study is needed to clarify this problem.

Information about the penetration of the ice by short-wave radiation (Untersteiner, 1961; Chernigovskii, 1963) is generally deficient.

This is unfortunate, as Cases 1 and 7 to 11 have shown the extent to which I_o can influence ice temperatures, ice thicknesses, and the annual pattern of mass changes at the boundaries. For a given oceanic heat flux, the equilibrium thickness is largely determined by the amount of surface ablation, which in turn is strongly influenced by the values of I_o and the albedo. Although I_o was assumed to be constant during the snow-free period, it is probably a function of time, depending upon the changing character of the surface. This time dependence probably does not affect the annual thickness.

To understand the interaction of solar energy with the ice, it is not sufficient simply to measure incoming and net short-wave radiation. These measurements should be combined with observations of surface ice ablation and calculations of I_o, preferably by both the indirect method of Untersteiner and the direct method of Chernigovskii. Given the uncertainties in the current estimates of average ice thickness and ablation at the surface, it has not been possible to establish definitely the magnitude of I_o from the model. On the basis of observed and calculated temperature profiles (Figs. 5 and 6) and the calculations of Untersteiner (1961), we are inclined to accept a value for I_o of 2.0 to 2.5 kcal/cm^2 year and a slightly lower ice albedo than suggested by Marshunova (Table 1).

Representative surface albedos for the ice during the summer ablation season pose a major problem in treating the arctic energy budget. We have seen in Cases 5 and 27 that an albedo of 0.45 results in a rapid disappearance of the ice. However there is accumulating evidence that large-area averages for July may indeed be this low. Measurements from high towers (Langleben, 1968) and calculations using satellite data (Raschke, unpublished) indicate similar values. How is it possible to resolve predictions of the model with these albedos? Unless these estimates are all grossly in error, the explanation must lie in the way in which melt ponds and leads absorb energy and interact with the surrounding ice.

Typical albedos over melting ice range from 0.55 to 0.70; an integrated average over bare ice, melt ponds, and leads must be lower. In Section 2.4.5 a tentative argument was presented to show that melt

ponds have little net effect on equilibrium thickness. If this argument is valid, then for a given oceanic heat flux, ice thickness is determined by ablation of the bare ice, and hence only ice albedos are important in determining equilibrium thickness. Even if the average ice thickness is not directly dependent upon the amount of solar energy absorbed by the leads and melt ponds, their presence will influence the magnitude of the other energy fluxes over the bare ice and thus will affect ice ablation to some extent. Presumably this influence is included in the albedo values given by Marshunova and Doronin (Table 1).

An important process needing clarification is the way melt ponds dispose of absorbed short-wave energy. A melt pond with an albedo of 0.20 absorbs 17 kcal/cm^2 during July and August, about 10 kcal/cm^2 more than the bare ice. Since melt ponds are usually about 40 cm in depth (Untersteiner, 1961), the ponds have to lose roughly 7 kcal/cm^2 more energy during this period than the bare ice. This energy must be lost through larger turbulent fluxes, more outgoing long-wave radiation, and perhaps most important, a greater I_o under the melt ponds, but the magnitudes of the required increases are unknown.

Although we have suggested one possible way to interpret the discrepancies in summer albedos and have pointed out some basic questions regarding the melt ponds, final analysis can only be made on the basis of observational evidence. A comprehensive program to define the characteristics and behavior of melt ponds is needed. Energy budgets over large melt ponds should be determined and compared with similar ones for bare ice. The distribution, the depth, and the duration of melt ponds should be investigated, along with measurements of temperature distribution in the water and I_o under the ponds. It would also be of considerable interest to determine how rapidly the ponds freeze in the autumn. If the differences between observed temperatures and those predicted by the model are due to a latent-heat release by the melt ponds, then it is expected that complete freezing does not occur until early December.

Neither the energy budget of Vowinckel and Orvig (1966, 1967) nor that of Fletcher (1965) seems entirely satisfactory. The use of

Fletcher's heat budget in Case 1 produced remarkable agreement with observations. Paradoxically, it is for this reason that it cannot be considered truly representative of a large-scale average. Because of the effects of leads and melt ponds, a large-scale average cannot be applied to a one-dimensional model of the ice. By assuming an average summer surface albedo of 0.64, Fletcher underestimates the average amount of short-wave radiation absorbed at the surface in the Central Arctic. Although the extent of leads is uncertain, it is known that melt ponds cover 20 to 40 percent of the ice during July. Thus, 1 to 2 kcal/cm^2 year more energy is absorbed at the surface than Fletcher assumes. Year-to-year variations appear to be considerably larger than this. How this affects his suggested values for the other energy fluxes has not been determined.

The heat budget of Vowinckel and Orvig describes the gross features, but its quantitative accuracy remains to be verified because some of the energy fluxes are implicit in their formulation of the energy balance. For this reason, their budget cannot be used to describe physical changes at the surface.

The most serious limitation in the present model lies in the simplifications made in stating the boundary conditions. The independent energy fluxes all depend, to some extent, on physical conditions at the boundaries. In the present model, only the absorbed short-wave radiation and the outgoing long-wave radiation respond to changes at the upper surface. The turbulent fluxes, at least, should show a similar dependence. To solve this problem it would be necessary to reformulate the boundary conditions and express the turbulent fluxes in terms of the gradients of humidity, temperature, and wind speed in the atmospheric boundary layer. If temperature, humidity, and wind speed were specified at the top of the boundary layer, it might be possible to link the ice model to a model of the atmosphere. A one-dimensional model of the ice could then supply realistic information at each surface grid point of a model of the atmosphere. Before this is attempted, it may be more expedient, as a next step, to develop a suitable one-dimensional model of the oceanic convection under the ice

and under a free water surface. Combined with the sea-ice model, this would enable us to approach the central problem of the transition from an ice-free to an ice-covered state of the Arctic Ocean.

Appendix

THE COMPUTER PROGRAM

The program described in this section is written in FORTRAN IV and has been used with the IBM 7090/7094 System at the University of Washington Research Computer Laboratory. The program has been generalized so that the physical parameters of the ice, grid spacing, snow accumulation, and the independent energy fluxes are treated as input data. Several options allow considerable latitude in the specification of input and output data. The flexible design of the program permits it to be easily extended. With only minor modifications, one could, for example, include a time-dependent oceanic heat flux or a depth-dependent extinction coefficient, or incorporate more complex boundary conditions.

The program is divided into five basic sections: the main program, and Subroutines YARIT, FLIP, SALPR, and RITE. The main program reads in the input data, initializes the internal variables of the program, and summarizes the results of each year's integration. Subroutine YARIT calculates the temperature and thickness changes of the ice and snow for each time step during the year. Subroutine FLIP takes the monthly values of the independent energy fluxes at the upper boundary (F_r, F_L, F_s, F_ℓ) and produces smoothed values for each time step, according to the method described in Section 3.3. Subroutine SALPR calculates the salinity profile at each time step [see Eq. (34)]. Finally, Subroutine RITE writes the temperature profile, ice thickness, and mass changes for each 10-day period throughout the year.

The FORTRAN IV symbols for the input parameters are defined below, the units being modified for convenience of machine computation:

SPH Specific heat of pure ice (cal °K/gm)

RC Density × specific heat for pure ice (cal/cm^3 °K)

DESS Snow density (gm/cm^3), $T_s < 273°K$

DESJ Density of melting snow (gm/cm^3)

QS1 Latent heat of fusion for fresh water (cal/cm^3)

QI Latent heat of fusion for pure ice (cal/cm^3)

QB Latent heat of fusion for sea ice at the lower boundary (cal/cm^3)

CONO Thermal conductivity for pure ice (cal/cm °K hr)

EXC Bulk extinction coefficient for sea ice (cm^{-1})

EXLW Long-wave emissivity and absorptivity of the surface

WST Melting temperature of snow (°K)

WIT Melting temperature of sea ice at the upper boundary (°K)

WTAB Temperature of sea ice at the ice/water interface (°K)

ABM Average albedo of melting sea ice

SL1 Ice salinity at the upper boundary [$(gm/cm^3) \cdot 10^3$]

SL2 Ice salinity at z_1' (see Section 3.4) [$(gm/cm^3) \cdot 10^3$]

SL3 Ice salinity at z_2' (see Section 3.4) [$(gm/cm^3) \cdot 10^3$]

SL4 Ice salinity at the lower boundary [$(gm/cm^3) \cdot 10^3$]

DT Time increment (hrs)

DZ Depth increment (cm)

PF Percent of net short-wave radiation which penetrates the ice during the snow-free period

FW Oceanic heat flux (cal/cm^2 year)

TMSN Amount of snow which must melt before the snow layer is assumed to be isothermal (cm)

GAM Constant (γ) in Eq. (3) (cal °K gm)

BTA Constant (β) in Eq. (4) ($cal\ cm^2/gm\ hr$)

SBC Stefan-Boltzmann constant [$(cal/°K^4\ cm^2\ hr) \cdot 10^{12}$]

MZZ1 Number of cases to be integrated

Snow accumulation (as described in Section 2.4.4) is specified by the following symbols:

SC1 Date of Spring increase in the rate of snow accumulation (day; e.g., 1 May = 120)

SC2 Date of the onset of fall snow accumulation (day)

SC3 Date of winter decrease in the rate of snow accumulation (day)

SC4 Date of the end of snow accumulation (day)

TSI1 Amount of winter (SC3 to SC1) snow accumulation (cm)

TSI2 Amount of spring (SC1 to SC4) snow accumulation (cm)

TSI3 Amount of autumn (SC2 to SC3) snow accumulation (cm)

The independent energy fluxes may be specified by either of two methods. If MFX $\neq$ 0, Subroutine FLIP is called. The fluxes of latent heat (F1), sensible heat (F2), incoming long-wave radiation (FDL), and incoming short-wave radiation (FIN), expressed in cal/cm^2 month, are read into the program. Smoothed values for FIN and F1 + F2 + FDL are then generated for each time increment (DT) and transferred back to the main program. If punched-card output is also desired, IPN is set equal to zero, otherwise IPN must be set equal to 1. The punched card output of FLIP may be read directly into the main program during future runs by specifying MFX = 0. In the main program, FSN corresponds to F_r and FLX to $F_L + F_s + F_\ell$.

Termination of program execution is determined by the choice of MNY, MXJ, and EQP. The program may be stopped at any predetermined time by specifying the year and iteration number. If, for example, it is desired that the integration end on 1 July of the tenth year, then MNY = 10 and MXJ = number of time increments between 1 January and 1 July. Normally, MXJ is set equal to zero. Equilibrium is defined through EQP. The ice thickness on each successive 1 January is compared; when the year-to-year change is less than EQP (0.1 cm in the cases discussed in Chapter IV), equilibrium is assumed to have been achieved. Before the execution is terminated, the ice thickness and temperature profile, along with the internal variables of the program, are stored on logical tape 4.

Specification of LRT completes the initialization of the program. If LRT = 1, logical tape 4 is read. It is thus possible to continue the integration of an interrupted case. If LRT = 0, corresponding to a new case, it is also necessary to specify:

ALBD Monthly albedo (ABM overrides the specified values during the snow-free period)

FS Flux of sensible heat (cal/cm^2 month)

FL Flux of latent heat (cal/cm^2 month)

ITK Initial ice thickness (cm)

SSTM Initial ice temperature at the snow surface (°K)

SIT Initial temperature at the ice/snow interface (°K)

If R5 = 1, temperature profiles will be printed on every tenth day. If R5 = 0, only ice and snow thicknesses and the mass changes will be printed. A summary of results is printed out each year, regardless of the value of R5. When the ice has attained equilibrium, the annual temperature-and-thickness field is printed out for 5 day intervals and deposited on logical tape 3 to facilitate numerical plotting.

MAIN COMPUTER PROGRAM

```
C      SEA ICE STUDIES-MAIN PROGRAM
       DIMENSION BSA(11,12)
       COMMON /BLK1/TF(12,80),BSM(11,13),T1(600),EPM(12),ABL(12),SND1(12)
      1,DTB(12),RIT(12)/BLS1/SL(600)/BLA1/FLX(12,60),FSN(12,60),IMM(5,4),
      2ALBD(12),FS(12),FL(12),T3(600)
       COMMON /BLSK/ISB,IDZ,DZ,DZX/BLK2/ISF,ISI,KK1,JJ2,JJ4,J17,J18,M1,LC
      1I,ITR,MXI,K5,DZP,DZY,EPC,EPTC,TSD,TSDP,WTAB,WST,FTK,VTK,GEP,ADD,R5
      2/BLS2/SL1,SL2,SL3,SL4,A1,A2,PI,U1,U2,ILB/BLA2/ITT1,ITT2,ITT3,ITT4,
      3ITC,II8,IDT,IZ1,ITO,ITK,IT4,JJ1,JJ3,JA4,JJ5,K7,KK2,KK8,LOX,LRT,MNY
      4,MXJ,MX2,MM1,MM2,MM3,MIF,NR,ABM,AIST,ASST,A,L1,NTW ,ABI,BTA,CONO,C
      5ONS,SWLO,DT,DESS,DESJ,DES,DV1,DV2,DS1,DS2,DS3,DZT,DT1,EXC,EPT,EPS,
      6FI,FIC,FIC,FW,FIOC,FI8,FK8,FZ1,GAM,PF,QI,QB,QS,QS1,RC,RCSP,RTK,SPH
      7,SOG,SBC,SND,TAC,VA,VB,VC,VD,WIT,XX1,XX5,XX2,XX0,YYO,K9,K10,K11
 1     FORMAT(5F4.0,3F5.1,5F4.2,4F5.0/2F6.0,4F6.1, F6.2,F6.3,2F7.5/4F5.2,
      15I3,2I5,3F4.1,F5.2)
 2     FORMAT(12F5.0)
 3     FORMAT(12F6.0)
 4     FORMAT(12F5.2)
 5     FORMAT(I4,2F6.1)
 6     FORMAT(12F6.1)
 10    FORMAT(12(2X,F8.6))
 15    FORMAT(80H
     1                                )
 16    FORMAT(18H SW LOSS TO OCEAN=F6.1/34H FLUX BALANCE FOR ENTIRE ICE S
      1LAB=F6.3/////////)
 17    FORMAT(1H1,115X,6H YEAR I3/28X,20H MONTH   DAY    HOUR//20H SNOW B
      1EGINS MELTING,4X,3(5X,I3)/20H ICE  BEGINS MELTING,4X,3(5X,I3)/20H
      2ICE  STOPS  MELTING,4X,3(5X,I3)/22H BOTTOM ACCRETION ENDS,2X,3(5X,
      3I3)/21H BOTTOM ABLATION ENDS,3X,3(5X,I3)///////)
 18    FORMAT(116X,6H YEAR I3)
 19    FORMAT(26X,3HJAN,5X,3HFEB,5X,3HMAR,5X,3HAPL,5X,3HMAY,5X,3HJUN,5X,3
      1HJUL,5X,3HAUG,5X,3HSEP,5X,3HOCT,5X,3HNOV,5X,3HDEC,4X,4HYEAR//22H A
      2VERAGE SURFACE TEMP ,13F8.2/22H AVERAGE SURF ICE TEMP,13F8.2/15H A
      3VERAGE ALBEDO,23X,8F8.2/16H NET SHORT WAVE ,5X,12F8.1,F9.3 /15H PE
      4NETRATING SW,6X,12F8.1,F9.3/14H NET LONG WAVE,7X,12F8.0,F9.3/18H F
      5LUX THRU SURFACE,3X,12F8.1,F9.3/17H FLUX THRU BOTTOM,4X,12F8.1,F9.
      63/21H SURFACE FLUX BALANCE,1X,13F8.2/ 18H ACTUAL BOT GROWTH,4X,13F
      78.2/18H AVERAGE  ICE THICK,4X,13F8.1//)
       REWIND 3
       REWIND 4
       MZZ=0
925    READ(5,15)
       READ(5,1) DT,DZ,QB,QS1,QI,TSI1,TSI2,TSI3,SPH,ABM,DESS,DESJ,RC,SC1,
      1SC2,SC3,SC4,GAM,FW,WTAB,WST,BTA,CONO,EXC,SBC,PF,SL1,SL2,SL3,SL
      24,MNY,MZZ1,LRT,MFX,NTW,MXI,MXJ,TMSN,R5,EQP,EXLW
       IF(MFX.EQ.0) GO TO 45
       CALL FLIP(EXLW)
       GO TO 49
45     DO 46 I=1,12
46     READ(5,6) (FLX(I,J),J=1,60)
```

```
      DO 47 I=1,12
47    READ(5,6) (FSN(I,J),J=1,60)
49    DO 50 I=1,12
      DO 50 J=1,60
      FSN(I,J)=FSN(I,J)*DT/12.0
50    FLX(I,J)=FLX(I,J)*DT/12.0
      SBC=SBC*DT*EXLW
      ITT1=SC1*24.0/DT
      ITT2=SC2*24.0/DT
      ITT3=SC3*24.0/DT
      ITT4=SC4*24.0/DT
      SL1=SL1*0.001
      SL2=SL2*0.001
      SL3=SL3*0.001
      SL4=SL4*0.001
      K10=12.0/DT
      A1=(SL4+SL1)/2.0
      A2=(SL4-SL1)/2.0
      PI=3.1415926S
      U1=ALOG(0.5+((ARSIN((2.0*SL2-SL4-SL1)/(SL4-SL1)))/PI))
      U2=ALOG(0.5+((ARSIN((2.0*SL3-SL4-SL1)/(SL4-SL1)))/PI))
      HAB=0.0
      SWLO=0.0
      L1=0
      IDZ=DZ
      IDT=DT
      TSDP=TSI1+TSI2+TSI3
      ADD1=TSDP+10.0
      ADC=ADD1
      ISI=(ADD1/DZ)+1.0
      JJ5=8640/IDT+1
      J17=600/IDZ-1
      J18=ISI+1
      FZ1=10.0/DZ
      IZ1=FZ1
      FI8=360.0/DT
      II8=FI8
      KK8=II8/3
      FK8=KK8
      ITC=II8*2
      ITO=II8*2/3
      IT4=II8*8
      FW=FW*DT/(24.0*360.0)
      DS1=TSI1*DT/((SC1+360.0-SC3)*24.0)
      DS2=TSI2*DT/((SC4-SC1)*24.0)
      DS3=TSI3*DT/((SC3-SC2)*24.0)
      DV1=3.0*SBC
      DV2=0.04*SBC
      XX0=SBC*((WST/100.0)**4)
      XX1=SBC*((WIT/100.0)**4)
```

```
      DES=DESS
      CONS=0.0068*(DES**2)*3600.0*DT
      CONO=CONO*DT
      BTA=BTA*DT
      A=1.0/(DZ*DZ)
      YYO=FW/(2.0*QB)
      IF(LRT.EQ.0) GO TO 105
      READ(4)  TF,BSM,T1,SL,SND1,RIT,DTB,ABL,EPM,ALBD,IMM,FS,FL
      READ(4)  MX1,MX2,ITR,LOX,KK1,KK2,JJ1,JJ2,JJ3,JJ4,ILB,ISB,ISF,LCI,K
     15,K7,MM1,MM2,MM3,MIF,M1,K9,K11
      READ(4)  DZT,DZX,DZP,DZY,EPTC,EPC,DES,RCSP,QS,SOG,FI,FIC,FIOC,TSD,
     1XX2,VA,VB,VC,VD,AIST,ASST,GEP,FTK,TAC
      LCI=1
      M1=1
      IF(ITR.LT.JJ5-1) GO TO 100
      ITR=1
      K7=0
      GO TO 165
100   JA4=ITR
      GO TO 170
105   READ(5,4) (ALBD(I),I=1,12)
      READ(5,3) (FS(I),I=1,12)
      READ(5,2) (FL(I),I=1,12)
      READ(5,5) ITK,SIT,SSTM
      VD=0.0
      AIST=0.0
      ASST=0.0
      DES=DESS
      RCSP=DES*SPH
      ILB=ISI+(ITK/IDZ)
      ISB=ISI
      FTK=ITK
      JJ1=ISB+1
      KK2=ISB-1
      JJ2=ILB-1
      JJ4=JJ2+1
      M1=1
      DZP=DZ
      DZY=0.0
      SND=TSI3+(DS1*((360.0-SC3)*24.0)/DT)
      I=SND/DZ
      KK1=ISB-I+1
      ISF=KK1-2
      ZZ=I
      DZX=SND-ZZ*DZ
      DZT=DZX+DZ
      XX2=DZX
      MX1=10
      CALL SALPR(FTK,MX1,TAC)
      Y=(WTAB-SIT)/FTK
```

```
      X=0.0
      DO 110 I=ISB,ILB
      T1(I)=SIT+X*Y
  110 X=X+DZ
      DO 135 I=ILB,600
  135 T1(I)=WTAB
      DO 140 I=2,ISF
  140 T1(I-1)=WST
      T1(ISF)=SSTM/100.0
      CON=CONO+((BTA*SL(JJ1))/(T1(JJ1)-273.0))
      T1(KK2)=T1(ISB)+(CON*(T1(ISB)-T1(JJ1)))/CONS
      VA=VA+ALBC(LOX)
      AP=CONS/(SND-DZ)
      BP=-(CONS*T1(KK2))/(SND-DZ)-FLX(1,1)
  145 X=T1(ISF)
      T1(ISF)=(DV1*(X**4)-BP)/((DV2*(X**3)+AP)*100.0)
      Y=ABS(X-T1(ISF))
      IF(Y.GT..0000001) GO TO 145
      VD=VD+FLX(1,1)-(SBC*(T1(ISF)**4))
      T1(ISF)=T1(ISF)*100.0
      T1(ISF+1)=T1(ISF)+((DZX*(T1(KK2)-T1(ISF)))/(SND-DZ))
      AIST=AIST+T1(ISB)
      ASST=ASST+T1(ISF)
      Y=(T1(KK2)-T1(ISF+1))/(SND-DZT)
      X=0.0
      DO 150 I=ISF,KK2
      T1(I+1)=T1(ISF+1)+X*Y
  150 X=X+DZ
      CCN=CONO+((BTA*SL(JJ4))/(T1(JJ4)-273.0))
      T1(JJ2)=WTAB-((FW*DZ)/CON)
  152 TF(1,1)=0.0
      DO 155 K=2,60
      I=((K-1)*10)/IDZ+1
  155 TF(1,K)=273.0-T1(I)
      DO 160 K=1,12
  160 ABL(K)=0.0
      K5=1
      K7=1
      EPTC=0.0
      ITR=2
      FIC=0.0
      GEP=0.0
      FIOC=0.0
      MIF=0
      MM1=0
      MM2=0
      MM3=1
      VA=0.0
      VB=0.0
      VC=0.0
```

```
161   QS=QS1*DES
      SOG=CONS/(DZ*DZ*RCSP)
      TSD=SND
      SND1(1)=TSD
      RIT(1)=FTK+GEP
      DTB(1)=FTK+ADD+GEP
      ABL(1)=0.C
      EPM(1)=0.0
      LCI=1
165   MX2=4
      MX1=10
      RTK=RIT(1)
      LOX=1
      JA4=1
      FI=0.0
      EPC=0.0
      KS=0
      K11=0
      VTK=0.0
170   CALL YARIT(MX1,TSI3,TMSN)
      TSDP=TSI1+TSI2+TSI3
      ADD=ADD1
      J20=ISB-ISI
      ISB=ISI
      KK2=ISI-1
      JJ1=ISI+1
      ISF=ISF-J20
      KK1=KK1-J20
      ILB=ILB-J20
      JJ2=ILB-2
      JJ3=ILB-3
      JJ4=ILB-1
      DO 190 I=ISF,ILB
      J=I+J20
190   T1(I)=T1(J)
      DO 195 I=ILB,J17
195   T1(I)=WTAB
      DO 200 I=ISB,ILB
      J=I+J20
200   SL(I)=SL(J)
      WRITE(6,10) (SL(I),I=ISB,ILB)
      WRITE(6,18) LCI
      WRITE(6,15)
      DO 205 I=1,5
      X=IMM(I,1)
      J=X/(2.0*FI8)
      IMM(I,2)=J+1
      Y=J
      Z=(X-2.0*Y*FI8)*DT/24.0
      IMM(I,3)=Z
```

```
      Y=IMM(I,3)
205   IMM(I,4)=(Z-Y)*24.0
      IF(LOX.EQ.13) GO TO 212
      DO 210 K=LOX,13
      DO 210 J=1,11
210   BSM(J,K)=0.0
      GO TO 220
212   DO 214 I=1,11
      X=0.0
      DO 213 J=1,12
213   X=X+BSM(I,J)
214   BSM(I,13)=X
      BSM(1,13)=BSM(1,13)/12.0
      BSM(2,13)=BSM(2,13)/12.0
      BSM(11,13)=BSM(11,13)/12.0
      DO 215 I=3,8
215   BSM(I,13)=BSM(I,13)/1000.0
220   WRITE(6,17) LCI,(IMM(1,I),I=2,4),(IMM(2,I),I=2,4),(IMM(3,I),I=2,4)
     1,(IMM(4,I),I=2,4),(IMM(5,I),I=2,4)
      WRITE(6,19) (BSM(1,I),I=1,13),(BSM(2,I),I=1,13),(BSM(3,I),I=3,10),
     1(BSM(4,I),I=1,13),(BSM(5,I),I=1,13),(BSM(6,I),I=1,13),(BSM(7,I),I=
     21,13),(BSM(8,I),I=1,13),(BSM(9,I),I=1,13),(BSM(10,I),I=1,13),(BSM(
     311,I),I=1,13)
      X=BSM(5,13)-BSM(8,13)-BSM(7,13)-(SWLO/1000.0)
      WRITE(6,16) SWLO,X
      SWLO=0.0
      WRITE(6,15)
      LCI=LCI+1
      IF(MNY.LE.LCI) GO TO 225
      ITR=1
      K7=0
      IF(ABS(RTK-RIT(1)).GE.EQP) GO TO 165
      MXJ=0
      R5=1.0
      MNY=LCI
      TF(1,1)=0.0
      DO 227 I=2,60
      J=((I-1)*10)/IDZ+1
227   TF(1,I)=273.0-T1(J)
      GO TO 165
225   IF(MXJ.EQ.0) GO TO 230
      MXJ=0
      ITR=1
      K7=0
      R5=1.0
      GO TO 165
230   CONTINUE
235   REWIND 4
      WRITE(4) TF,BSM,T1,SL,SND1,RIT,DTB,ABL,EPM,ALBD,IMM,FS,FL
      WRITE(4) MX1,MX2,ITR,LOX,KK1,KK2,JJ1,JJ2,JJ3,JJ4,ILB,ISB,ISF,LCI,K
```

```
15,K7,MM1,MM2,MM3,MIF,M1,K9,K11
 WRITE(4) DZT,DZX,DZP,DZY,EPTC,EPC,DES,RCSP,QS,SOG,FI,FIC,FIOC,TSD,
1XX2,VA,VB,VC,VD,AIST,ASST,GEP,FTK,TAC
 MZZ=MZZ+1
 IF(MZZ.LT.MZZ1) GO TO 925
 REWIND 3
 STOP
  END
```

```
C      YEARLY ITERATION SUBROUTINE
       SUBROUTINE YARIT(MX1,TSI3,TMSN)
       DIMENSION T(600),TT(600)
       COMMON /BLK1/TF(12,80),BSM(11,13),T1(600),EPM(12),ABL(12),SND1(12)
      1,DTB(12),RIT(12)/BLS1/SL(600)/BLA1/FLX(12,60),FSN(12,60),IMM(5,4),
      2ALBD(12),FS(12),FL(12),T3(600)
       COMMON /BLSK/ISB,IDZ,DZ,DZX/BLK2/ISF,ISI,KK1,JJ2,JJ4,J17,J18,M1,LC
      1I,ITR,MXI,K5,DZP,DZY,EPC,EPTC,TSD,TSDP,WTAB,WST,FTK,VTK,GEP,ADD,R5
      2/BLS2/SL1,SL2,SL3,SL4,A1,A2,PI,U1,U2,ILB/BLA2/ITT1,ITT2,ITT3,ITT4,
      3ITC,II8,ICT,IZ1,ITO,ITK,IT4,JJ1,JJ3,JA4,JJ5,K7,KK2,KK8,LOX,LRT,MNY
      4,MXJ,MX2,MM1,MM2,MM3,MIF,NR,ABM,AIST,ASST,A,L1,NTW ,ABI,BTA,CONO,C
      5ONS,SWLO,DT,DESS,DESJ,DES,DV1,DV2,DS1,DS2,DS3,DZT,DT1,EXC,EPT,EPS,
      6FI,FIC,FIC,FW,FIOC,FI8,FK8,FZ1,GAM,PF,QI,QB,QS,QS1,RC,RCSP,RTK,SPH
      7,SOG,SBC,SND,TAC,VA,VB,VC,VD,WIT,XX1,XX5,XX2,XXO,YYO,K9,K10,K11
 10    FORMAT(16F8.3)
 11    FORMAT(3I5,10X,2F10.2)
 12    FORMAT(15H SHEARING ERROR)
       DO 565 JJ=JA4,JJ5
       IF(ITC.NE.K7) GO TO 100
       BSM(1,LOX)=273.0-(ASST/(2.0*FI8))
       BSM(2,LOX)=273.0-(AIST/(2.0*FI8))
       BSM(3,LOX)=VA/(2.0*FI8)
       BSM(4,LOX)=VB+FIOC
       BSM(5,LOX)=FIOC
       BSM(6,LOX)=VD-FS(LOX)-FL(LOX)
       BSM(7,LOX)=VC
       BSM(8,LOX)=FIC
       BSM(9,LOX)=BSM(4,LOX)-BSM(5,LOX)+BSM(6,LOX)+BSM(7,LOX)+FS(LOX)+FL(
      1LOX)+VMF
       VMF=0.0
       BSM(10,LOX)=EPC-FI
       BSM(11,LOX)=VTK/(2.0*FI8)
       VTK=0.0
       VA=0.0
       VB=0.0
       VC=0.0
       VD=0.0
       FIOC=0.0
       ASST=0.0
       AIST=0.0
       FIC=0.0
       LOX=LOX+1
       K9=0
       K11=0
       IF(12.LT.LOX) GO TO 570
       FI=EPC
       K7=0
100    K7=K7+1
       K9=K9+1
       IF(K9.LE.K10.AND.K9.NE.1) GO TO 104
```

```
      K9=1
      K11=K11+1
      FLW=FLX(LOX,K11)
      FSW=FSN(LOX,K11)
  104 GO TO(200,240,240,265,120,125,155,160,170,105,110),MX1
  105 IF(ITT1.GE.ITR) GO TO 170
      MX1=11
  110 IF(ITT4.LT.ITR) GO TO 115
      TSD=TSD+DS2
      XX2=XX2+DS2
      GO TO 180
  115 DZX=0.0
      DZT=DZ
      MX1=1
      MX2=1
      TSD=TSDP
      KK1=ISF+1
      GO TO 200
  120 IF(ITT2.GE.ITR) GO TO 185
      MX1=6
      DZX=0.0
      ALBD(LOX)=ALBD(LOX+1)
      MX2=2
      MIF=0
      TSD=0.0
      JJ1=KK1+1
      DES=DESS
      QS=QS1*DES
      RCSP=DES*SPH
      CONS=0.0068*(DES**2)*3600.0*DT
      SOG=CONS/(DZ*DZ*RCSP)
  125 IF(ITT3.LT.ITR) GO TO 150
      TSD=TSD+DS3
      DZX=DZX+DS3
  130 IF(2.0*DZ.LT.TSD) GO TO 140
      IF(DZ.LT.TSD) GO TO 135
      ISF=ISB-1
      GO TO 380
  135 IF(MX2.EQ.3) GO TO 380
      ISF=ISB-2
      MX2=3
      DZX=DZX-DZ
      GO TO 380
  140 MX2=4
      MX1=8
      ISF=ISB-3
      XX2=TSD-2.0*DZ
      KK1=ISB-1
      KK2=ISB-1
      JJ1=ISB+1
```

```
145   DZX=XX2
      DZT=DZ+XX2
      GO TO 200
150   MX1=7
155   TSD=TSD+DS1
      DZX=DZX+DS1
      GO TO 130
160   IF(ITT3.LT.ITR) GO TO 165
      TSD=TSD+DS3
      XX2=XX2+DS3
      GO TO 180
165   MX1=9
170   TSD=TSD+DS1
175   XX2=XX2+DS1
180   IF(DZ.GE.XX2) GO TO 145
      XX2=XX2-DZ
      KK1=KK1-1
      ISF=ISF-1
      GO TO 180
185   X=(1.0-ABM)*FSW
      VC=VD+FLW
      FIO=X*PF
      FIOC=FIOC+FIO
      FNW=FLW-FIO+X
      VA=VA+ABM
      VB=VB+X-FIO
190   RCP=RC+(GAM*SL(KK1))/((T1(KK1)-273.0)**2)
      CON=CONO+((BTA*SL(KK1))/(T1(KK1)-273.0))
      SIG=A*CON/RCP
      AP=CON/((1.0+SIG)*DZ)
      BP=-FNW-(CON*((1.0-SIG)*T1(KK1)+SIG*T1(KK1+1)))/((1.0+SIG)*DZ)
      Y=T1(ISI)/100.0
195   ET=(DV1*(Y**4)-BP)/((DV2*(Y**3)+AP)*100.0)
      X=ABS(ET-Y)
      Y=ET
      IF(X.GT..COCCOC1) GO TO 195
      VD=VD-(SB(*(Y**4))
      T(ISI)=Y*100.0
      IF(WIT.GE.T(ISB)) GO TO 380
      T(ISI)=WIT
      GO TO 380
200   X=(1.0-ALBD(LOX))*FSW
      VC=VD+FLW
      VA=VA+ALBD(LOX)
      VB=VB+X
      FNW=FLW+X
      IF(DZX.EQ.0.0) GO TO 205
      AP=CONS/((1.0+SOG)*DZ+DZX)
      BP=-FNW-(CONS*((1.0-SOG)*T1(KK1)+SOG*T1(KK1+1)))/((1.C+SOG)*DZ+DZX
     1)
```

```
      GO TO 210
205   AP=CONS/((1.0+SOG)*DZ)
      BP=-FNW-(CONS*((1.0-SOG)*T1(KK1)+SOG*T1(KK1+1)))/((1.0+SOG)*DZ)
210   Y=T1(ISF)/100.0
215   ET=(DV1*(Y**4)-BP)/((DV2*(Y**3)+AP)*100.0)
      X=ABS(ET-Y)
      Y=ET
      IF(X.GT..000001) GO TO 215
      T(ISF)=Y*100.0
      IF(WST.GE.T(ISF)) GO TO 219
      VD=VD-XXO
      MX1=1
      MX2=1
      GO TO 235
219   GO TO(225,380,380,220),MX2
220   T(KK1-1)=((1.0+SOG)*DZ*T(ISF)+DZX*((1.0-SOG)*T1(KK1)+SOG*T1(KK1+1)
     1))/((1.0+SOG)*DZ+DZX)
      T3(KK1-1)=T(KK1-1)
225   DO 230 K=KK1,KK2
230   T(K)=((1.0-SOG)*T1(K)+SOG*(T1(K+1)+T(K-1)))/(1.0+SOG)
      VD=VD-(SBC*((T(ISF)/100.0)**4))
      GO TO 380
235   IF(MM1.NE.0) GO TO 240
      MM1=1
      IMM(1,1)=ITR
      IF(TSD.GE.TSDP) GO TO 240
      TSDP=TSD
240   T(ISF)=WST
      GO TO(270,245,255),MX1
245   IF(KK1.GT.KK2) GO TO 260
      DO 250 K=KK1,KK2
      T(K)=WST
250   TT(K)=WST
255   T(ISB)=WIT
      TT(ISB)=WIT
      X=ABM+(TSD*ABI/TSDP)
      VD=VD+FLW-XXO
      Y=(1.0-X)*FSW
      FNW=FLW+Y
      VA=VA+X
      VB=VB+Y
      EPT=(XXO-FNW)/QS
      VMF=VMF+EPT*QS
      GO TO 275
260   MX1=3
      GO TO 255
265   RCP=RC+(GAM*SL(KK1))/((T1(KK1)-273.0)**2)
      CON=CONO+((BTA*SL(KK1))/(T1(KK1)-273.0))
      SIG=A*CON/RCP
      T(ISB)=WIT
```

```
      X=(1.0-ABM)*FSW
      VC=VD+FLW-XX1
      FIO=X*PF
      FIOC=FIOC+FIO
      FNW=FLW-FIO+X
      VA=VA+ABM
      VB=VB+X-FIO
      X=(XX1-FNW)/(2.0*QI)
      Y=((1.0+SIG)*DZ+DZX)/2.0
      EPT=X-Y+SQRT((X+Y)**2+CON *(WIT+(SIG-1.0)*T1(KK1)-SIG*T1(KK1+1))/Q
     1I)
      VMF=VMF+EPT*QI
      GO TO 275
  270 X=(XXC-FNW)/(2.0*QS)
      Y=((1.0+SCG)*DZ+DZX)/2.0
      EPT=X-Y+SQRT((X+Y)**2+CONS*(WST+(SOG-1.0)*T1(KK1)-SOG*T1(KK1+1))/Q
     1S)
      VMF=VMF+EPT*QS
  275 EPTC=EPTC+EPT
      TSD=TSD+EPT
      DZT=DZT+EPT
      DZX=DZT-DZ
      IF(MX1.GE.2) GO TO 285
      IF(EPTC.GT.TMSN) GO TO 285
      MX1=2
      DES=DESJ
      TSD=DESS*TSD/DESJ
      ABI=((ALBC(LOX)-AEM)*TSDP)/TSD
      EPTC=TSD-TSDP
      K=TSD/DZ
      Z=K
      KK1=ISB-K+1
      ISF=ISB
      DZX=TSD-DZ*Z
      DZT=DZ+DZX
      QS=QS1*DES
      RCSP=DES*SPH
      CONS=0.0068*(DES**2)*3600.0*DT
      SCG=CONS/(DZ*DZ*RCSP)
      MM1=0
      DO 280 K=KK1,KK2
      T(K)=WST
  280 TT(K)=WST
      T(ISB)=WIT
      TT(ISB)=WIT
  285 IF(DZT.GE.DZ.AND.DZT.LT.2.0*DZ) GO TO 305
      IF(DZT.GE.2.0*DZ) GO TO 300
      DZT=DZT+DZ
      KK1=KK1+1
      DZX=DZT-DZ
```

```
      GO TO(295,285,285,290),MX1
290   JJ1=KK1+1
      ISB=KK1-2
      L1=1
      ISF=ISB
      GO TO 285
295   IF(KK1-ISF-2.LE.C) GO TO 285
      ISF=ISF+1
      GO TO 285
300   DZT=DZT-DZ
      KK1=KK1-1
      ISF=ISF-1
      DZX=DZT-DZ
      GO TO 285
305   GO TO(315,375,310,330),MX1
310   IF(TSD.GT.0.) GO TO 375
      MX1=4
      ISB=KK1-2
      ISF=ISB
      MIF=1
      IMM(2,1)=ITR
      JJ1=KK1+1
      GO TO 330
315   T(KK1)=((1.0-SOG)*T1(KK1)+SOG*(T1(KK1+1)+(1.0-DZX/DZT)*WST))/(1.0+
     1SOG*(1.0-DZX/DZT))
      TT(KK1)=T(KK1)
      IF(EPTC.GE.0.) GO TO 320
      T(KK1-1)=WST+(((T(KK1)-WST)*DZX)/DZT)
      T3(KK1-1)=T(KK1-1)
320   J20=KK1+1
      DO 325 K=J20,KK2
325   T(K)=((1.0-SOG)*T1(K)+SOG*(T1(K+1)+T(K-1)))/(1.0+SOG)
      GO TO 375
330   RCP=RC+(GAM*SL(KK1))/((T1(KK1)-273.0)**2)
      CON=CONO+((BTA*SL(KK1))/(T1(KK1)-273.0))
      SIG=A*CON/RCP
      T(KK1)=((1.0-SIG)*T1(KK1)+SIG*T1(KK1+1)+SIG*(1.0-DZX/DZT)*WIT)/(1.
     10+SIG*(1.0-DZX/DZT))
      TT(KK1)=T(KK1)
      T(KK1-1)=WIT+(DZX*(T(KK1)-WIT))/DZT
      T3(KK1-1)=T(KK1-1)
      T3(ISB)=WIT
      IF(EPT.LT.0.) GO TO 375
      MX1=5
      L1=1
      IMM(3,1)=ITR
      VD=VD+XX1
      EPTC=EPTC-EPT
      VMF=VMF-EPT*QI
      ABL(K5+1)=TSDP+EPTC
```

```
      DZT=DZT-EPT
      DZX=DZT-DZ
      K=JJ2
      J2C=KK1-2
      Y=DZ-DZX
      IF(DZX.GT.5.0) GO TO 335
      ISF=KK1-1
      ISB=ISF
      GO TO 340
  335 KK1=KK1-1
  340 T1(ISF)=WIT
      Z=FTK+GEP+TSDP+EPTC
      J=Z/DZ
      ZZ=(J-1)*IDZ
      DZP=Z-ZZ
      JJ2=J+ISF-1
      ACD=(ISF-1)*IDZ
      JJ4=JJ2+1
      ILB=JJ2+2
      JJ3=JJ2-1
      JJ1=KK1
      DZX=C.0
      DZT=DZ
      DZY=DZP-DZ
      TAC=DZY
      DO 345 J=KK1,JJ2
      J20=J20+1
  345 T(J)=T1(J20)+(Y*(T1(J20+1)-T1(J20)))/DZ
      T1(JJ4+1)=WTAB
      T1(ISB-1)=WST
      IF(J20+1-K)355,35C,360
  350 T(JJ4)=T1(J20+1)+(Y*(T1(J20+2)-T1(J20+1)))/DZ
      GO TO 365
  355 WRITE(6,12)
      GO TC 365
  360 IF(J20.NE.K) GO TC 355
      T(JJ4)=T1(J20+1)+(Y*(WTAB-T1(J20+1)))/(DZP-DZ)
  365 DO 37C  J=KK1,JJ2
  370 T1(J)=T(J)
      FTK=FTK+GEP+TSDP+EPTC
      CALL SALPR(FTK,MX1,TAC)
      GEP=0.0
      EPTC=C.0
      TSD=0.0
      IF(ITT2.GE.ITR) GC TO 190
      X=ITT3-ITR
      DS3=TSI3/X
      VA=VA-ABM
      VB=VB+FIO+((ABM-1.0)*FSW)
      VC=VD-FLW
```

```
      FIOC=FIOC-FIO
      GO TO 120
  375 CONTINUE
  380 JJ3=JJ2-1
      RCP=RC+(GAM*SL(JJ2))/((T1(JJ2)-273.0)**2)
      CON=CONO+((BTA*SL(JJ2))/(T1(JJ2)-273.0))
      SIG=A*CON/RCP
      Y=((1.0+SIG)*DZ+DZY)/2.0
      XYT=(T1(JJ2)+WTAB)/2.0
      XYS=(SL(JJ2)+SL4)/2.0
      CCN=CONO+(BTA*XYS/(XYT-273.0))
      EPS=-YYO-Y+SQRT((Y-YYO)**2+(CON *(WTAB-(1.0-SIG)*T1(JJ2)-SIG*T1(JJ
     13)))/QB)
      DZP=DZP+EPS
      DZY=DZP-DZ
      TT(JJ2)=(DZP*((1.0-SIG)*T1(JJ2)+SIG*T1(JJ3))+SIG*DZ*WTAB)/((1.0+SI
     1G)*DZ+DZY)
      IF(1.NE.MIF) GO TO 383
      Z=FTK+GEP-DZP
      DZP=DZP-EPS
      IF(MX1.EQ.5) GO TO 381
      Z=Z+TSDP+EPTC
  381 RCP=RC+(GAM*SL(JJ2)/((TT(JJ2)-273.0)**2))
      X=TT(JJ2)+(EXC*FIO*EXP(-Z*EXC)/RCP)
      XYT=(X+WTAB)/2.0
      CCN=CONC+(BTA*XYS/(XYT-273.0))
      EPS=-YYO-(DZP/2.0)+SQRT(((DZP/2.0)-YYO)**2+(CON*(WTAB-X)/QB))
      DZP=DZP+EPS
      DZY=DZP-DZ
      FIC=FIC+(CON*(X-WTAB)/DZP)
      GO TO 384
  383 FIC=FIC+(CON*(TT(JJ2)-WTAB)/DZP)
  384 EPC=EPC+EPS
      GEP=GEP+EPS
      T(JJ4)=WTAB+((DZY*(TT(JJ2)-WTAB))/DZP)
      TT(JJ4)=T(JJ4)
      IF(EPS)385,410,4CC
  385 IF(MM2.NE.0) GO TO 390
      MM2=1
      MM3=0
      IMM(4,1)=ITR
  390 IF(DZP.GE.DZ) GO TO 410
      DZP=DZP+DZ
      DZY=DZP-DZ
      T(JJ2)=TT(JJ2)
      JJ2=JJ2-1
      JJ3=JJ2-1
      JJ4=JJ4-1
      TT(JJ2)=(DZP*T(JJ2+1)-DZ*WTAB)/DZY
      IF(ILB-JJ4-1.LE.C) GO TO 395
      ILB=ILB-1
```

```
395   T(ILB)=hTAB
      TT(ILB)=HTAB
      GO TO 385
400   IF(MM3.NE.0) GO TC 405
      MM2=0
      MM3=1
      IMM(5,1)=ITR
405   IF(DZP.LT.2.0*DZ) GO TO 410
      DZP=DZP-DZ
      DZY=DZP-DZ
      JJ2=JJ2+1
      JJ4=JJ4+1
      ILB=ILB+1
      T(JJ4)=T(JJ2)+((DZ*(hTAB-T(JJ2)))/DZP)
      TT(JJ4)=T(JJ4)
      GO TO 400
410   IF(MX1.GT.1.AND.MX1.LT.6) GO TO 450
      DO 415 J=JJ1,JJ3
      K=JJ3+JJ1-J
      RCA=RC+(GAM*SL(K))/((T1(K)-273.0)**2)
      CAN=CONO+((BTA*SL(K))/(T1(K)-273.0))
      SAG=A*CAN/RCA
415   TT(K)=((1.0-SAG)*T1(K)+SAG*(T1(K-1)+TT(K+1)))/(1.0+SAG)
      IF(MX2.EQ.1.OR.MX2.EQ.4) GO TO 435
      RCP=RC+(GAM*SL(KK1))/((T1(KK1)-273.0)**2)
      CON=CONO+((BTA*SL(KK1))/(T1(KK1)-273.0))
      SIG=A*CON/RCP
      MX3=1
      TT(KK1)=(((1.0-SIG)*T1(KK1))+SIG*(T1(KK1-1)+TT(KK1+1)))/(1.0+SIG)
      XX5=(CON*TSD)/(CONS*DZ)
      AP=CON/(DZ*(1.0+XX5))
      X=(1.0-ALBD(LOX))*FSW
      VC=VD+FLW
      VA=VA+ALBD(LOX)
      VB=VB+X
      FNW=FLW+X
      BP=-FNW-(AP*TT(KK1))
      Y=T1(ISF)/100.0
420   ET=(DV1*(Y**4)-BP)/((DV2*(Y**3)+AP)*100.0)
      X=ABS(ET-Y)
      Y=ET
      IF(X.GT..0000001) GO TO 420
      TT(ISF)=Y*100.0
      IF(MX3.EQ.2) GO TC 430
      T(ISB)=(TT(ISF)+XX5*TT(KK1))/(1.0+XX5)
      DO 425 J=KK1,JJ3
      RCP=RC+(GAM*SL(J))/((T1(J)-273.0)**2)
      CON=CONO+((BTA*SL(J))/(T1(J)-273.0))
      SIG=A*CON/RCP
425   T(J)=((1.0-SIG)*T1(J)+SIG*(T1(J+1)+T(J-1)))/(1.0+SIG)
```

```
      T3(KK1)=(T(KK1)+TT(KK1))/2.0
      CON=CONO+((BTA*SL(KK1))/(T1(KK1)-273.0))
      AP=CON/(DZ*(1.0+XX5))
      BP=-FNW-(AP*T3(KK1))
      Y=TT(ISF)
      MX3=2
      GO TO 420
  430 T(ISF)=TT(ISF)
      VC=VC-(SBC*(T(ISF)/100.0)**4))
      RCP=RC+(GAM*SL(KK1))/((T1(KK1)-273.0)**2)
      CON=CONO+((BTA*SL(KK1))/(T1(KK1)-273.0))
      SIG=A*CON/RCP
      T3(ISB)=(T(ISF)+XX5*T3(KK1))/(1.0+XX5)
      IF(MX2.LT.3) GO TO 460
      T3(ISB-1)=T(ISF)+(((T3(ISB)-T(ISF))*(TSD-DZ))/TSD)
      GO TO 460
  435 CON=CONO+((BTA*SL(JJ1))/(T1(JJ1)-273.0))
      T(ISB)=((CON*TT(JJ1))/CONS+T(KK2))/(1.0+CON/CONS)
      TT(ISB)=T(ISB)
      DO 440 J=JJ1,JJ3
      RCP=RC+(GAM*SL(J))/((T1(J)-273.0)**2)
      CON=CONO+((BTA*SL(J))/(T1(J)-273.0))
      SIG=A*CON/RCP
  440 T(J)=((1.0-SIG)*T1(J)+SIG*(T1(J+1)+T(J-1)))/(1.0+SIG)
      DO 445 K=KK1,KK2
      J=KK1+KK2-K
  445 TT(J)=((1.0-SOG)*T1(J)+SOG*(T1(J-1)+TT(J+1)))/(1.0+SOG)
      GO TO 460
  450 DO 455 J=JJ1,JJ3
      K=JJ3+JJ1-J
      RCA=RC+(GAM*SL(K))/((T1(K)-273.0)**2)
      RCP=RC+(GAM*SL(J))/((T1(J)-273.0)**2)
      CON=CONO+((BTA*SL(J))/(T1(J)-273.0))
      CAN=CONO+((BTA*SL(K))/(T1(K)-273.0))
      SIG=A*CON/RCP
      SAG=A*CAN/RCA
      TT(K)=((1.0-SAG)*T1(K)+SAG*(T1(K-1)+TT(K+1)))/(1.0+SAG)
  455 T(J)=((1.0-SIG)*T1(J)+SIG*(T1(J+1)+T(J-1)))/(1.0+SIG)
  460 RCP=RC+(GAM*SL(JJ3+1))/((T1(JJ3+1)-273.0)**2)
      CON=CONO+((BTA*SL(JJ3+1))/(T1(JJ3+1)-273.0))
      SIG=A*CON/RCP
      T(JJ3+1)=((1.0-SIG)*T1(JJ3+1)+SIG*(T1(JJ3+2)+T(JJ3)))/(1.0+SIG)
      DO 465 J=KK1,JJ4
  465 T3(J)=(T(J)+TT(J))/2.0
      IF(MX1.GT.1.AND.MX1.LT.8) GO TO 470
      CON=CONO+((BTA*SL(JJ1))/(T1(JJ1)-273.0))
      T3(ISB)=((CON*T3(JJ1))/CONS+T3(KK2))/(1.0+CON/CONS)
  470 IF(1.NE.MIF) GO TO 490
      IF(MX1.NE.5) GO TO 475
      Z=DZ
```

```
      J20=KK1
      GO TO 480
  475 Z=DZX
      J20=KK1-1
  480 DO 485 J=J20,JJ4
      RCP=RC+(GAM*SL(J))/((T3(J)-273.0)**2)
      T3(J)=T3(J)+(EXC*FIO*EXP(-Z*EXC))/RCP
  485 Z=Z+DZ
      SWLO=SWLO+FIC*EXP(-Z*EXC)
  490 DO 495 K=KK1,JJ4
  495 T1(K)=T3(K)
      GO TO(500,520,520,515,520,500,500,515,515,515,515),MX1
  500 GO TO(505,515,510,515),MX2
  505 IF(WST.GT.T(ISF)) GO TO 520
      T1(KK1-1)=T(KK1-1)
      GO TO 520
  510 T1(KK1-2)=T3(KK1-2)
  515 T1(KK1-1)=T3(KK1-1)
  520 IF(MX1.GT.1.AND.MX1.LT.5) GO TO 525
      T1(ISF)=T(ISF)
      GO TO 530
  525 T1(ISB)=WIT
  530 TAC=TAC+EPS
      IF(MX1.NE.4) GO TO 535
      TAC=TAC+EPT
      HAB=TSDP+EPTC
      GO TO 540
  535 IF(TAC.LT.DZ.AND.TAC.GT.0.0) GO TO 545
  540 HTK=FTK+GEP+HAB
      L1=0
      HAB=0.0
      CALL SALPR(HTK,MX1,TAC)
  545 ASST=ASST+T1(ISF)
      IF(R5.NE.1.0) GO TO 555
      IF(MOD(ITR,KK8))555,550,555
  550 WRITE(3) T1,ISF,ILB,DZX,DZY
      WRITE(6,10) (T1(J),J=1,ILB)
      WRITE(6,11) ISF,ILB,ITR,DZX,DZY
  555 AIST=AIST+T1(ISB)
      VTK=VTK+FTK+GEP
      GO TO(560,563,563,561,561,556,556,556,556,556,556),MX1
  556 GO TO(560,558,559,560),MX2
  557 VC=VC+((CCN*(T1(KK1)-T1(ISF)))/(DZ+DZX))
      GO TO 563
  558 VC=VC+(CONS*(T1(ISB)-T1(ISF))/DZX)
      GO TO 563
  559 VC=VC+(CONS*(T1(ISB)-T1(ISF))/(DZ+DZX))
      GO TO 563
  560 CCN=CONS
      GO TO 557
```

```
561   CON=CONO+((BTA*SL(KK1))/(T1(KK1)-273.0))
      IF(MX1.EQ.5) GO TO 557
      VTK=VTK+TSDP+EPTC
      GO TO 557
563   IF(MOD(ITF,ITO))565,564,565
564   CALL RITE(MX1,MX3)
      GO TO(565,570),MX3
565   ITR=ITR+1
570   RETURN
      END
```

```
C      FLUX INTERPOLATION SUBROUTINE
       SUBROUTINE FLIP(EXLW)
       COMMON /BLA1/FLX(12,60),FSN(12,60),IMM(5,4),ALBD(12),FS(12),FL(12)
      1,T3(600)
       DIMENSION FIX(60),FS1(20),FLMT(60),F1(20),F2(20),FDL(20),FIN(20),F
      1(60),FLX2(60),F3(60)
 2     FORMAT(12F5.0)
 4     FORMAT(F5.1,I3)
 5     FORMAT(12F6.1)
 6     FORMAT(10F7.0)
 7     FORMAT(12F6.0)
 10    FORMAT(10(F8.1,5X))
 11    FORMAT(1H1,20X,9H DELTA T=,F5.1,6H HOURS//)
 12    FORMAT(1HC)
 13    FORMAT(15HO TOTAL FLX(I)=F8.1,10X,12H TOTAL F(I)=F8.1)
       READ(5,4) DT,IPN
       READ(5,7) (F1(I),I=2,17)
       READ(5,2) (F2(I),I=2,17)
       READ(5,6) (FDL(I),I=2,17)
       READ(5,6) (FIN(I),I=2,17)
       FI9=720.0/DT
       II9=FI9
       WRITE(6,11) DT
       LIX=0
       F1(1)=0.0
       F2(1)=0.0
       FDL(1)=0.0
       FIN(1)=0.0
       DO 100 I=2,17
       F1(I)=F1(I)/FI9
       F2(I)=F2(I)/FI9
       FDL(I)=(FDL(I)*EXLW)/FI9
 100   FIN(I)=FIN(I)/FI9
       DO 105 I=2,17
 105   F1(I)=F1(I)+F2(I)+FDL(I)
       X=((DT/720.0)**3)/2.0
       X2=720.0/DT
       X3=2.0*720.0/DT
       X4=3.0*720.0/DT
       M1=1
       L1=0
       M4=1
       I9=II9/2
       K1=2
       K2=5
       ITR=0
       IJ8=II9+1
       DO 200 I=2,13
       DO 110 K=1,17
 110   FS1(K)=F1(K)
```

```
      DO 115 K=1,60
115   FIX(K)=0.C
120   A1=(FS1(I+1)-FS1(I+2)+(FS1(I+3)-FS1(I))/3.0)*X
      A2=(((X2+X3+X4)*FS1(I)-(X2+X3)*FS1(I+3))/3.0+(X2+X4)*FS1(I+2)-(X3+
     1X4)*FS1(I+1))*X
      A3=(X3*X4*FS1(I+1)-X2*X4*FS1(I+2)+(X2*X3*FS1(I+3)-(X2*X3+X2*X4+X3*
     1X4)*FS1(I))/3.0)*X
      A4=(X2*X3*X4*FS1(I)*X)/3.0
      Y=FI9
      DO 135 J=1,II9
      L1=L1+1
      Y=Y+1.0
      FLMT(J)=A1*(Y**3)+A2*(Y**2)+A3*Y+A4
      GO TO(130,125),M1
125   F(L1)=FLMT(J)
      GO TO 135
130   FIX(L1)=FLMT(J)
135   CONTINUE
      L1=0
      GO TO(140,150),M1
140   DO 145 K=K1,K2
145   FS1(K)=FIN(K)
      M1=2
      GO TO 120
150   K1=K1+1
      K2=K2+1
      ITR=ITR+1
      M1=1
      GO TO(155,165),M4
155   DO 160 J=1,II9
      FLX2(J)=FIX(J)
160   F3(J)=F(J)
      M4=2
      GO TO 200
165   DO 170 J=1,I9
      K=I9+J
      FLMT(J)=F3(K)
      FLMT(K)=F(J)
      F3(K)=F(K)
      F(J)=FLMT(J)
      F(K)=FLMT(K)
      FLMT(J)=FLX2(K)
      FLMT(K)=FIX(J)
      FLX2(K)=FIX(K)
      FIX(J)=FLMT(J)
170   FIX(K)=FLMT(K)
175   LIX=LIX+1
      DO 180 J=1,II9
      FLX(LIX,J)=FIX(J)
180   FSN(LIX,J)=F(J)
```

```
      SUMX=0.0
      SUMF=0.0
      DO 185 J=1,II9
      SUMX=SUMX+FIX(J)
185   SUMF=SUMF+F(J)
      WRITE(6,13) SUMX,SUMF
      WRITE(6,12)
      WRITE(6,10) (FIX(K),K=1,II9)
      WRITE(6,12)
      WRITE(6,10) (F(K),K=1,II9)
      IF(12-ITR)200,190,200
190   ITR=ITR+1
      DO 195 J=1,I9
      K=I9+J
      FIX(J)=FL>2(K)
      FIX(K)=FL>2(J)
      F(J)=F3(K)
195   F(K)=F3(J)
      GO TO 175
200   CONTINUE
      DO 205 I=1,60
      FSN(1,I)=0.0
      FSN(2,I)=0.0
      FSN(11,I)=0.0
205   FSN(12,I)=0.0
      IF(IPN.EQ.1) GO TO 220
      DO 210 I=1,12
210   PUNCH 5,(FLX(I,J),J=1,60)
      DO 215 I=1,12
215   PUNCH 5,(FSN(I,J),J=1,60)
220   RETURN
      END
```

```
C       SALINITY PROFILE ADJUSTMENT
        SUBROUTINE SALPR(THK,MX1,TAC,HK1)
        COMMON /BLS1/SL(600)
        COMMON /BLSK/ISB,IDZ,DZ,DZX/BLS2/SL1,SL2,SL3,SL4,A1,A2,PI,U1,U2,IL
       1B
        Z1=(10.0*THK)/34.C
        Z2=(20.0*THK)/34.C
        SL(ISB)=SL1
        SL(ILB)=SL4
        EP1=U1/ALCG(Z1/THK)
        EP2=U2/ALCG(Z2/THK)
        G1=((1.0/EP2-1.0/EP1)*THK)/(Z2-Z1)
        G2=1.0/EP1-(G1*Z1/THK)
        J1=ISB+1
        J2=ILB-1
        IF(MX1.NE.4) GO TO 101
        Z=DZX
        GO TO 102
 101    Z=DZ
 102    DO 1C0 I=J1,J2
        ZP=Z/THK
        EP=1.0/(G1*ZP+G2)
        SL(I)=A1+A2*SIN(PI*((ZP)**EP-0.5))
 100    Z=Z+DZ
        I=THK/DZ
        Z=I*IDZ
        TAC=THK-Z
        RETURN
        END
```

```
C      OUTPUT SUBROUTINE
       SUBROUTINE RITE(MX1,MX3)
       COMMON /BLK1/TF(12,80),BSM(11,13),T1(600),EPM(12),ABL(12),SND1(12)
      1,CTB(12),RIT(12)
       COMMON /BLSK/ISB,IDZ,DZ,DZX/BLK2/ISF,ISI,KK1,JJ2,JJ4,J17,J18,M1,LC
      1I,ITR,MXI,K5,DZP,DZY,EPC,EPTC,TSD,TSDP,WTAB,WST,FTK,VTK,GEP,ADD,R5
  10   FORMAT(13X,2H 1,7X,3H 10,7X,3H 20,8X,2H 1,7X,3H 10,7X,3H 20,8X,2H
      11,7X,3H 1C,7X,3H 20,8X,2H 1,7X,3H 10,7X,3H 20//)
  11   FORMAT(2X,I3,5H CM. ,12(F8.3,2X))
  12   FORMAT(//10H ACCRETION,12(F8.3,2X)/10H BOT DEPTH,12(F8.3,2X)//)
  13   FORMAT(1H1,115X,6H YEAR I2/10H SNO DEPTH,12(F8.3,2X)/10H ICE THICK
      1,12(F8.3,2X)/10H ICE ABLTN,12(F8.3,2X)//)
  14   FORMAT(8H    DEPTH,13X,7HJANUARY,23X,8HFEBRUARY,23X,5HMARCH,25X,5HA
      1PRIL)
  15   FORMAT(8H    DEPTH,15X,3HMAY,27X,4HJUNE,26X,4HJULY,24X,6HAUGUST)
  16   FORMAT(8H    DEPTH,12X,9HSEPTEMBER,22X,7HOCTOBER,23X,8HNOVEMBER,22X
      1,8HDECEMBER)
  17   FORMAT(7H1  CATE,10X,10H SNO DEPTH,10X,10H ICE THICK,10X,10H ICE A
      1BLTN,10X,10H ACCRETION,10X,10H BOT DEPTH)
  18   FORMAT(2X,2I3,9X,5(F8.3,12X))
       K5=K5+1
       EPM(K5)=EPC
       CTB(K5)=FTK+GEP+ADD
       SND1(K5)=TSD
       IF(MX1.NE.4) GO TO 130
       ABL(K5)=TSDP+EPTC
       SND1(K5)=C.0
       RIT(K5)=FTK+ABL(K5)+GEP
       GO TO 135
 130   RIT(K5)=CTB(K5)-ADD
 135   DO 140 K=JJ4,J17
 140   T1(K+1)=WTAB
       DO 145 K=2,ISF
 145   T1(K-1)=WST
       IF(R5.EQ.C.0) GO TO 155
       DO 150  K=2,60
       I9=((K-1)*10)/IDZ+1
 150   TF(K5,K)=273.0-T1(I9)
 155   IF(ITR.GE.MXI) GO TO 160
       IF(K5-12)200,160,160
 160   IF(R5.EQ.C.0) GO TO 191
       WRITE(6,12) LCI,(SND1(J),J=1,12),(RIT(J),J=1,12),(ABL(J),J=1,K5)
       GO TO(170,175,180,165),M1
 165   M1=1
 170   WRITE(6,14)
       GO TO 185
 175   WRITE(6,15)
       GO TO 185
 180   WRITE(6,16)
 185   WRITE(6,10)
```

```
      DO 190 J=1,50
      I6=(J-1)*10
  190 WRITE(6,11) I6,(TF(K,J),K=1,K5)
      WRITE(6,12) (EPM(J),J=1,12),(DTB(J),J=1,K5)
      GO TO 194
  191 IF(M1.NE.1) GO TO 192
      J6=1
      J7=-10
      WRITE(6,17)
  192 DO 193 K=1,12
      J7=J7+10
      IF(J7.NE.30) GO TO 193
      J6=J6+1
      J7=0
  193 WRITE(6,18) J6,J7,SND1(K),RIT(K),ABL(K),EPM(K),DTB(K)
      IF(M1.NE.3) GO TO 194
      M1=0
  194 M1=M1+1
      DO 195 K=1,K5
  195 ABL(K)=0.0
      DO 196 I=1,12
      SND1(I)=0.0
      RIT(I)=0.0
  196 EPM(I)=0.0
      K5=0
      IF(ITR.GE.MXI) GO TO 205
  200 MX3=1
      GO TO 210
  205 MX3=2
      ITR=ITR+1
  210 RETURN
      END
```

REFERENCES

Abels, G., Measurement of the snow density at Ekaterinburg during the winter of 1890-1891, Academia Nauk, Memoirs, 69, 1892.

Ambach, W., and H. Mocker, Messungen der Strahlungsextinktion mittels eines kugelformigen Empfängers in der oberflächennahen Eisschicht eines Gletschers und im Altschnee, Arch. Meteorol. Geophys. Bioklimatol., B, 10, 84-99, 1959.

Ambach, W., and H. L. Habicht, Untersuchungen der Extinktionseigenschaften des Gletschereises und Schnees, Arch. Meteorol. Geophys. Bioklimatol., B, 11, 512-532, 1962.

Badgley, F. I., Heat balance at the surface of the Arctic Ocean, Proc. Western Snow Conf., Spokane, Washington, 101-104, 1961.

Badgley, F. I., Heat budget at the surface of the Arctic Ocean, Proceedings of the Symposium on the Arctic Heat Budget and Atmospheric Circulation, The Rand Corporation, Santa Monica, California, RM-5233-NSF, 267-278, December 1966.

Barnes, H. T., Ice Engineering, Renouf, Montreal, 1928.

Bilello, M., Formation, growth and decay of sea ice in the Canadian Arctic Archipelago, Arctic, 14, 2-25, 1961.

Bilello, M., Method for predicting river and lake ice formation, J. Applied Meteorol., 3, 38-44, 1964.

Briazgin, N. N., The problem of the albedo on the surface of drifting ice, Probl. Arkt. Antarkt., No. 1, 33-39. [Transl. for GRD by American Meteorological Society on contract AF 19(604)6113].

Brooks, C. E. P., Climate Through the Ages, McGraw-Hill, New York, 1949.

Budyko, M. I., Polar ice and climate, Proceedings of the Symposium on the Arctic Heat Budget and Atmospheric Circulation, The Rand Corporation, Santa Monica, California, RM-5233-NSF, 3-22, December 1966.

Callaway, E. B., An Analysis of Environmental Factors Affecting Ice Growth, U. S. Navy Hydrographic Office, TR-7, September 1954.

Carslaw, H. H., and J. C. Jaeger, Conduction of Heat in Solids, Second Edition, Clarendon Press, Oxford, 1959.

Chernigovskii, N. T., Radiational properties of the Central Arctic ice coat, Soviet Data on the Arctic Heat Budget and Its Climatic Influence, The Rand Corporation, Santa Monica, California, RM-5003-PR, May 1966.

Crary, A. P., Arctic ice island and shelf ice studies, Scientific Studies at Fletcher's Ice Island, T-3, 1952-1955, 3, GRD-AFCRC, Geophysics Research Paper 63, 1960.

Dingle, A. N., and C. Young, Computer Applications in the Atmospheric Sciences, College of Engineering, University of Michigan, 1965.

Doronin, Yu. P., On the problem of sea ice accretion (in Russian), Probl. Arkt. Antarkt., 1, 73-80, 1959.

Doronin, Yu. P., On the heat balance of the Central Arctic (in Russian), Proceedings of the Arctic and Antarctic Scientific Research Institute, 253, 178-184, Leningrad, 1963.

Doronin, Yu. P., Characteristics of the heat exchange, Proceedings of the Symposium on the Arctic Heat Budget and Atmospheric Circulation, The Rand Corporation, Santa Monica, California, RM-5233-NSF, 247-266, December 1966.

Dunbar, M., and W. Wittmann, Some features of ice movement in the Arctic Basin, Proc. Arctic Basin Symp., Oct. 1962, Arctic Institute of North America, Washington, D. C., 90-108, 1963.

Ewing, M., and W. L. Donn, A theory of ice ages, I, Science, 123, 1061-1066, 1956.

Ewing, M., and W. L. Donn, A theory of ice ages, II, Science, 127, 1159-1162, 1958.

Ewing, M., and W. L. Donn, A theory of ice ages, III, Science, 152, 1706-1712, 1966.

Fletcher, J. O., The Heat Budget of the Arctic Basin and its Relation to Climate, The Rand Corporation, Santa Monica, California, R-444-PR, October 1965.

Fletcher, J. O., Ice Extent on the Southern Ocean and its Relation to World Climate, The Rand Corporation, Santa Monica, California, RM-5793-NSF, March 1969.

Forsythe, G. E., and W. R. Wasow, Finite-Difference Methods for Partial Differential Equations, John Wiley & Sons, Inc., New York, 1960.

Gavrilova, M. K., Radiation Climate of the Arctic, Hydrometeorological Publishing House, Leningrad, 1963. [Translation for NSF by Israel Program for Scientific Translations, 1966].

Giese, J. H., Numerical analysis, Recent Soviet Contributions to Mathematics, MacMillan Co., 86-88, 1962.

Hanson, A. M., Studies of the mass budget of arctic pack-ice floes, J. Glaciology, 5, 701-709, 1965.

Hanson, K. J., The albedo of sea ice and ice islands in the Arctic Ocean Basin, Arctic, 14, 188-196, 1963.

Hildebrand, F. B., Introduction to Numerical Analysis, McGraw-Hill, New York, 1956.

Hisdal, V., The diurnal temperature variation during the polar night, Quart. J. Roy. Meteor. Soc., 86, 104-106, 1960.

Holton, J. R., A stable finite difference scheme for the linearized vorticity and divergence equation system, J. Applied Meteorol., 6, 519-522, 1967.

Hunkins, K., and H. Kutschale, Quaternary sedimentation in the Arctic Ocean, Proceedings of the Seventh INQUA Congress, 1965.

Kellogg, W. W., K. J. K. Buettner, and E. C. May, Meteorological Sattellite Observations of Thermal Emission, The Rand Corporation, Santa Monica, California, RM-4392-NASA, December 1964.

Kolesnikov, A. G., On the theory of ice accretion on the sea surface (in Russian), Problems of Marine Hydrological Forecasts, Leningrad, 1946.

Kolesnikov, A. G., On the growth rate of sea ice, Arctic Sea Ice, National Academy of Sciences Publication 598, 157-161, 1958.

Ku, T. L., and W. S. Broecker, Rates of sedimentation in the Arctic Ocean, Proceedings of the Seventh INQUA Congress, 1965.

Laktionov, A. F., Recent Soviet investigations in the polar regions (in Russian), Sea Transport Publishing, 347-426, 1955. [Translation by Air University Document Study, Maxwell AFB, 1956].

Lamb, H. H., and A. I. Johnson, Climate variation and observed changes in the general circulation, Parts I and II, Geografiska Annaler, 41, 94-134, 1959.

Lamb, H. H., and A. I. Johnson, Climate variation and observed changes in the general circulation, Part III, Geografiska Annaler, 43, 363-400, 1961.

Langleben, M. P., Albedo measurements on an arctic ice cover from high towers, J. Glaciology, 7, 289-298, 1968.

Larkin, B. K., Stable difference approximations to the diffusion equation, Mathematics of Computation, 18, 196-202, 1964.

Larsson, P., and S. Orvig, Atlas of mean monthly albedo of arctic surfaces, McGill Univ. Publ. Meteorol., 45, 1961.

Larsson, P., and S. Orvig, Albedo of arctic surfaces, McGill Univ. Publ. Meteorol., 54, 1962.

Liljequist, G. H., Energy exchange of an Antarctic snowfield, Scientific Results of the Norwegian-British-Swedish Antarctic Expedition, 3, Norsk Polarinstitutt, Oslo, 1956.

Lyon, W., Ocean and Sea Ice Research in the Arctic Ocean, Translation by New York Academy of Sciences, Series II, 23, 1961.

Makarova, V. S., A. M. Mkhitaryan, A. A. Trapeznikov, and T. G. Fedorova, The use of monomolecular films for decreasing evaporation from a water surface (in Russian), Transactions of the All-Union Scientific Conference, 4, 460-470, 1962.

Malmgren, F., On the properties of sea ice, The Norwegian Polar Expedition "Maud", Scientific Results, 1a:5, 1-67, 1927.

Marshunova, M. S., "Principal Characteristics of the Radiation Balance of the Underlying Surface and of the Atmosphere in the Arctic" (in Russian), Proc. Arctic and Antarctic Res. Institute, 229, Leningrad, 1961. [Translated by the Rand Corporation, RM-5003-PR, 1966].

Mellor, M., Properties of Snow, CRREL Science and Engineering Report, III-A1, Hanover, New Hampshire, 1964.

Mellor, M., Optical Measurements on Snow, CRREL Research Report 169, Hanover, New Hampshire, 1965.

Milne, W. E., Numerical Calculus, Princeton Univ. Press, Princeton, New Jersey, 1949.

Mosby, H., Water, salt and heat balance in the North Polar Sea, Proc. Arctic Basin Symp., Arctic Institute of North America, Washington, D.C., 69-84, 1963.

Ono, N., Specific heat and heat of fusion of sea ice, Physics of Snow and Ice, Volume I, Institute of Low Temperature Science, Hokkaido, Japan, 599-610, 1967.

Panov, V. V., and A. O. Shpaikher, Influence of Atlantic waters on some features of the hydrology of the Arctic Basin and adjacent seas, Deep-Sea Research, 11, 275-285, 1964.

Petrov, I. G., Physical-mechanical properties and thickness of the ice cover, Observational Data of the Scientific-Research Drifting Station of 1950-1951, 2:6, 1954. [Translation for GRD by American Meteorological Society under contract AF(604)-1936.]

Rakipova, L. R., The influence of the Arctic ice cover on the zonal distribution of atmospheric temperature, Proceedings of the Symposium on the Arctic Heat Budget and Atmospheric Circulation, The Rand Corporation, Santa Monica, California, RM-5233-NSF, 411-442, December 1966.

Richtmyer, R. D., Difference Methods for Initial Value Problems , Interscience, New York, 1957.

Sauliev, V. K., A method of numerical solution for the diffusion equation (in Russian), Dokl. Akad. Nauk SSSR(NS), 115, 1077-1079, 1957a.

Sauliev, V. K., Numerical integration of parabolic equations (in Russian), Dokl. Akad. Nauk SSSR(NS), 117, 36-39, 1957b.

Schwarzacher, W., Pack ice studies in the Arctic Ocean, J. Geophys. Res., 64, 2357-2367, 1959.

Schwerdtfeger, P., The thermal properties of sea ice, J. Glaciology, 4, 789-807, 1963.

Schwerdtfeger, P., An analogue computer for solving growth problems of floating ice, Gerlands Beitrage zur Geophysik, 73:1, 44-52, 1964.

Stefan, J., Über die Theorie der Eisbildung, insbesondere über die Eisbildung im Polarmeere, Ann. Physik, 3rd Ser., 42, 269-286, 1891.

Timofeev, V. T., An approximate determination of the heat balance of Arctic Basin waters, Problemy Arktiki, 4, 23-28, 1958. [Translation for AFCRC by American Meteorological Society, contract AF19(604)-1936].

Toporkov, L. G., Is it possible to remove the ice cover of the Northern Arctic Ocean?, Priroda, 11, 93-97, 1963. [Translation for AFCRL by Emmanuel College Research Language Center, E-T-R-64-23].

Treshnikov, A. F., The ice of the Southern Ocean, Proceedings of the Symposium on Pacific-Antarctic Sciences, 11th Pacific Science Congress, Tokyo, 1966.

U. S. Naval Civil Engineering Laboratory, Theoretical Study of an Arctic Ocean Environment Simulator, Port Hueneme, California, Report No. 3039, August 1965.

Untersteiner, N., On the mass and heat budget of arctic sea ice, Arch. Meteorol. Geophys. Bioklimatol., A, 12, 151-182, 1961.

Untersteiner, N., Ice budget of the Arctic Ocean, Proceedings of the Arctic Basin Symposium, Arctic Institute of North America, Washington, 219-226, 1962.

Untersteiner, N., Calculations of temperature regime and heat budget of sea ice in the Central Arctic, J. Geophys. Res., 69, 4755-4766, 1964.

Untersteiner, N., Calculating the thermal regime and mass budget of sea ice, Proceedings of the Symposium on the Arctic Heat Budget and Atmospheric Circulation, The Rand Corporation, Santa Monica, California, RM-5233-NSF, 203-214, December 1966.

Untersteiner, N., Natural desalination and equilibrium salinity profile of perennial sea ice, J. Geophys. Res., 73, 1251-1257, 1968.

Untersteiner, N., and F. I. Badgley, Preliminary results of thermal budget studies on arctic pack ice during summer and autumn, Arctic Sea Ice, Natl. Acad. Sci., Publ. 598, 85-95, 1958.

Vowinckel, E., Cloud amount and type over the Arctic, McGill Univ. Publ. Meteorol., 51, 1962.

Vowinckel, E., Ice Transport between Greenland and Spitzbergen and its causes, McGill Univ. Publ. Meteorol., 59, 1963.

Vowinckel, E. and S. Orvig, Water balance and heat flux of the Arctic Ocean, Arctic, 15, 205-223, 1962a.

Vowinckel, E., and S. Orvig, Relation between solar radiation income and cloud type in the Arctic, McGill Univ. Publ. Meteorol., 48, 1962b.

Vowinckel, E., and S. Orvig, Insolation and absorbed solar radiation at the ground in the Arctic, McGill Univ. Publ. Meteorol., 53, 1962c.

Vowinckel, E., and S. Orvig, Long wave radiation and total radiation at the surface in the Arctic, McGill Univ. Publ. Meteorol., 62, 1963.

Vowinckel, E., and S. Orvig, Radiation balance of the troposphere and of the earth-atmosphere system in the Arctic, McGill Univ. Publ. Meteorol., 63, 1964.

Vowinckel, E., and S. Orvig, Energy balance of the Arctic. V: The heat budget of the Arctic Ocean, Arch. Meteorol. Geophys. Bioklimatol., 14, 303-325, 1966.

Vowinckel, E., and S. Orvig, Climate change over the Polar Ocean. I: The radiation budget, Arch. Meteorol. Geophys. Bioklimatol., 15, 1-23, 1967.

Vowinckel, E., and B. Taylor, Evaporation and sensible heat flux over the Arctic Ocean, McGill Univ. Publ. Meteorol., 66, 1964.

Wittmann, W. I., and J. J. Schule, Comments on the mass budget of arctic pack ice, Proceedings of the Symposium on the Arctic Heat Budget and Atmospheric Circulation, The Rand Corporation, Santa Monica, California, RM-5233-NSF, 215-246, December 1966.

Yakoviev, G. N., Solar radiation as the chief component of the heat balance of the arctic ice, Arctic Sea Ice, National Academy of Sciences Publication 598, 181-184, 1958.

Yanes, A. V., Melting of snow and ice in the Central Arctic, Problems of the Arctic and the Antarctic, No. 11, Leningrad, 1962. [Translated for AINA, May 1966].